AJS American Journal of Science
publishing earth-sciences research since 1818

Trapp-Müller, G., Aller, R. C., Sluijs, A., & Middelburg, J. J. (2025). Silicate weathering and diagenetic reaction balances in deltaic muds. *American Journal of Science*, Article 10.
https://doi.org/10.2475/001c.134118

Science Paper

Silicate Weathering and Diagenetic Reaction Balances in Deltaic Muds

Gerrit Trapp-Müller[1][a], Robert C. Aller[2], Appy Sluijs[1], Jack J. Middelburg[1]

[1] Department of Earth Sciences, Utrecht University, [2] School of Marine and Atmospheric Sciences, Stony Brook University

Keywords: terrigenous marine sediments, mobile muds, mineral authigenesis, silicate alteration, alkalinity

https://doi.org/10.2475/001c.134118

American Journal of Science

Reactions between terrigenous sediments, marine-biogenic substances and seawater modulate multiple biogeochemical cycles, but the dynamics and factors governing these reactions are poorly constrained. Deltaic mobile muds are a major sedimentary facies along river-dominated ocean margins through which most terrigenous sediment transits and mixes with marine-biogenic matter, representing efficient and globally significant batch reactors. Here, we present a process-based model that combines equilibrium aqueous chemistry with kinetic concepts from sediment biogeochemistry and mineral sciences to explore the solution-mediated interplay of organic and inorganic matter alteration in episodically reworked deltaic muds. The model reproduces observed diagenetic conditions and product suites over the seasonal timescales relevant to deltaic systems and indicates a systematic and dynamic coupling between the sedimentary cycles of H^+, C, P, Fe, S, Si, Mg, K, and Ca. We used the model in combination with published field observations and concepts of authigenic mineral occurrences to develop a generalized explanatory framework for silicate weathering fluxes and diagenetic reaction balances in marine sediments. Diagenetic silicate weathering is represented by a continuum of reaction balances with acid (reverse) and alkaline (forward) endmembers that is moderated by sediment sources, which determine the sediment's weathering *potential*, and depositional environments, which govern the *expression* of this potential. Reverse weathering dominates in seasonally reworked, low-latitude deltaic muds, where green clays form rapidly from lateritic river sediments and biogenic silica under suboxic conditions. High mineral precipitation rates and protracted sediment remobilization drive large solute fluxes from/to these sediments. Net forward silicate weathering becomes more likely under steady, sustained anoxic conditions, particularly in volcanically-influenced settings and at minimal pre-weathering of sediment sources. These results further our understanding of the role silicate weathering and marine sediments play in global biogeochemistry and Earth system evolution, and can aid targeted 'enhanced weathering' strategies to environmental governance.

1. INTRODUCTION

Chemical silicate weathering (CSW) denotes the low-temperature transformation of silicate materials (minerals and amorphous substances) by coupled dissolution-precipitation reactions (Hellmann et al., 2012; Ruiz-Agudo et al., 2016). CSW is ubiquitous and quantitatively redistributes elements among Earth's solid and fluid reservoirs, affecting natural acid-base equilibria, global biogeochemistry, and Earth surface conditions (E. K. Berner & Berner, 2012; Ébelmen, 1845; Kump et al., 2000; Urey, 1952). Enhancing CSW in terrestrial and marine environments is discussed as a viable option aiding ocean alkalinization and societal decarbonization (CO_2 removal from the atmosphere) (Hartmann et al., 2013; Longman et al., 2020; Matter et al., 2016; Meysman & Montserrat, 2017). While natural CSW fluxes are traditionally ascribed to either continental or oceanic crust weathering (R. A. Berner et al., 1983; Caldeira, 1995; Hartmann et al., 2014; Hilton & West, 2020), CSW in marine sediments is increasingly recognized as a common part of shallow diagenetic reaction networks, exerting biogeochemical fluxes that potentially rival crustal weathering (R. C. Aller & Wehrmann, 2025; Isson et al., 2020; Jeandel & Oelkers, 2015; Mackenzie & Garrels, 1965; Michalopoulos & Aller, 1995; Rahman et al., 2017; Rude & Aller, 1989; Sillén, 1967; Wallmann et al., 2008, 2023). However, the corresponding biogeochemical fluxes, particularly of alkalinity and carbon, and the underlying reaction patterns are poorly constrained (Trapp-Müller et al., in press; Wallmann et al., 2023).

A substantial body of research has concentrated on disentangling diagenetic weathering dynamics and constrain-

a Corresponding author: g.muller@uu.nl

ing the resulting biogeochemical fluxes and their governing factors, largely using chemical analyses of sediments and porewaters and/or sediment mineralogy and petrography (Ehlert et al., 2016; Maher et al., 2006; Meister et al., 2022; Michalopoulos & Aller, 2004; Rahman & Trower, 2023; Torres et al., 2020, 2022; Wallmann et al., 2023).

Measurements of sediment composition and porewater chemistry in combination with reaction-transport models are then used to quantify reaction rates and related elemental fluxes (Du et al., 2022; Ehlert et al., 2016; Maher et al., 2006; Wallmann et al., 2008). However, interpretations and comparison of model results can be complicated by analytical artifacts, such as temperature and pressure effects on solubility (Cetiner et al., 2023; De Lange et al., 1992; Siever et al., 1965) or physical disturbance of the sediment-water interface upon sampling. Additional problems may arise from missing observational constraints and differences in the kinetic formulations applied. For example, dissolution and precipitation rates or operationally defined net weathering rates are commonly quantified by numerical fitting of parameters in study-specific rate laws (Meister et al., 2022; Wallmann et al., 2008). Although informative, kinetic constants obtained in this way often lack a mechanistic basis, are scarce, and cannot be compared directly, impeding generalizations and predictions (Hellevang et al., 2013; Krissansen-Totton & Catling, 2020; Tosca et al., 2016; Tosca & Masterson, 2014).

Si-isotopic data of marine sediments and porewaters in particular have elucidated the relative roles and contributions of lithogenic, biogenic and authigenic silicates to benthic Si fluxes (Closset et al., 2022; Ehlert et al., 2016; Geilert et al., 2023; Luo et al., 2022; Rahman et al., 2017; Ward et al., 2022). Moreover, Sr isotope systematics in active margin sediments have demonstrated a tight coupling between diagenetic CSW and carbonate authigenesis (Hong et al., 2020; Torres et al., 2020). In addition, isotopic signatures of Mg and K in various marine sediments attest to widespread silicate authigenesis (Chanda et al., 2023; Higgins & Schrag, 2015; Li et al., 2022; Santiago Ramos et al., 2018). However, a full assessment of net reaction balances and environmental influences, information required to generalize findings from such isotopic studies and to quantitatively assess biogeochemical impacts, is generally lacking (Trapp-Müller et al., in press; Wallmann et al., 2023). For example, the relative contributions of cation-depleted vs cation-enriched Al-sources to clay authigenesis and ambient solution chemistry may determine whether the reactions net produce alkalinity and sequester CO_2 (‘forward weathering’) or produce acidity and release CO_2 (‘reverse weathering’), but Al dynamics are rarely considered in much detail (Trapp-Müller et al., in press; Wallmann et al., 2023). Although qualitative, observation-based frameworks for occurrences of marine authigenic minerals exist and have partly been linked to terrestrial and marine reactant supplies (Aplin & Taylor, 2012; R. A. Berner, 1981; Kastner, 1999; Müller, 1967), these frameworks have not yet been tested against thermodynamic and kinetic constraints, nor linked to concepts of diagenetic weathering fluxes, depositional environments and Earth’s weathering feedback (R. C. Aller & Wehrmann, 2025; Mackenzie & Garrels, 1966; Torres et al., 2020; Trapp-Müller et al., in press; Wallmann et al., 2023).

Episodically reworked, deltaic ‘mobile’ muds are a major sedimentary facies along the river-dominated ocean margins (Bao et al., 2019; Kuehl et al., 1986, 2019; Liu et al., 2018; McKee et al., 2004). A dominant fraction of the terrigenous sediments reaching the ocean transits through them for multiple years, entraining large amounts of reactive marine-biogenic particles and exchanging materials with ocean and shoreline before eventually reaching longer term depocenters (Anthony et al., 2010; Kuehl et al., 2019; Song et al., 2022) (fig. 1). Low latitude mobile muds represent efficient batch reactors, organic carbon ‘incinerators’, and global hotspots of K, Mg and F consumption, biogenic Si sequestration and likely reverse weathering, (R. C. Aller et al., 2008; R. C. Aller & Blair, 2006; Bao et al., 2018; Ku & Walter, 2003; Michalopoulos & Aller, 1995, 2004; Rahman et al., 2017; Rude & Aller, 1989, 1994; B. Zhao et al., 2017). These deltaic systems often remove substantial fractions of the corresponding riverine solute fluxes and biogenic particle inputs. For example, diagenetic silicate weathering in the Amazon-Guianas mobile muds alone may remove ~10 % of the global riverine K supply (R. C. Aller, 2004; Michalopoulos & Spiegel, 2021), ~2% of the global riverine F^- supply (Rude & Aller, 1994), up to 67 % of the Mg (Rude & Aller, 1989) , and ~50 % of the dissolved Si delivered by the Amazon river (Rahman et al., 2016). Due to seasonal reworking, the corresponding reaction-transport dynamics can deviate substantially from traditional (‘plug-flow’) diagenetic models, which assume steady and undisturbed sediment accummulation (R. C. Aller, 2004; R. A. Berner, 1980).

To constrain the main factors governing net reaction outcomes in deltaic mobile mud belts, we explored the evolution of diagenetic conditions within mobile muds and the coupled responses of silicate weathering and mineral authigenesis. First, we reviewed dominant features of marine diagenetic weathering, and then constructed a batch reaction model suitable for mobile mud diagenesis over the characteristic timescales of episodic deposition. The model combines equilibrium aqueous chemistry with kinetic concepts from sediment biogeochemistry (R. A. Berner, 1980; Soetaert et al., 1996) and mineral sciences (Aagaard & Helgeson, 1982; Hellevang et al., 2013; Tosca et al., 2016). We implemented two approaches to silicate precipitation: (I) an explicit formulation of nucleation-growth mechanisms (‘PHA’, based on Hellevang et al. (2013) and Pham et al. (2011)) and (II) a phenomenological pH-dependent, Si-limited batch rate law (‘TIP’, based on Isson and Planavsky (2018) and Tosca et al. (2016)). Both model setups were scaled to resemble quantitative and qualitative observations from mobile muds of the Amazon delta topset. Subsequent model experiments, linear global sensitivity analyses, and comparison to observations from a wide range of sedimentary environments were then used to develop a general, explanatory framework of diagenetic silicate weathering products and fluxes with respect to sediment sources and depositional environments.

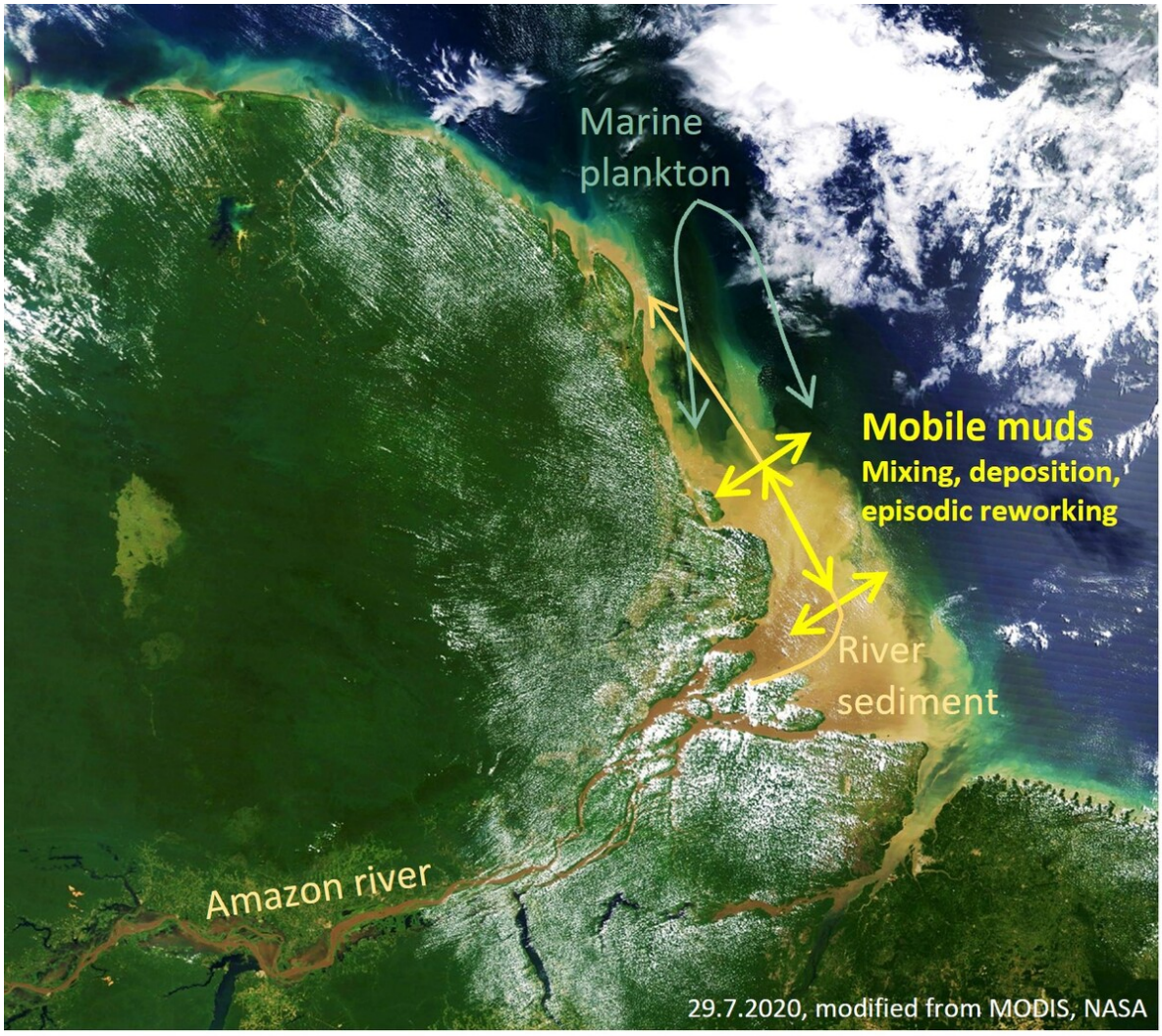

Figure 1. Satellite image (modified from MODIS, NASA) showing how terrestrial sediments (brown) and marine biogenic particles (green) are mixed, deposited and episodically reworked over vast distances (and timescales) in deltaic mobile muds of the Amazon shelf. Reworking of > 1 m thick mud layers within the delta topset is seasonal, and maintains reactivity and dominantly suboxic biogeochemical conditions.

2. WEATHERING REACTION BALANCES AND MARINE ENVIRONMENTS

2.1. Weathering reaction balances: 'forward' and 'reverse' components

The weathering process represents a dynamic continuum of intricately coupled dissolution and precipitation reactions releasing and/or consuming solutes (Hellmann et al., 2012; Niedermeier et al., 2009; O'Neil & Taylor, 1967):

$$Dissolution + Precipitation = Solute\ Flux \quad (1)$$

where *Dissolution* and *Precipitation* are each a series of reactions that are locally coupled at the dissolution front (Hellmann et al., 2012; Ruiz-Agudo et al., 2012, 2016) and may decouple in space and time, as suggested by Frings et al. (2014) and Wallmann et al. (2008). Congruent dissolution or homogeneous nucleation from an initially supersaturated solution are possible too. *Dissolution* exerts a flux to solution (> 0), while *Precipitation* consumes solutes (< 0) so that the resulting net *Solute Flux* can be either positive or negative. To maintain charge balance, the hypothetical 'net charge' of the direct *Solute Flux* after accounting for speciation is compensated by re-equilibration of local acid-base systems, primarily CO_2-HCO_3^--CO_3^{2-} transformations in Earth surface environments (Middelburg et al., 2020). Thus, the carbon cycle impact of weathering reactions is best quantified through changes in alkalinity, similar to other biogeochemical processes (Middelburg et al., 2020; Soetaert et al., 2007; Trapp-Müller et al., in press).

'Forward' and 'reverse' weathering can be described as two endmembers of a reaction continuum, transforming CO_2 to HCO_3^- (increasing alkalinity) or transforming HCO_3^- into CO_2 (reducing alkalinity), respectively (Isson et al., 2020; Mackenzie & Garrels, 1966b; Trapp-Müller et al., in press). Net forward silicate weathering typically transforms cation-rich silicates (e.g., feldspar or mafic minerals) into cation-depleted, Si-Al-enriched secondary phases (e.g., smectite, kaolinite or opal), e.g.:

$$\begin{aligned} &Cation-rich\ silicate + CO_2 + H_2O \\ &\quad \rightarrow Cation-poor\ silicate \\ &\quad + cations\left(Na^+, K^+, Ca^{2+}, Mg^{2+}, Mn^{2+}, Fe^{2+}\right) \\ &\quad + Si(OH)_4 + (Fe(OH)_3(s) + Al(OH)_3(s)) \\ &\quad + HCO_3^- \end{aligned} \quad (2)$$

Such a weathering stoichiometry is characteristic for dilute, acidic to circum-neutral continental freshwaters and forms the basis of the negative weathering feedback on atmospheric CO_2 and hydro-climate that stabilizes the carbon cycle over geological timescales (R. A. Berner, 1991; Brantley et al., 2023; Ruiz-Agudo et al., 2016). Reaction dynamics are further moderated by the physicochemical evolution of the altering grain's reactive interface (Hellmann et al., 2012; Luttge et al., 2019; Müller et al., 2022), and by tectonic-geomorphological boundary conditions (Stallard, 1985; von Blanckenburg, 2005; West et al., 2005).

While forward weathering in anoxic marine sediments has been observed (Torres et al., 2020; Wallmann et al., 2008), net alkalinity-neutral and reverse weathering balances become feasible in oceanic environments (Aloisi et al., 2004; Ku & Walter, 2003; Mackenzie & Garrels, 1965; Michalopoulos & Aller, 1995; Wallmann et al., 2023). Generally, the oceans high ionic strength promotes dissolution and weathering rates (Gruber et al., 2019; Rimstidt et al., 2016; Wallmann et al., 2023), while the higher pH and cation availability (compared to freshwaters) should also promote the precipitation of cation-rich secondary phases. In terrigenous marine muds, the dissolved and particulate products of (terrestrial) forward weathering (eq 2) and biogenic silica recombine, eventually reversing some of the large-scale effects of forward weathering (Ku & Walter, 2003; Mackenzie & Garrels, 1965, 1966; Michalopoulos & Aller, 1995), e.g.:

$$\begin{aligned} &Cation-poor\ silicate \\ &\quad + cations\left(Na^+, K^+, Ca^{2+}, Mg^{2+}, Mn^{2+}, Fe^{2+}\right) \\ &\quad + Si(OH)_4 + (Fe(OH)_3(s) + Al(OH)_3(s)) \\ &\quad + HCO_3^- \\ &\quad \rightarrow Cation-rich\ silicate + CO_2 + H_2O \end{aligned} \quad (3)$$

A variety (or sequence) of secondary minerals or amorphous substances (non-crystalline and by definition not a mineral) has been observed in marine sediments, including opal (Riech & von Rad, 1979; van Bennekom et al., 1989), 'palagonites' (amorphous replacement products of volcanic glasses) (Stroncik & Schmincke, 2002), clays (e.g., smectites, mica-group clays, chlorites and serpentines) (Aplin & Taylor, 2012; Müller, 1967), zeolites (Hay, 1966; Kastner, 1979; Stroncik & Schmincke, 2001) and even K-feldspar (Milliken, 2003; Müller, 1967), implying substantial variation in net reaction balances. Moreover, the precipitation kinetics may be moderated by metastable intermediates (Steefel & Van Cappellen, 1990; Tosca et al., 2016), which may or may not change in composition during recrystallization and ripening. The net weathering flux is the result of the balance between dissolution and precipitation, whose interplay depends on transport-phenomena and ambient reactions, such as organic matter degradation in marine sediments (Aplin & Taylor, 2012; Baldermann et al., 2013; Burst, 1958; Michalopoulos & Aller, 1995; Wallmann et al., 2008). Thus, weathering reaction balances and net fluxes in marine sediments vary laterally and vertically with reactant mixture (sediment sources) and physical and biogeochemical boundary conditions (sediment dynamics, diagenesis) (R. C. Aller & Wehrmann, 2025).

2.2. Marine weathering environments

In marine sediments, transitions between (carbonate-forming) forward weathering, near alkalinity-neutral and reverse diagenetic weathering occur in space and/or time as either reactant mixes (sediment provenance, compound depletion or involvement of oceanic crust) (Aplin & Taylor, 2012; Milliken, 2003; Torres et al., 2022) or biogeochemical conditions change (Aplin & Taylor, 2012; Scholz et al., 2013; Wallmann et al., 2008).

Generally, the forward weathering component is promoted by the presence of cation-rich reactants, such as feldspar, tephra or mafic minerals. Indeed, immersion of these materials in (oxic) standard seawater commonly results in substantial element release and, sometimes, alkalinity generation (Gruber et al., 2019; Jeandel & Oelkers, 2015; Jones et al., 2012; Montserrat et al., 2017). The reverse weathering component appears to strengthen with increasing degree of previous terrestrial alteration and porewater Si concentrations (Delerce et al., 2023; Mackenzie & Garrels, 1965; Mackin, 1986). Weathering of common clays, i.e., terrestrial weathering products, in oxygenated standard seawater and analogues often results in acidification and cation-uptake (Caillère & Hénin, 1949; Mackenzie & Garrels, 1965; Swindale & Fan, 1967). A portion of terrestrial weathering products is composed of amorphous Si-Al(-Fe)(oxy-)hydroxide nanoparticles (C. V. Putnis & Ruiz-Agudo, 2021) that are hard-to-detect but appear to cover large fractions of common clay surfaces (Tsukimura et al., 2021). The supply of these weathering products varies with climate and runoff (Müller et al., 2021; Poulton & Raiswell, 2002), eventually driving latitudinal diagenetic weathering patterns along the continental margins (Aplin & Taylor, 2012; Ku & Walter, 2003; Odin, 1990).

Besides reactant distributions, the net fluxes and acid-base impacts are moderated by variation in precipitation, strengthening the reverse component under seawater compared to freshwater conditions (Fuhr et al., 2022; Sillén, 1967; Trapp-Müller et al., in press; Wallmann et al., 2023). Besides internal reaction-transport feedbacks that can self-accelerate or inhibit the weathering process (Du et al., 2022; Hellmann et al., 2012; Müller et al., 2022), the balance of dissolution and precipitation and nature of precipitate are sensitive to ambient physical and biogeochemical conditions (Aplin & Taylor, 2012; R. A. Berner, 1981; Hellmann et al., 2012; Wallmann et al., 2008). In marine sediments, ambient biogeochemistry is largely governed by the effects of organic matter degradation, availability of dissolved and particulate electron acceptors (R. A. Berner, 1981; Froelich et al., 1979; Soetaert et al., 1996) and degree of physical or biological disturbance (R. C. Aller, 1994; R. C. Aller & Wehrmann, 2025; Bao et al., 2018).

Dissimilatory Mn and Fe reduction (DMR and DIR, respectively) in muddy and organic-bearing ocean margin sediments, promote manganous and ferruginous conditions

that facilitate the formation of cation-rich 'green clays' (Aplin & Taylor, 2012; Michalopoulos & Aller, 2004; Odin, 1990). Green clay stabilities depend critically on the *local* redox potential, particularly Fe^{2+}/Fe^{3+} (Burst, 1958; Cloud, 1955) and are thus often associated with microenvironments (Baldermann et al., 2013; Odin & Morton, 1988), fluctuating redox conditions (R. A. Berner, 1981; Cloud, 1955; Michalopoulos & Aller, 2004), and partially ventilated, iron-rich surface sediments (Giresse et al., 2021; Giresse, 2022; K. Wang et al., 2015; B. Zhao et al., 2017). Moreover, glauconite forms in some deep-sea environments that receive sufficient organic matter to deplete O_2 and NO_3^-, but not all metal (oxy-)hydroxides (R. A. Berner, 1981; Cloud, 1955). In tropical deltaic muds, metal (oxy-)hydroxides are often supplied by rivers in excess and episodic reworking, re-oxidation, and mixing with marine-biogenic matter (figs. 1, 2) cause ferruginous conditions to dominate the depositional periods (R. C. Aller, 1998, 2004).

Protracted reworking and material exchange with adjacent shelf environments enhance both, suboxic organic matter degradation and silicate weathering rates, driving globally significant biogeochemical fluxes (R. C. Aller et al., 2008; R. C. Aller & Blair, 2006; Bao et al., 2018; Michalopoulos & Aller, 2004; Rahman et al., 2016). Because green clays are comparably cation-rich and often form from cation-depleted lateritic sediments and biogenic silica (bSi), these reaction balances are thought to host significant reverse weathering (Ku & Walter, 2003; Michalopoulos & Aller, 1995). However, these presumably reverse weathering balances are offset towards neutrality by coupled DIR and the common involvement of feldspar as a reactant (Michalopoulos & Aller, 1995; Wallmann et al., 2023).

Many shallow continental margin sediments off the highly energetic and frequently disturbed regions stabilize for years or decades rather than seasons, so that most iron is trapped in authigenic minerals, and sulfidic or methanic conditions can develop (R. C. Aller, 2004; R. A. Berner, 1980). Both, detrital and authigenic clays, eventually (re-)dissolve under anoxic conditions, possibly producing alkalinity and authigenic carbonate (Meister et al., 2022; Zhang & Tutolo, 2021). Silicate dissolution could represent a relevant source of iron to FeS_x, net increasing alkalinity while sequestering reduced sulfur and iron (Boudreau & Canfield, 1988). In methanic Black Sea sediments, plagioclase-to-smectite weathering releases Ca and Sr, but consumes Na, K, Li and B, resulting in an approximately alkalinity-neutral weathering flux (Aloisi et al., 2004). If local Ca release and alkalinity generation become substantial, inorganic calcite precipitation may be induced, recycling these components in addition to carbon storage (Caldeira, 1995; Torres et al., 2020). Such *in situ* carbonation represents a solid sink of local respiratory rather than atmospheric CO_2 (Torres et al., 2020; Wallmann et al., 2008, 2023), i.e., an organic-inorganic carbon sink switch, similar to organic phosphorous retention authigenic phosphate minerals (Ruttenberg, 1992). Forward and carbonate-forming marine silicate weathering seem to be very common in slope sediments, particularly in those influenced by volcanic activity (Hong et al., 2020; Middelburg, 1990; Torres et al., 2020; Wallmann et al., 2008, 2023). The development of a predictive reaction-solute speciation model that incorporates organic matter diagenesis, mineral authigenesis and silicate weathering allows us to disentangle the roles of individual reactants and biogeochemical conditions in shaping weathering balances, and to test these relationships based on comparison of thermodynamic and kinetic data with field observations.

3. METHODS

Weathering reaction balances reflect reactant supply, diagenetic redox zonation, and transport conditions associated with specific depositional environments. Here we emphasize reaction patterns within fine-grained sediment mixed layers that are typical of the topset facies (delta front, delta shelf facies) within many energetic subaqueous deltas and estuarine turbidity maximum zones. In the delta topset, mud layers of ~0.1–1 m thickness are episodically mobilized, exposed to oxygenated water, and re-deposited (R. C. Aller et al., 2008; Kuehl et al., 1986, 2019; McKee et al., 2004). The timescales of such deltaic reworking typically vary from tidal (daily) to interannual, affecting smaller and larger sediment volumes, respectively (Anthony et al., 2010; Kineke et al., 1996). Here we consider conditions affecting relatively thick layers of sediment (> 0.1 m) that stabilize for ~3–9 months between episodes of flood-induced reworking in the Amazon delta (Mackin et al., 1988).

In this context, we developed a time-dependent chemical batch model in which equilibrium aqueous solution chemistry and (non-equilibrium) sediment composition evolve dynamically in response to the kinetics of organic matter degradation and a set of inorganic dissolution and precipitation reactions, including silicates, carbonates, (oxy-)hydroxides, sulfides and phosphates (table 1), and exchange of adsorbed Na^+, K^+, Mg^{2+}, and Ca^{2+} for NH_4^+, Mn^{2+} and Fe^{2+} on bulk sediment surfaces. We define the model domain as the center of a thick and freshly deposited mud layer, where macrofauna are absent and the sediment can be considered a closed, unsteady batch reactor over the characteristic timescale of episodic deposition (R. C. Aller, 2004). Thus, transport-phenomena are not included. The model requires initial sediment composition, solution chemistry (assumed to be standard seawater at salinity 35 (Brown et al., 1995) with biologically depleted N(V) and P(V) concentrations, table S1) and porosity (constant, 0.8) as inputs. It generates reaction rates, chemical fluxes, evolving solution chemistry and particle composition.

Because aqueous speciation is typically much faster than particle-water interactions, we model equilibrium aqueous speciation, including pH and alkalinity, and mineral saturation indices, stepwise using the PHREEQC-COM module (Parkhurst & Appelo, 2013). This module allows scripting model scenarios, mass balances, kinetics, and sensitivity analyses in MATLAB R2023b (The MathWorks, Inc., 2023) using parallel computing for computational efficiency. Activity coefficients are determined at each timestep through specific ion interaction theory (sit.dat) (Giffaut et al., 2014)

Table 1. Overview of solid phases, their composition and kinetics, and sorption processes in the model. TST: Transition state theory (eq 12), PHA: simplified nucleation-growth rate following equation (13) ('Pham-Hellevang-Aagard'), TIP: phenomenological precipitation rate following equation (14) ('Tosca-Isson-Planavsky'), MB: Mass balance (see text), DIR: Dissimilatory iron reduction, DMR: Dissimilatory manganese reduction. Amz and Ice are the endmember scenarios based on either Amazon or Icelandic bulk river sediment composition (see text). For the Amazon clay, the unit formula was divided by two to be better comparable to the thermodynamic calibration of illite-Fe^{2+}. The adsorbed fractions were calculated by the relative thermodynamic preference relative to NH_4X (eq 5).

Phase/Process	Abr.	Unit formula	Amz wt%	Ice wt%	Dissolution/ Degradation/ Solute release	Precipitation/ Solute consumption
Quartz	Qtz	SiO_2	28	0	TST	-
Plagioclase	Plg	$Na_{0.4}Ca_{0.6}Al_{1.6}Si_{2.4}O_8$	4	21.799	TST	-
K-feldspar	Kfs	KAlSi3O8	5	0	TST	-
Pyroxene	Px	$Ca_{0.35}Mg_{0.42}Fe_{0.23}SiO_3$	0	12	TST	-
Olivine	Olv	$(Mg_{0.7}Fe_{0.3})_2SiO_4$	0	7	TST	-
Basaltic Glass	BsG	$SiAl_{0.36}Fe_{0.19}Mg_{0.28}Ca_{0.26}Na_{0.08}K_{0.008}O_{3.31}$	0	35	TST (Al, am SiO_2)	-
$Fe(OH)_3$	FeOH3	$Fe(OH)_3Al_{0.0083}Si_{0.0083}$	2.6	0.17	DIR +RC	first-order
MnO_2	MnO2	$MnO_2Al_{0.0083}Si_{0.0083}$	0.026	0.001	DMR + RC	-
$AlOH_3$	AlOH3	$Al(OH)_3$	1	0.1	MB	-
Opal-A	bSi	SiO_2	1	0.1	TST	-
Opal-CT	Opc	$(SiO_2)_{0.92}(H_2O)_{0.07}$ $(Na_2O)_{0.002}(K_2O)_{0.001}$ $(MgO)_{0.004}(CaO)_{0.003}$	0	1	TST	TIP or PHA
Kaolinite	Kao	$Al_2Si_2O_5(OH)_4$	24.444	0	TST	TIP or PHA
Montmorillonite	Mmt	$Na_{0.34}Mg_{0.34}Al_{1.66}Si_4O_{10}(OH)_2$	6	3	TST	TIP or PHA
Fe-rich mixed layer smectite	Smx	$Na_{0.409}K_{0.025}Ca_{0.009}(Si_{3.738}Al_{0.262})$ $(Al_{1.598}Mg_{0.214}Fe_{0.173}Fe_{0.035})O_{10}(OH)_2$	6	3	TST	TIP or PHA
Chlorite	Chl	$(Mg_{2.5}Fe_{2.5})\,Al_2Si_3O_{10}(OH)_8$	3	2	TST	TIP or PHA
Chrysotile	Cry	$Mg_3Si_2O_5(OH)_4$	0	2	TST	TIP or PHA
Illite	Ill	$K_{0.85}Al_{2.85}Si_{3.15}O_{10}(OH)_2$	19	2	TST	TIP or PHA
Glauconite	Glc	$K_{0.75}Mg_{0.25}Fe_{1.5}Al_{0.5}Si_{3.75}O_{10}(OH)_2$	0	0	TST	TIP or PHA
Amazon clay	Amz	$Na_{0.03}K_{0.48}Fe_{0.45}Mg_{0.195}Al_{2.4}Si_{3.25}O_{10}(OH)_2$	0	0	TST	TIP or PHA
Organic (terr.)	OmT	$[CH_1O_{0.2}][NH_3]_{7.1/84.8}$ $[H_2S]_{0.5/84.8}[H_3PO_4]_{7.6/84.8}$	0.5	0.5	first order TEA	-
Organic (mar.)	OmM	$[CH_{1.2}O_{0.31}][NH_3]_{12/106}$	0.3	0.3	first order TEA	-

Phase/Process	Abr.	Unit formula	Amz wt%	Ice wt%	Dissolution/ Degradation/ Solute release	Precipitation/ Solute consumption
		$[H_2S]_{0.4/106}[H_3PO_4]_{1/106}$				
Mackinawite	Mcw	FeS	0	0	first order	first order
Calcite	Cal	$CaCO_3$	0.1	10	Mixed order	higher order or PHA
Siderite	Sid	$FeCO_3$	0	0	first order	first order or PHA
Ankerite	Ank	$Ca_{0.5}Fe_{0.3}Mg_{0.15}Mn_{0.05}CO_3$	0	0	first order	first order or PHA
Kutnahorite	Ktn	$Ca_{0.5}Mn_{0.5}CO_3$	0	0	first order	first order or PHA
Apatite(-OH)	Hap	$Ca_5[PO_4]_3(OH)$	0.03	0.03	TST	first order
Vivianite	Vvt	$(Fe)_3(PO_4)_2\ 8H_2O$	0	0	TST	first order
NH_4^+ sorption		$NH_4^+ + \chi^- \leftrightarrow NH_4\chi$			fixed adsorbed fraction (0.5)	fixed adsorbed fraction (0.5)
Mn^{2+} sorption		$Mn^{2+} + 2\ \chi^- \leftrightarrow Mn\chi_2$			fixed adsorbed fraction (0.59)	fixed adsorbed fraction (0.59)
Fe^{2+} sorption		$Fe^{2+} + 2\ \chi^- \leftrightarrow Fe\chi_2$			fixed adsorbed fraction (0.55)	fixed adsorbed fraction (0.55)
Na^+ sorption		$Na^+ + \chi^- \leftrightarrow Na\chi$			47.9% charge compensation	47.9% charge compensation
Ca^{2+} sorption		$Ca^{2+} + 2\ \chi^- \leftrightarrow Ca\chi_2$			12.7% charge compensation	12.7% charge compensation
Mg^{2+} sorption		$Mg^{2+} + 2\ \chi^- \leftrightarrow Mg\chi_2$			31.0% charge compensation	31.0% charge compensation
K^+ sorption		$K^+ + 2\ \chi^- \leftrightarrow K\chi$			8.4% charge compensation	8.4 % charge compensation

to account for the high ionic strength of seawater. To complete the thermodynamic database for our purposes, pyroxene, olivine and basaltic glass were added from literature (Aradóttir, Sonnenthal, Björnsson, et al., 2012) and chrysotile from phreeqc.dat (Supplementary Data S1). For plagioclase and chlorite, reaction enthalpy and solubility constants were estimated by linear interpolation between Ca-Na and Mg-Fe endmembers, respectively, in sit.dat. A K-Si-rich Fe^{2+}-mica (10 Å basal spacing) forms in Amazon sediments (Michalopoulos & Aller, 1995, 2004), but we lack thermodynamic data for inclusion. Celadonite, a potential substitute, is rarely observed in nature, is significantly more cation-rich and remains largely undersaturated under the observed bulk porewater conditions, so that it cannot be used as an adequate alternative. Thus, we also included the 'Amazon clay' with the measured composition (Michalopoulos & Aller, 1995) and the thermodynamic data of Fe^{2+}-rich illite from (sit.dat). Reaction rates and solute fluxes of OM degradation and inorganic dissolution-precipitation are described by a variety of approaches and the resulting differential equations are 'stiff' (e.g., Boudreau, 1997; Hellevang et al., 2013) and solved at discrete timesteps (0.056 days ~80 min), referenced to the composition at the previous timestep. The timestep was chosen to avoid negative concentration errors and facilitate computational efficiency. Stepwise amounts of solid phases and dissolved species (M = mol per liter solution) are then added or removed to/from the previous sediment (in MATLAB) and solution (*via* REACTION keyword in PHREEQC)) after a fraction of the NH_4^+, Mn^{2+} and Fe^{2+} fluxes are exchanged for Na^+, K^+, Mg^{2+}, and Ca^{2+} at surface sites. Thus, the mass balances for total molar concentration (M) of dissolved element C (and each oxidation state separately for redox-sensitive elements) at each timestep (dt) are given by:

$$\frac{d[C]}{dt} = \sum_{i}^{P} R_i \nu_{C,i} dt - F_{sorp} \quad (4)$$

P is the number of solid phases i considered in the model, t is the time (yr), R_i is the reaction rate (M/yr, i.e., normalized to one liter of solution (porewater) for all kinetic reactions) with respect to the solid i (dissolution/degradation: $R < 0$, precipitation: $R > 0$) and $\nu_{C,i}$ the stoichiometric coefficient (molar fraction) of element C in solid i. The sorption fluxes (F_{sorp}) of NH_4^+, Mn^{2+} and Fe^{2+} scale directly with the corresponding particle-water fluxes by a constant adsorbed fraction of C ($K_{\chi,C} = C\chi_q/C$, where χ is an adsorption site and q the cation charge) that is observationally constrained to ~0.5 for NH_4^+ (calculated from 1.3 µmol/g/M (Mackin & Aller, 1984a) assuming a porosity of 0.8 and sediment density of 2.7 g/cm^3) and calculated for Mn^{2+} (0.55) and Fe^{2+} (0.59) by rearranging mass action laws, reflecting relative thermodynamic preferences:

$$\frac{C\chi_2}{C} = \frac{\left(K_{NH_4^+}\right)^2}{K_C} \left(\frac{NH_4^+}{NH_4\chi}\right)^2 \quad (5)$$

The thermodynamic constants ($K_{\chi,C}$) and reaction stoichiometries are taken from phreeqc.dat. Our calculated values for $K_{\chi,Mn}$ are somewhat higher than available field-based estimates from Skagerrak sediments (~0.1–0.01 µmol/g/M) (Canfield et al., 1993). These sorption fluxes are charge balanced by Na^+, K^+, Mg^{2+}, and Ca^{2+} fluxes in equivalent fractions corresponding to seawater-equilibrated clays (Sayles & Mangelsdorf, 1977). This simplified, phenomenological treatment assumes unbounded availability of sorption sites and exchangeable Ca^{2+} and Na^+, but does not require numerical solutions, improving model efficiency. Sorption is also implicit in the choice of exchangeable cation in the (charge-balanced) composition of smectites (montmorillonite and mixed-layer smectite). Moreover, $Fe(OH)_3$ includes small amounts of Si and Al (Mackin & Aller, 1984c) (table 1). For particles, mass balances are given by:

$$\frac{dX_i}{dt} = R_i + \sum_{j}^{P(\neq i)} R_j \nu_{i,j} dt \quad (6)$$

X_i (mol/L) is the molar concentration of i and j is another solid phase that directly affects i during its reaction, which applies only to MnO_2 and $Fe(OH)_3$ through anaerobic respiration and to $Al(OH)_3$ through clays. Because porosity is fixed, the total volume of sediment and solution are both conserved, while solid composition is updated at each timestep by considering individual molar mass changes and normalizing to the given total solid phase volume. Mass changes of solid phases are rather small in this study (< 1 wt%) so that these simplifications (fixed porosity) do not significantly affect our results and conclusions. The carbonate assemblage (calcite, kutnahorite, ankerite, siderite, table 1) was chosen according to observations from the Amazon delta and elsewhere (R. C. Aller & Wehrmann, 2025; Mucci, 2004; Z. Zhu et al., 2002). The clay assemblage was limited to a minimum set that resembles the most common authigenic clays found at continental margins: kaolinite, smectites (dioctahedral montmorillonite and Fe-rich mixed-layer smectite, micas (illite, glauconite, Amazon clay), chlorite and serpentine (chrysotile) (Aplin & Taylor, 2012; Baldermann et al., 2013; Burdige, 2006; Giresse, 2022; Michalopoulos & Aller, 2004; Müller, 1967; Rude & Aller, 1989; Worden & Burley, 2003). We did not include generally undersaturated authigenic clays (e.g., berthierine or cronstedtite) and extremely supersaturated Mg-clays, such as saponite and sudoite (> 10^3–10^5 times in the initial Si-poor solution, calculation not shown) that are rather rarely observed in shelf sediments (Aplin & Taylor, 2012; Müller, 1967; Odin, 1990). Note that possible effects of sudoite- and saponite-like (Mg-rich) clays on reaction balances are largely covered by chlorite and chrysotile. The two most common diagenetic phosphates, apatite and vivianite were included (Egger, Jilbert, et al., 2015; R. A. Jahnke et al., 1983; M. Zhao et al., 2020). Solid solutions are not considered here for simplicity, although they are likely (Mackin, 1986; Middelburg et al., 1987). All kinetic rate laws used are detailed in sections 3.1–3.4, section 3.5 gives an overview over the model scenarios, and section 3.6 describes the sensitivity analysis. Parameter values, references and assumed properties of individual solid phases (density, specific surface area, molar mass, stoichiometry, and reference names in our modified database) are provided in tables 1–2 and S1–S2, and Supplementary Data S1. Model codes are available from the corresponding author upon request.

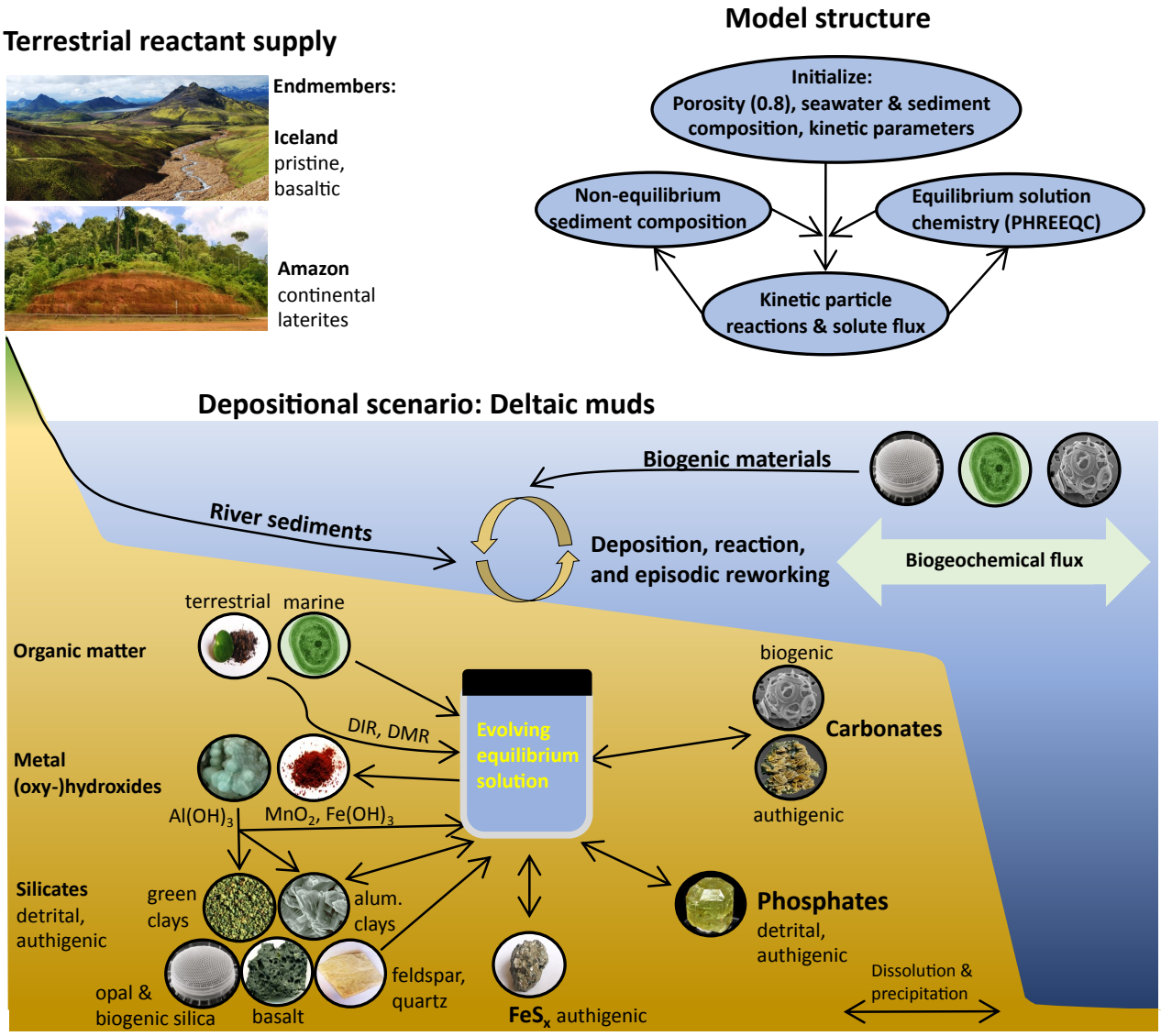

Figure 2. Conceptual model of marine and terrestrial particle mixing and the batch reaction mode of mobile mud belts, and how different detrital, biogenic and authigenic phases interact through an evolving batch solution. Individual processes are discussed in the text, parametrization and equations involved are summarized in the Methods section. Note that FeS_x is represented by FeS only in the model. DIR: Dissimilatory iron reduction, DMR: Dissimilatory manganese reduction. $Al(OH)_3$ is directly consumed by clay authigenesis and maintains a steady state Al concentration in solution (through a mass balance approach). The landscape images from Iceland (Petr Broz) and French Guiana (Claude Maisch), and images of the cyanobacteria, diatom (CSIRO), apatite and $Al(OH)_3$ (Rob Lavinsky) are publicly available under a Creative Commons Attribution-Share Alike 3.0 Unported license (https://creativecommons.org/licenses/by-sa/3.0/deed.en), the coccolith ("NEON_ja") under Attribution-Share Alike 2.5 Generic (https://creativecommons.org/licenses/by-sa/2.5/deed.en), the vesicular olivine basalt (James St. John) under Attribution -2.0 Generic (https://creativecommons.org/licenses/by/2.0/deed.en), and siderite (Didier Descouens) under Attribution-Share Alike 4.0 International (https://creativecommons.org/licenses/by-sa/4.0/deed.en).). The other images are public domain and made by the authors.

3.1. Organic matter degradation

Microbial organic matter oxidation and fermentation were described using a simple 2-G approach (two reactivity pools), differentiating labile marine ($k_{OM,M}$ ~0.7 yr^{-1} (R. C. Aller et al., 1996; R. C. Aller & Blair, 2006)) and refractory terrestrial (low reactivity, $k_{OM,T}$ = 0.1 $k_{OM,M}$, arbitrary slower) organic matter with slightly different composition (table 1, Supplementary Data S1). OM degradation was partitioned along the characteristic succession of terminal electron acceptor using formulations of established diagenetic models (table S2: Boudreau, 1996; Van Cappellen & Wang, 1996):

$$R_{OM,G} = \sum_{TEA}^{N_{TEA}} k_{OM,G} X_{OM,G} f(TEA) \qquad (7)$$

where $X_{OM,G}$ is the molar concentration (M) of the respective particulate organic matter pool G. *f(TEA)* is one or a sum of Monod-type and inhibition term(s) related to a specific metabolic pathway (Boudreau, 1996) (table S2). Parameter values were taken from (Boudreau, 1996) without alterations, and initial tests demonstrated that these parameters have little effects. However, here we refer to the 'reactive' fraction of residual MnO_2 and $Fe(OH)_3$, which is calculated similar to a reactive continuum approach (Postma, 1993): $(X_i/X_{i,0})_r = (X_i/X_{i,0})^\gamma$. In the absence of reasonable constraints, a wide range of values for γ (1–750) were tested. In addition, sulfate-mediated anaerobic oxidation of methane (AOM) was included (Martens & Berner, 1977; Y. Wang & Van Cappellen, 1996).

3.2. Inorganic reactions from established diagenetic models

Reduced metabolites from OM degradation may react to form carbonate, sulfide, or phosphate minerals, or be re-oxidized. Because re-oxidized Fe^{3+} rapidly (minutes) precipitates as $Fe(OH)_3$ upon oxidation (Stumm & Morgan, 2013), Fe^{3+} is 'scavenged' in the model with a rate constant of 0.25 yr^{-1} ($R_{p,Fe(OH)3}$ in M/yr, (Raiswell & Canfield, 2012))

$$R_{Fe(OH)_3} = 0.25\left[Fe^{3+}_{tot}\right] \quad (8)$$

Dissolution of $Fe(OH)_3$ and MnO_2 proceeds solely *via* dissimilatory manganese and iron reduction (DMR and DIR, respectively) in our model. Dissolution (R_d, M/yr) and precipitation rates (R_p, M/yr) of carbonates and sulfides (Van Cappellen & Wang, 1996), and precipitation of phosphates (M. Zhao et al., 2020) and opal-CT (cf. Khalil et al., 2007), were described by first-order ($p = q = 1$) kinetics with respect to the specific mineral saturation state Ω (with mineral subscript, dropped for simplicity in equations but implied in reactant-product sets), except calcite, which follows variable orders of dissolution (depending on Ω_{cal}) and high order during precipitation (Sulpis et al., 2022).

$$\Omega = \frac{\prod_C^{N_C}\{C\}^{\nu_C}}{K_{SP}} \quad (9)$$

$$R_d = k_d X(1-\Omega)^p \quad (10)$$

$$R_p = k_p(1-\Omega)^q \quad (11)$$

{C} is the activity of a solute *C*, N_c the total number of solutes, and K_{SP}, k_d and k_p are the particle-specific solubility constant (subscripts dropped here for simplicity), dissolution constant (yr^{-1}) and precipitation constant (M/yr) of the particle in question (assuming $\{X_i\}= 1$). In our time-evolving model runs, Ω values vary widely, from strong undersaturation to supersaturation for most phases included. The initial parameters were chosen according to experiments and field observations (Sulpis et al., 2022; Y. Wang & Van Cappellen, 1996; M. Zhao et al., 2020; Supplementary Data S1) and were then scaled to approximate the observations from the Amazon delta (section 3.6).

3.3. Dissolution and transition state theory

Silicate dissolution kinetics were described by 'linear' transition state theory (TST) (Aagaard & Helgeson, 1982; Hellevang et al., 2013; Heřmanská et al., 2022, 2023):

$$R_{TST} = RSA\sum_m^{N_m} A_m e^{\frac{-E_{a,m}}{RT}}\prod_C^{N_C}\{C\}^{n,c}(1-\Omega) \quad (12)$$

where RSA is the reactive and accessible surface area of a particle relative to solution volume (m^2/L), commonly approximated by geometric constraints or by gas adsorption techniques and a unitless correction factor (Heřmanská et al., 2022; Marty et al., 2015; Wallmann et al., 2023). Here we calculated *bulk* surface areas from individual mineral volumes using densities (g/m^3) and gas adsorption-measured specific surface areas (m^2/g, Supplementary Data S1). Estimating the reactivity and accessibility of the so calculated surfaces is a long-standing and unsolved problem in geosciences and chemistry. RSA estimates are complicated by its time and scale dependence, and by textural relationships, but is commonly accounted for by applying a (unitless) correction factor in the order of $0.1–10^{-5}$ (e.g., Beckingham et al., 2017; Maher et al., 2006; Schnoor, 1990; White & Brantley, 2003). Consistent with the theoretical and observational constraints of comparably high reaction rates in marine settings (Geilert et al., 2023; Gruber et al., 2019; Michalopoulos & Aller, 1995; Wallmann et al., 2023), we chose a relatively high factor of 0.1, i.e., 10 % of the bulk surface area of a given mineral is assumed to be reactive at the relevant timescales (except bSi, which is assumed to be twice as reactive as abiotic opal-A, table 2). $A_m e^{\frac{-E_{a,m}}{RT}}$ is an Arrhenius term (A_m: Arrhenius constant (mol/$m^{-2}yr^{-1}$), $E_{a,m}$: apparent activation energy of m (J/mol), R: universal gas constant ($Jmol^{-1}K^{-1}$), T: absolute temperature (K)) describing the temperature dependence of reaction mechanism m. $E_{a,m}$ reflects the energetic barrier to dissolution and regulates the temperature dependence of the dissolution rate. While incorporated in the model, temperature (27°C) was not varied, because activation energies were not available for all precipitation rates considered. $\{C\}^{n,c}$ reflects a dependence of mechanism *m* on the molar activity of species C (here exclusively $\{H^+\}$, except for basaltic glass which is inhibited by dissolved Al) of order *n*. For vivianite, quartz, pyroxene and glauconite, no parameters for base-catalyzed dissolution (at high pH) and no parameters for neutral olivine and opal-CT dissolution were available (Heřmanská et al., 2022, 2023). However, the range of modelled pH values is comparably small (~7–8) so that the induced inaccuracy is rather limited. Dissolution of phosphates was also described in this way, although neither apatite nor vivianite dissolved under the modeled conditions.

TST has been criticized for its mechanistic inaccuracy (Müller et al., 2022; Truesdale & Greenwood, 2015), especially when dealing with mass transport-controlled reactions (R. A. Berner, 1980; Ruiz-Agudo et al., 2016), metastable substances (Müller et al., 2022) or complex textural relationships (Altree-Williams et al., 2015; Hellmann et al., 2012; Müller et al., 2022). For example, basaltic glass forms through rapid cooling of high temperature melts so that no actual equilibrium with the solution can exist. Thus, basaltic glass can dissolve independently from its 'saturation state'. However, glass dissolution in our model ceases as amorphous silica becomes saturated. Despite all these pitfalls, currently available TST calibrations docu-

Table 2. Overview of kinetic parameters that result in porewater concentrations and reaction rates resembling porewater observations. RC: reactive continuum exponent, f[]: first-order coefficient with respect to the bracketed value, κ_1: linear scaling factor for TIP approach, m: linear scaling factor for mixed rate law approach of (Sulpis et al., 2022). Dimensionless dissolution factors are linear surface scaling factors for TST and growth rate laws (i.e., reflecting the roughness and reactivity surface area). Asterisks mark values for which comparison to literature values is problematic: For RC, context differs substantially from the original formulation, for k_g reactive surface area estimates may impede quantitative comparison. Moreover, many of the literature values have been applied to different ambient conditions, thermodynamics databases, and phase assemblages, further complicating comparisons.

Phase	Dissolution factor (first-order, TST, RC*) [literature range]	Precipitation factor (first-order, mixed, κ_1) [literature range]	Ω_{crit}	k_N*	k_g*	Γ [literature range]
Qtz	0.1 (TST) [10^{-5}–10^{-1}]	-	-	-	-	-
Plg	0.1 (TST) [10^{-5}–10^{-1}]	-	-	-	-	-
Kfs	0.1 (TST) [10^{-5}–10^{-1}]	-	-	-	-	-
Px	0.1 (TST) [10^{-5}–10^{-1}]	-	-	-	-	-
Olv	0.1 (TST) [10^{-5}–10^{-1}]	-	-	-	-	-
BsG	0.1 (TST) [10^{-5}–10^{-1}]	-	-	-	-	-
$Fe(OH)_3$	115 (RC) [1.1–4.7]*	0.25 yr^{-1} (f[Fe^{3+}]) [0.25]	-	-	-	-
MnO_2	115 (RC) [as FeOH3]*	-	-	-	-	-
$AlOH_3$	1 (RC) [-]	-	-	-	-	-
bSi	2.0 (TST) [-]	-	-	-	-	-
Opc	0.1 (TST) [10^{-5}–10^{-1}]	0.1 Myr^{-1} (f[Ω_{Opc}]) [-]	-	10^{-3} (M/s) [1]	1.4 10^{-26} (M/m^2s) [1.4 10^{-13}]	10^6 [1 - 3 10^{10}]
Kao	0.1 (TST) [10^{-5}–10^{-1}]	1 (κ_1) [1]	10^8 [-]	10^{-9} (M/s) [1]	5.8 10^{-28} (M/m^2s) [5.8 10^{-15}]	2 10^{10} [1 - 3 10^{10}]
Mmt	0.1 (TST) [10^{-5}–10^{-1}]	0.1 (κ_1) [1]	10^7 [-]	10^{-9} (M/s) [1]	2.2 10^{-28} (M/m^2s) [2.2 10^{-15}]	3 10^{10} [1 - 3 10^{10}]
Smx	0.1 (TST) [10^{-5}–10^{-1}]	2 (κ_1) [1]	10^6 [-]	10^{-9} (M/s) [1]	2.2 10^{-28} (M/m^2s) [Mmt]	3 10^9 [1 - 3 10^{10}]
Chl	0.1 (TST) [10^{-5}–10^{-1}]	30 (κ_1) [1]	10^5 [-]	10^{-9} (M/s) [1]	2.2 10^{-28} (M/m^2s) [Mmt]	7 10^9 [1 - 3 10^{10}]
Cry	0.1 (TST) [10^{-5}–10^{-1}]	0.1 (κ_1) [1]	10^6 [-]	10^{-9} (M/s) [1]	2.2 10^{-28} (M/m^2s) [Mmt]	1 10^{10} [1 - 3 10^{10}]
Ill	0.1 (TST) [10^{-5}–10^{-1}]	30 (κ_1) [1]	10^6 [-]	10^{-9} (M/s) [1]	6.2 10^{-29} (M/m^2s) [6.2 10^{-16}]	5 10^9 [1 - 3 10^{10}]
Glc	0.1 (TST) [10^{-5}–10^{-1}]	1 (κ_1) [1]	10^6 [-]	10^{-9} (M/s) [1]	6.2 10^{-29} (M/m^2s) [Ill]	1 10^9 [1 - 3 10^{10}]

Phase	**Dissolution factor (first-order, TST, RC*) [literature range]**	**Precipitation factor (first-order, mixed, κ_1) [literature range]**	**Ω_{crit}**	**k_N***	**k_g***	**Γ [literature range]**
Amz	0.1 (TST) [10^{-5}–10^{-1}]	75 (κ_1) [1]	10^8 [-]	10^{-1} (M/s) [1]	6.2 10^{-29} (M/m^2s) [III]	10 10^{10} [1 - 3 10^{10}]
OmT	0.07 yr^{-1} (f[OM]) [0.1 – 0.001 k_{OmM}]	-	-	-	-	-
OmM	0.7 yr^{-1} (f[OM]) [0.2 – 0.66]	-	-	-	-	-
Mcw	10^{-3} yr^{-1} (f) [10^{-3}]	5 10^{-5} Myr^{-1} (f[Ω_{Mcw}]) [1.5 10^{-5}]	-	-	-	-
Cal	0.1 yr^{-1} (f) [1]	5 10^{-5} Myr^{-1} (m[Ω_{Cal}]) [1]	-	7.5 10^{-4} (M/s) [1]	10^{-16} (M/m^2s)	0.25 10^{10} [2 - 4 10^{10}]
Sid	0.1 yr^{-1} (f) [0.1]	5 10^{-5} Myr^{-1} (f[Ω_{Sid}]) [< 10^{-2}–4.5 10^{-5}]	-	5 10^{-7} (M/s) [1]	1.6 10^{-17} (M/m^2s) [1.6 10^{-17}–4.5 10^{-25}]	0.35 10^{10} [2 - 4 10^{10}]
Ank	0.1 yr^{-1} (f) [0.1]	1 10^{-6} M/yr^{-1} (f[Ω_{Ank}]) [< 10^{-2}–4.5 10^{-5}]		5 10^{-7} (M/s) [1]	1.6 10^{-17} (M/m^2s) [1.6 10^{-17}–4.5 10^{-25}]	0.7 10^{10} [2 - 4 10^{10}]
Ktn	0.1 yr^{-1} (f) [0.1]	5 10^{-5} M/yr^{-1} (f[Ω_{Ktn}]) [< 10^{-2}–4.5 10^{-5}]	-	2.5 10^{-7} (M/s) [1]	1.6 10^{-17} (M/m^2s) [1.6 10^{-17}–4.5 10^{-25}]	0.4 10^{10} [2 - 4 10^{10}]
Hap	0.1 (TST) [10^{-5}–10^{-1}]	2.7 10^{-11} M/yr^{-1} (f[Ω_{Hap}]) [2.7 10^{-8}]	-	-	-	-
Vvt	0.1 (TST) [10^{-5}–10^{-1}]	2.7 10^{-8} M/yr^{-1} (f[Ω_{Vvt}]) [2.7 10^{-8}]	-	-	-	-

ment the relative reactivities of different substances and their relationships to solution chemistry and temperature from a plethora of experiments conducted over decades (Aradóttir, Sonnenthal, & Jónsson, 2012; Heřmanská et al., 2022; Velbel, 1993). To date, TST-calibrated databases provide the only compilation of silicate dissolution kinetics across a wide range of settings and materials, and represent today's standard in geoscientific and mineralogical research (Heřmanská et al., 2022; Palandri & Kharaka, 2004). Therefore, we use these TST rate laws to represent silicate and phosphate dissolution kinetics in our model.

3.4. Precipitation

Nucleation rather than growth may determine the overall precipitation rate during diagenesis (Wilkinson, 2015) and there is a 'critical supersaturation' at which stable authigenic nuclei can be formed (Kashchiev, 2011; Kashchiev & van Rosmalen, 2003), so that extension of TST towards supersaturation leads to extreme overestimation of precipitation rates (Hellevang et al., 2013). Thus, two different approaches to clay precipitation were tested: (I) a mechanistic, theory-based nucleation-growth law (Pham-Hellevang-Aagard, PHA) (Hellevang et al., 2013; Pham et al., 2011) and (II) a phenomenological Si-limited, pH-dependent composite batch rate law (Tosca-Isson-Planavsky, TIP) (Isson & Planavsky, 2018; Tosca et al., 2016). The PHA approach was also applied to carbonate precipitation, for which it has been tested successfully (Pham et al., 2011), while carbonates precipitate according to equation (11) in the TIP setup (table 1).

3.4.1. Nucleation-growth (PHA)

The PHA approach is based on a simplified form of classical nucleation theory combined with dislocation-controlled growth (Burton et al., 1949; Hellevang et al., 2013; Pham et al., 2011) and an additional term for $Al(OH)_3$-limitation of Al-bearing clays (all except chrysotile) ($r_{Al(OH)3}$, unitless, see 'Al dynamics' below):

$$R_{PHA} = \left(k_g RSA(\Omega-1)^2 + k_N e^{\left(-\Gamma\left(\frac{1}{T^{1.5}\ln(\Omega)}\right)^2\right)}\right) r_{Al(OH)_3} \quad (13)$$

where k_g is the growth constant (M $m^{-2}yr^{-1}$), k_N the nucleation rate (M/yr) and Γ a functional factor that lumps together molar volume, a shape factor, and surface tensions of substrate and precipitate (Hellevang et al., 2013). While values of k_g are available from seeded growth experiments (Marty et al., 2015; Yang & Steefel, 2008), k_N and Γ are essentially unknown for most substances and situations, but experiments and sensitivity analyses indicate that Γ ~1–3 * 10^{10} for most clays, carbonates and opal (Hellevang et al., 2013). Although they allow for first order constraints on how variation of saturation during diagenesis drives precipitation dynamics, equation (13) does not directly reflect Si-limitation or pH-dependent kinetics (as opposed to indirect effects via Ω), which may be essential to marine and diagenetic weathering (Ehlert et al., 2016; Isson & Planavsky, 2018; Loucaides et al., 2010; Michalopoulos & Aller, 2004; Tosca et al., 2016; Tosca & Masterson, 2014).

3.4.2. Phenomenological silicate precipitation law (TIP): Si-limitation & pH-dependence

In addition to classical nucleation theory, we develop a novel, phenomenological silicate precipitation rate law that is based on previous studies of clay formation and reverse weathering (Isson & Planavsky, 2018; Tosca et al., 2016). This approach uses data from unseeded, anoxic batch experiments of homogeneously nucleated greenalite precipitation (Tosca et al., 2016) to empirically derive a batch precipitation rate law solely dependent on pH (note logarithmic scale) and dissolved Si concentration (Isson & Planavsky, 2018):

$$\begin{aligned} R_{TIP,max} &= k_{TIP}(pH)\left([Si] - [Si]_{as}(pH)\right) \\ &= 1.01\ 10^{-19}\ pH^{22.4}\left([Si] - 2.02^{-5.57pH}\right) \end{aligned} \quad (14)$$

where $k_{TIP}(pH)$ (in yr^{-1}) is a pH-dependent constant and $[Si]_{as}(pH)$ (in M) is a pH-dependent 'asymptotic' (low) Si concentration at which precipitation ceases. Although critiqued for its extreme pH dependence (Krissansen-Totton & Catling, 2020), this approach allows scaling of clay authigenesis directly to Si dynamics, while providing an upper limit of the pH-effect of OM diagenesis on silicate weathering. However, this rate law does not take mineral saturation states (Ω, eq 9) into account, i.e., if a driving force exists. Hence, it is strictly only applicable to systems that are *a priori* supersaturated enough to facilitate nucleation (Ω >> *10*) and to the clay formed in the original experiments (greenalite). To be able to apply this rate law to different phases and conditions, we extended this empirical law by a critical saturation value and a *tangens hyperbolicus* term:

$$R_{TIP} = R_{TIP,max}\kappa_1 \tanh\left(\frac{\kappa_2 \frac{\Omega}{\Omega_{crit}}}{R_{TIP,max}}\right) r_{Al(OH)_3} \quad (15)$$

Similar to the PHA approach, $r_{Al(OH)3}$ is a factor for $Al(OH)_3$-limitation (see below), κ_1 is a unitless scaling coefficient, and the factor κ_2 (in M/yr) governs the dependence on saturation and ensures that the argument of the hyperbolic function becomes dimensionless. Given excess $Al(OH)_3$ or dissolved Al (e.g., from feldspar dissolution): At high supersaturation $\frac{\Omega}{\Omega_{crit}} \gg 1$, the hyperbolic function yields 1, essentially representing $R_{TIP,max}$ (Isson & Planavsky, 2018; Tosca et al., 2016). This reflects an excess in driving force and rapid, pH-dependent reaction kinetics, so that the reaction becomes limited by the supply of Si to the site of precipitation via transport and coupled reactions (e.g., bSi or feldspar dissolution). At low supersaturation $\frac{\Omega}{\Omega_{crit}} \ll 1$, the hyperbolic function yields $\left(\frac{\kappa_2 \frac{\Omega}{\Omega_{crit}}}{R_{TIP,max}}\right)$, so that the rate becomes linearly dependent on supersaturation level $\left(\kappa_1\kappa_2 \frac{\Omega}{\Omega_{crit}}\right)$, hence on the chemical activity of its compounds and the resulting thermodynamic driving force. The rate becomes negligibly slow at low supersaturation $\frac{\Omega}{\Omega_{crit}} <\sim 10^{-5}$. Values for Ω_{crit} in the range of 10^6 to 10^9 were applied to the various secondary silicates, so that values of Ω between 10 and 10^4 are required to initiate quantitatively significant precipitation (table 2). Comparable composite rate laws have been introduced to address the observation of different dissolution mechanisms operating at different distances from equilibrium (Burton et al.,

1949; Lasaga & Luttge, 2001; Sulpis et al., 2022). Similar to k_N and Γ, κ_1 and Ω_{crit} were scaled to observations from the Amazon delta and to induce competition among potential secondary silicates, while κ_2 was held constant at 1 M/yr.

3.4.3. Aluminum dynamics and limiting concentrations

Resolving these ~ mM/yr major cation fluxes with an accuracy that complies with maximum Al concentrations of a few hundred nM is numerically (and analytically) challenging (Maher et al., 2006; Meister et al., 2022). Moreover, supply *via* dissolution of most detrital silicates, including plagioclase (Wallmann et al., 2023), is comparably slow (observations in the order of ~10–100 µM/yr), so that an additional, highly reactive source (and/or limit) of Al may be required to sustain authigenesis as inferred from Amazon delta porewater chemistry (Mackin, 1986; Michalopoulos & Aller, 2004). Besides Fe-Mn hydroxide-related Al (Mackin & Aller, 1984b), detrital Al-hydroxide (e.g., gibbsite, boehmite or amorphous) and/or (nanoparticulate) amorphous Al(-Si-Fe) phase(s) are alternative and potentially large sources of Al, mainly supplied via terrestrial weathering and subsequent erosion (e.g., Aplin & Taylor, 2012; Loucaides et al., 2010; Tsukimura et al., 2021). Detrital quartz and feldspar grains are often coated by clays and metal (oxy-)hydroxides that contain several weight percent of Al, depending on iron mineralogy (cf., Gibbs, 1973; Schwertmann & Taylor, 1989) and eventually inhibit the dissolution of the underlying grains (Beckingham et al., 2017). While amorphous nanoparticles are nearly invisible to many conventional techniques (Tsukimura et al., 2021), a more readily detectable, crystalline form of $Al(OH)_3$, gibbsite, seems common in some of the southern lowland tributaries of the Amazon river (Gibbs, 1967). Thus, we introduce minor amounts (⩽ 1 wt%, near the detection limit of crystalline silicates in standard X-ray diffractometry) of $Al(OH)_3$, the dissolution rate (R_{Al} [M Al/yr]) of which is constrained by a mass balance based on an empirical relationship between dissolved Al, Si and pH that appears to be widely applicable in mobile mud settings—strictly at pH > 7.3 and low 'dissolved' organic matter concentrations (see Mackin, 1986; Mackin & Aller, 1984c):

$$\begin{aligned}[Al]_{MA} &= 10^{-(13.98-0.828\{H^+\}-0.429[Si])} \\ &= [Al] - R_{Al}dt - \sum_{i}^{N_{sil}} R_i \nu_{Al,i} dt \leftrightarrow R_{Al}dt \\ &= \left([Al]_{MA} - [Al] + \sum_{i}^{N_{sil}} R_i \nu_{Al,i} dt \right)\end{aligned} \quad (16)$$

where $[Al]_{MA}$ is the predicted dissolved concentration (Mackin & Aller, 1986). Strictly speaking, $[Al]_{MA}$ predictions are not corrected for log-transformation bias. Because of the good quality of the fit, standard deviation of residuals should be small so that the correction factor is close to 1. Thus, the error introduced is a constant offset to lower values in the order of a few % (i.e., at pM levels) and its influence on reaction patterns can be neglected given the many approximations and scaling procedures involved. Because limited supply of this particulate Al-source may restrict maximum precipitation rates, $r_{Al(OH)3}$ (= $X_{Al(OH)3}/(X_{Al(OH)3})_0$) was introduced as a limiting factor for Al-clay precipitation in both, PHA and TIP rate laws (eqs 12, and 14).

Note that '$Al(OH)_3$' here represents an idealized model-phase, whose the composition and properties in nature are not very well defined. The various Al-sources (e.g., crustal aluminosilicates, clays and Al-Fe-Mn (oxy-)hydroxides, coatings) and their relative contribution to clay authigenesis and alkalinity cycling require more analytical in-depth research. Comparable, but less dynamic approaches have been implemented into previous diagenetic models to tackle a similar problem and a lack of measurements (Maher et al., 2006; Meister et al., 2022). The approach and parameter values are strictly only valid at pH > 7.3 and in Amazon delta-like sediments with relatively low Fe^{2+} concentrations (Mackin, 1986; Mackin & Aller, 1986), possibly affecting aluminosilicate saturation under various conditions. If Al is not excessively consumed, it is allowed to deviate from this relationship, i.e., it can rise if aluminosilicate dissolution fluxes exceed those of clay formation. Moreover, if consumption at the calculated reaction rate of any phase would exceed the dissolved reservoir, it is set to 10% of that solute concentration, resembling concentration-limited precipitation similar to $R_{Fe(OH)3}$ (e.g., glauconite may become limited by Fe^{3+} under deeply ferruginous, Si-rich conditions) and preventing negative concentration errors.

3.5. Scenarios and strategy

We modeled two primary scenarios which represent time evolution of realistic end-member reactant mixtures: (I) a mobile mud layer at the Amazon delta topset facies (Amz) that incorporates pre-weathered terrigenous sediment (largely clay, quartz, Mn-Fe (oxy-)hydroxides and smaller amounts of feldspar), marine organic matter, and biogenic silica, and (II) a comparably un-weathered, mafic sediment approximating Icelandic rivers in a similar depositional setting (Ice) (fig. 2, table 1). These model end-members were complemented by additional intermediate scenarios and a sensitivity analysis. Only input sediment concentrations were adjusted in these scenarios, all other parameters were kept constant and both model setups (TIP & PHA, table 1) were applied to each scenario.

First, we model a mobile mud layer at the Amazon delta topset facies (Amz) that stabilizes for a characteristic timescale of ~6 months (McKee et al., 2004). The input sediment composition approximates observations from Amazon River and delta sediments (table 1) (R. C. Aller et al., 1996; Gibbs, 1967; Michalopoulos & Aller, 2004; Poulton & Raiswell, 2002; Rousseau et al., 2019). The resulting rates and porewater concentrations were compared to some of the most detailed studies on mobile mud diagenesis and clay authigenesis conducted so far (R. C. Aller et al., 1996; R. C. Aller & Blair, 2006; Mackin & Aller, 1986; Michalopoulos et al., 2000; Michalopoulos & Aller, 1995, 2004; Rude & Aller, 1989; Spiegel et al., 2021; Wallmann et al., 2023; Z. Zhu et al., 2002). Kinetic constants were first initialized within the range of published values (table 2)

and then adjusted manually (within an order of magnitude, table 2) to match the observed porewater concentrations and estimated reaction rates in the Amazon delta topset facies.

A (pseudo-)first-order rate constant with respect to organic matter (OM) degradation was taken from literature (R. C. Aller et al., 1996; R. C. Aller & Blair, 2006), and MnO_2 and $FeOH_3$ reactivity coefficients were adjusted to roughly match Mn^{2+} and Fe^{2+} concentrations and facilitate sustained ferruginous conditions in the Amz scenario. Silicate dissolution kinetics were then scaled using a (high) surface reactivity constant (0.1) that is common to all silicates, preserving relative reactivities except for bSi, to account for the complex shapes and highly reactive surfaces of fresh biogenic silica compared to pre-weathered and abiotic amorphous silica (Van Cappellen et al., 2002). A reactivity scaling factor of two for bSi dissolution was required to harmonize relatively stable, sub-millimolar Si concentrations with net K and Mg consumption at a ~ mM/yr scale later on. Carbonate, phosphate and sulfide dissolution were practically irrelevant and have not been scaled. Carbonate precipitation was scaled to match observed dissolved inorganic carbon (DIC) and Mn concentrations at the given OM degradation rate, and facilitate competition among the various carbonate minerals. First order (with respect to saturation) carbonate precipitation constants are about an order of magnitude lower than in previous diagenetic models (Y. Wang & Van Cappellen, 1996), possibly due to the higher number of carbonates included (four instead of two) and different thermodynamic databases used. First order (with respect to saturation) phosphate precipitation rates constants were decreased by a factor 0.01 relative to literature values (of carbonate-fluor apatite), preventing negative P concentration errors and facilitating P storage by authigenic minerals in the order of magnitude of P release (Ruttenberg, 1992). The first order rate constant of FeS precipitation of ~5 $\times 10^{-5}$ was found adequate, rapidly consuming Fe^{2+} upon sulfate reduction as observed in nature, and is about a factor three higher than previously applied values (Y. Wang & Van Cappellen, 1996). Silicate precipitation was significantly more difficult to scale because sufficient constraints on relative nucleation and growth kinetics, or temperature and pH dependences are not available. Nucleation barriers were chosen to facilitate precipitation at the highest degrees of supersaturation during test runs, were adjusted to approximate observed porewater concentrations of K, Mg and Si, and to facilitate competition between different clay species. In the mechanistic nucleation growth setup, nucleation parameter choices were guided by published sensitivity analyses (Hellevang et al., 2013). The linear precipitation coefficients (mainly k_N) were further adjusted to match the observed order of magnitude of K, Mg and Si consumption by clays, and pH changes. No reference data were available for our newly developed phenomenological clay precipitation rate law (TIP), so that the initial values of these parameters were chosen in comparison to the PHA parameters and improved iteratively. During the scaling procedure, the system appeared most sensitive to organic matter degradation and metal (oxy-)hydroxide reactivity, to clay nucleation barriers, and to the ratio of bSi and detrital silicate dissolution rate constants (in this order). Note that comparison to literature values is complicated for some parameters because of the different model environment (thermodynamic databases, ambient conditions, selected phase assemblages and reactants) or inadequate ranges (literature may not reflect the actual variability in nature). For the MnO_2 and $Fe(OH)_3$ reactivity parameters, our formulation differed substantially from the original use of the metal-oxide reactive continuum concept (Postma, 1993) (here coupled to OM degradation) impeding direct comparison.

After scaling, we explored the effects of terrestrial sediment sources and weathering intensity on diagenetic weathering (Michalopoulos & Aller, 2004; Trapp-Müller et al., in press; Wallmann et al., 2008, 2023), using a series of mixtures between an Amazon delta scenario (Amz), a highly weathered endmember, and a scenario approximating glaciated, Icelandic river sediments (Ice) (Poulton & Raiswell, 2002; Thorpe et al., 2019). A series of intermediate scenarios was created by linear mixing of the two endmembers to investigate the dynamic transition. Finally, we conducted a grouped linear global sensitivity analysis (see section Sensitivity analyses) to quantify the relative influences of OM, silicate, carbonate, and sulfide reaction kinetics on solute fluxes (H^+, dissolved inorganic carbon (DIC), Ca, Mg, K, Si and Fe^{2+}), at three time slices representing oxygenated, suboxic and anoxic conditions. Moreover, the global sensitivity analysis allows an estimation of the extent of interactions and nonlinearity in the model.

3.6. Global Sensitivity analyses

To quantify the sensitivity of solution chemistry (H^+, DIC, Ca, Mg, K, Si, Fe^{2+}) to different reaction groups (related to organic matter, silicate, carbonate and sulfides) we perturbed the corresponding rate laws linearly by pseudo-random factors (+/- 10 %) sampled from a Latin hypercube distribution (OM degradation: D OM, bSi dissolution: D bSi, inorganic silicate dissolution: D sil, silicate precipitation: P sil, carbonate precipitation: P carb, FeS precipitation: P FeS). For the sensitivity analysis, we used a reference scenario (30 % Amz- 70% Ice and $\gamma_{Fe(OH)3}$ = 115) that allows observation of the transition from net reverse to forward weathering within a limited simulation time of 1 year in both model setups. As a quantitative measure for the influence of a process on a specific concentration change, Standardized Regression Coefficients (SRC) (Saltelli et al., 2008) are calculated by regressing the resulting concentration of an element of interest (C_{dt}) at a timestep of interest (here 1 day, 90 days and 325 days, reflecting oxygenated, suboxic and sulfidic conditions, respectively) against the perturbation factors of each process (*PF*) using a linear model:

$$C_{dt} = I + \beta_1 PF_1 + \beta_2 PF_2 + \beta_3 PF_3 + \beta_4 PF_4 + \beta_5 PF_5 + e \quad (17)$$

where I is the intercept, β the ordinary regression coefficient of a *PF* and e the error of approximation of C_{dt}. For well-performing models, β can be used to assess the influence of a specific PF on the model outcome. Scaling to the

standard deviation of C_{dt} (σ_{Cdt}) and PF (σ_{PF}) ensures that SRCs are independent of parameter units and scales.

$$SRC = \beta \frac{\sigma_{PF}}{\sigma_{C_{dt}}} \quad (18)$$

Positive values reflect an increasing influence, negative value reflect a decreasing effect. We express the relative contribution of each parameter to the model prediction as

$$SRC\% = 100 \frac{SRC^2}{R^2} \quad (19)$$

In the following, we present and discuss SRC% and the direction of SRC. This method allows for robust sensitivity analysis in complex models with a limited number of runs (Saltelli et al., 2008; van Hoek et al., 2021). Given a reasonably good model performance, the 'unexplained variability' (100(1-R^2)) quantifies the amount of nonlinearity and interactions, which is not accounted for in the simple linear model. However, the small size of the perturbations (< 10%) provokes a quasi-linear response over the studied range, ensuring a good quality linear fit. Stabilizing standard deviations of concentration changes demonstrate 200 runs were sufficient for the five perturbed groups in the chosen scenario for both, the TIP and PHA setups (figs. S5, S7).

4. RESULTS

4.1. Tropical mobile muds

In mobile muds of the Amazon delta, porewater chemistry evolves systematically over ~3–9 months as indicated by the measurement-based red shading and arrows in figure 3. The kinetic parameters were roughly scaled to approximate these changes in porewater composition (fig. 3) and are summarized along with published reference values in table 2. The results also reproduce the dominant authigenic clay species identified in Amazon delta sediments (chlorite + ferrous, Si-rich mica) (Michalopoulos & Aller, 1995, 2004; Rude & Aller, 1989) with additional small amounts of illite and mixed-layer clays in the TIP scenario (figs. 4, S1). Moreover, the model reproduces the variation of authigenic mineral suites over the suboxic gradient in solution chemistry as detailed below. These parameter values were considered as a reference for subsequent model experiments. Generally, trends in solution chemistry are very similar in both model setups (PHA and TIP), but there are relatively small differences in pH, Si, Al, Mn^{2+} and Fe^{2+} concentrations (figs. 3–4, S1–S2). The differences are, however, less than an order of magnitude and rather affect the exact shape of the coupled trends.

OM is sequentially oxidized by O_2 and NO_3^- within the first days, dominantly by MnO_2 within weeks, and subsequently by mainly $Fe(OH)_3$ with minor decreasing contributions of MnO_2 and increasing contributions of SO_4^{2-}, consistent with published estimates (R. C. Aller, 2004). This sequence of terminal electron acceptors (TEA) directly causes pronounced and systematic changes in first decreasing and then increasing pH, and increasing DIC, alkalinity, P, N(-III) (= NH_4^+ + NH_3), and sequentially increasing Mn, Fe, S(-II) (= H_2S + HS^- + S^{2-}), and CH_4 concentrations. A total of ~3.5 mM and ~0.6 mM of marine and terrestrial organic carbon (~12 % and ~1.2 % of initial), respectively, are respired over a 6-month run, approximating the lower limit inferred from Amazon delta porewaters (R. C. Aller et al., 1996).

The evolution of porewater chemistry influences and is moderated by the dissolution of detrital and biogenic silicates, here mainly plagioclase, quartz and bSi (fig. 4). The corresponding solute accumulation (Si, Al, Na, K, Mg, Ca, Fe) and response of acid-base chemistry then determine the identity and rate of formation of inorganic precipitates, and net solute fluxes. The modelled P concentrations are consistent with those observed in the Amazon delta at relatively high $Fe(OH)_3$ reactivity (low $\gamma_{Fe(OH)3}$) and are largely moderated by apatite formation, which is generally consistent with a wide range of field observations, although inorganic/organic phosphorous ratios in Amazon shelf sediment are comparably low (R. A. Jahnke et al., 1983; Ruttenberg, 1992; Ruttenberg & Goñi, 1997). P levels vary largely as a function of pH for a given P release (k_{Om}), hence, are governed by the amount and reactivity of metal (oxy-)hydroxides and by simultaneous silicate and carbonate reactions. Calcite dissolves upon acidification, more readily and rapidly with decreasing $Fe(OH)_3$ reactivity (figs. 4, S2). Effects of pH on calcite dissolution seem to be stronger than those of DIC, so that calcite does not dissolve at high $Fe(OH)_3$ reactivity, particularly in the PHA setup (fig. S2). Authigenic carbonate mineralogy transitions from kutnahorite (Mn-Ca) to ankerite (Fe-Mg-Ca-Mn) and, at high $Fe(OH)_3$ reactivity, siderite (Fe) with their relative rates largely being set by dissolved Mn^{2+} and Fe^{2+} release from DMR and DIR (figs. 3–4). Siderite formation is more sensitive to $Fe(OH)_3$ reactivity in the PHA setup, similar to calcite dissolution. These carbonate mineral patterns are consistent with inferences from stable carbon isotope ratios and sequential extractions in Amazon-derived sediments of the Amapá shelf (Z. Zhu et al., 2002). In our model, authigenic carbonates sequester ~15–50 % of the respired organic carbon, decreasing with $Fe(OH)_3$ reactivity, approximating inferences from measurements in Amazon shelf sediments muds (~10–30 %) (R. C. Aller et al., 1996). Thus, the relative rates of OM degradation and carbonate precipitation dominate the evolution of DIC and alkalinity, and their interplay is moderated by $Fe(OH)_3$ reactivity and the coupled effects of carbonate and silicate dissolution and of clay and sulfide precipitation on Fe^{2+}, S(-II), the major cations and pH. The evolution of clay mineralogy follows the TEA sequence too: During aerobic and nitrogenous OM degradation smectite (montmorillonite and mixed-layer smectite) +/- illite precipitate relatively slowly (~0.1–1 mM/yr) and are subsequently outcompeted by a series of green clays (smectite + chrysotile glauconite (TIP only) + smectite Amazon clay + chlorite Amazon clay +/- smectite +/- illite) during DIR (fig. 4). The small individual stability fields of different green clay species depend largely on dissolved Fe^{2+}/Fe^{3+} and pH (given sufficient dissolved Si and solid $Al(OH)_3$ in these scenarios).

The chlorite stability field and related Mg consumption expand significantly with increasing Fe^{2+} supply and the corresponding increase in pH, while K consumption by the

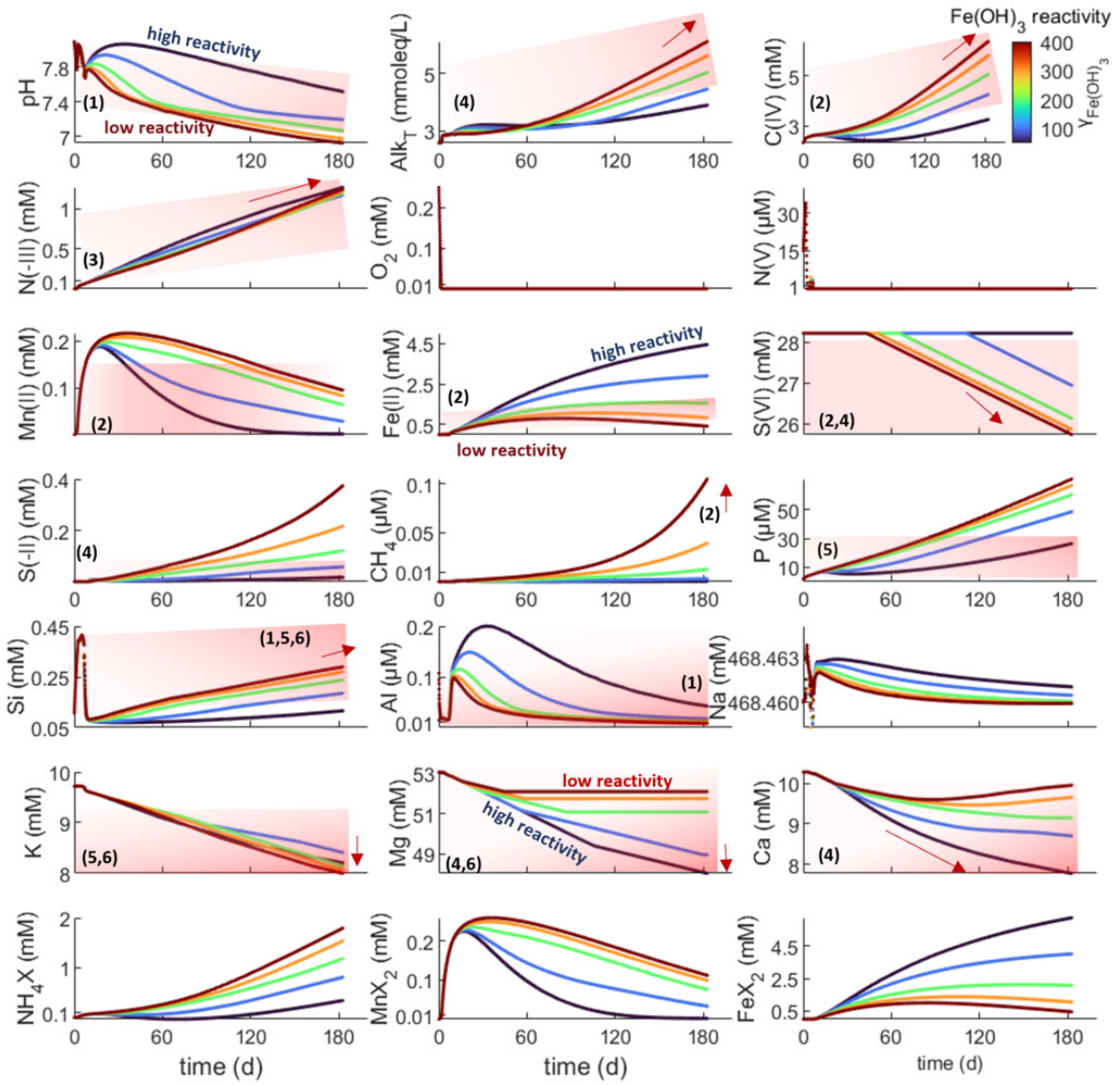

Figure 3. Evolution of porewater chemistry in the Amz scenario for different $Fe(OH)_3$ reactivities ($\gamma_{Fe(OH)3}$) (TIP setup). Red fields approximately indicate the observed range (red shading indicates direction of change in time, arrows indicate that measured maxima/minima are higher/lower than the visible range). References: (1): (Mackin & Aller, 1986), (2): (R. C. Aller et al., 1996), (3): (Mackin et al., 1988), (4): (R. C. Aller et al., 1986), (5): (Spiegel et al., 2021), (6): (Michalopoulos & Aller, 2004).

Amazon clay varies insignificantly over a wide range of $Fe(OH)_3$ reactivities in both model setups (figs. 3–4, S1–S2). The sequence of green clay precipitation is more readily established in the TIP setup as glauconite and illite precipitation are muted by the stronger competetive effect in the PHA setup. While the difference in precipitation kinetics influence the shape of trends in pH, Si, Al, Mn^{2+} and Fe^{2+} levels, it is only marginally relevant to the overall changes in solution chemistry (figs. 3–4 and S1–S2). Green clays precipitate rapidly (up to15 mM/yr), exceeding experimental and leaching-based estimates of ~1.5 mM Fe^{2+}-mica /yr (~2.8 μM K/g/yr (Michalopoulos & Aller, 2004)). However, such high green clay precipitation rates are required to fit the oberserved K decrease in porewaters Amazon delta (Michalopoulos & Aller, 2004; Spiegel et al., 2021). Because detrital plagioclase dissolution (~0.15 mM/yr) is about an order of magnitude slower than the observed green clay authigenesis under deeply ferruginous conditions, while quartz, K-feldspar and detrital clays quickly saturate, substantial amounts of $Al(OH)_3$ are required to sustain this cation consumption (up to 80 mM/yr, fig. 4) in our model, implying acidification *via* reverse weathering (cf. Michalopoulos & Aller, 1995; Wallmann et al., 2023). Our predicted plagioclase dissolution rates approximate the upper limit estimated for plagioclase-rich, anoxic sediments off Iceland (< 0.1 mM/yr) (Maher et al., 2006) and exceed maximum forward weathering rates of anoxic mafic sediments in the Sea of Okhotsk (~0.01–0.015 mM/yr) (Wallmann et al., 2008). Because feldspar grains in pre-weathered, tropical sediments may become passivated by clay and metal (oxy-)hydroxide coatings, our model rate likely overestimates feldspar dissolution. Thus, the extent of $Al(OH)_3$

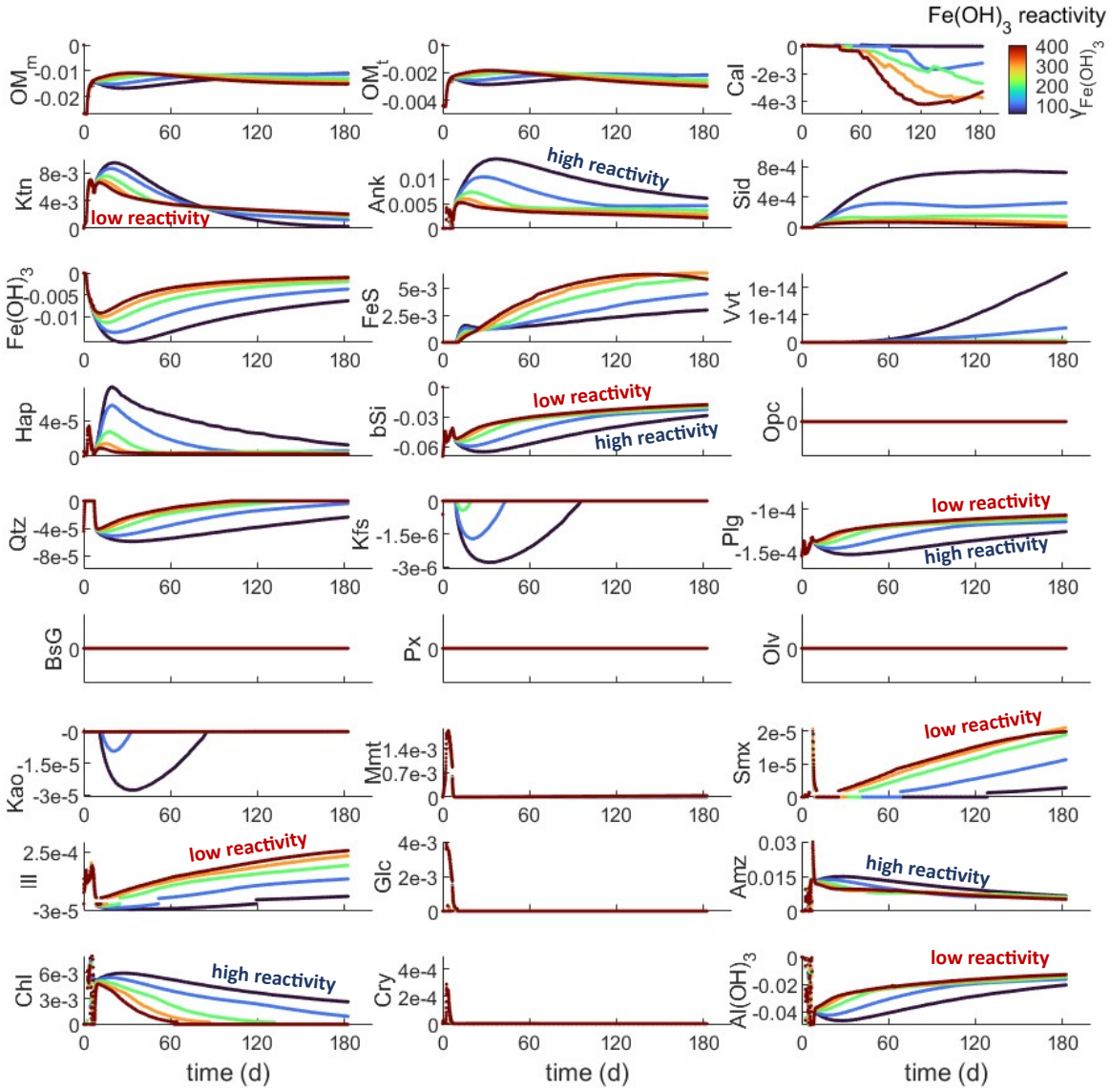

Figure 4. Evolution of reaction rates (M/yr) in the Amazon (Amz) scenario for different $Fe(OH)_3$ reactivities ($\gamma_{Fe(OH)3}$) (TIP setup). Mineral abbreviation key as in table 1.

consumption and related shifts to more reverse weathering seem plausible. However, during reduction, Fe-Mn-based coatings may dissolve, releasing Al and reactivating the underlying grain surfaces. Moreover, direct µm-scale feedback between dissolution and precipitation may allow for faster dissolution, even of nominally (super-)saturated detrital silicates (Ruiz-Agudo et al., 2016), such as K-feldspar and some detrital clay. As Fe^{2+} and pH decrease in response to precipitation, particularly of FeS, green clays eventually become undersaturated and the precipitating clay assemblage shifts back to a comparably slowly precipitating (0.1–0.3 mM/yr) aluminous clays (here dominantly illite and smectite in the PHA setup). The onset and duration of FeS precipitation and related acidification and modelled changes in authigenic mineralogy vary as a function of $Fe(OH)_3$ reactivity (for a given k_{OmM}) (figs. 3–4).

4.2. The role of terrestrial sediment sources and depositional timescale

For the given amount and reactivity of OM, the prevailing biogeochemical conditions at a given point in time vary primarily as a function of TEA availability and depositional timescale (figs. 3,5). Thus, terrestrial sediment sources, particularly metal (oxy-)hydroxide content, and the timescale of episodic reworking have a clear and dramatic effect on the evolution of the metabolic pathways of organic matter degradation, porewater composition and mineral authigenesis (fig. 5). Particularly DMR and DIR are regulated by metal (oxy-)hydroxides availability and exert a large effect on pH, mineral saturation states, weathering, and authigenesis (fig. 6). Moreover, sediment sources regulate the supply, composition and reactivity of detrital silicates. Both, metal (oxy-)hydroxide reduction and reactive detrital silicate supply affect the magnitude and direction of silicate weathering fluxes, and responses of authigenic

carbonates, sulfide, phosphates, and porewater chemistry, also on interannual timescales (figs. 5–6). There is a fundamental difference in the late stage pH and Fe^{2+}/S(-II) evolution of $Fe(OH)_3$-rich and $Fe(OH)_3$-poor scenarios upon sulfate reduction because FeS formation and related acidification eventually become limited by Fe^{2+} rather than S(-II) availability at low pre-weathering intensities (low %Amz). This condition allows for sulfide accumulation in solution, resulting in increases of pH and alkalinity that facilitates calcite precipitation (R. A. Berner et al., 1970; Boudreau & Canfield, 1993). The latter trend is consistent with global scale patterns of $CaCO_3$ authigenesis in marine sediments (Schrag et al., 2013; Turchyn et al., 2021) and does not occur in Fe-rich, acidic scenarios, where calcite and siderite eventually dissolve during sulfate reduction (figs. 4, 6). This reflects a FeS-related bistability in the coupled Fe-S cycles, where small perturbations of OM/$Fe(OH)_3$ input ratios within a specific critical range can fundamentally alter the systems biogeochemical state (van de Velde et al., 2020; Wijsman et al., 2002) and drive changes in weathering and authigenesis.

Generally, dissolved Mn and Fe concentrations and the duration of dominantly suboxic conditions increase with increasing pre-weathering intensity (%Amz), while dissolved Si, Na, K, Mg, K and P decrease. This is because higher amounts of $Fe(OH)_3$ and $Al(OH)_3$ allow for larger and more rapid Fe, Mn and related Al release, and inhibit the transition to sulfidic conditions. All of these factors are beneficial to green clay formation, element consumption and reverse weathering. However, K consumption within the modelled timeframe is maximized at ~75 %Amz, because of lower initial MnO_2 concentrations and an earlier onset of DIR and transition to ferrous conditions, and a higher pH.

On the longer term, K consumption in the Amazon scenario would exceed that of the less pre-weathered scenarios, highlighting the role of depositional timescales. Higher amounts of mafic minerals and basaltic glass with decreasing %Amz increase the release of mainly Si and Mg and some K and Al, countering the effects of green clay formation on solution chemistry (fig. 6). The modelled dissolution rates of plagioclase, pyroxene and basaltic glass are comparable but slightly exceed those inferred from porewaters of anoxic mafic sediments (~0.01–0.1 mM/yr) (Maher et al., 2006; Wallmann et al., 2008). The modeled olivine dissolution rates coincide with those suggested for coastal environments (several mM/yr) (Montserrat et al., 2017). In the near Iceland scenario (figs. 5, S3), trends in Mg (post-ferruginous increase, 'U-shaped' at 25–50%Amz in fig. 5), K (stable to slight decrease), Ca (mM fluctuation, slight early increase and strong late-stage consumption), Si (rapid increase to opal saturation) and Al (slight increases at low %Amz in figs. 5, S3) resemble those in anoxic mafic sediment cores (Middelburg, 1990; Wallmann et al., 2008). Note that our approach to maintain Al mass balance at high clay precipitation rates approaches the limits of its validity limits (high Fe^{2+} or pH < 7.3) in some scenarios, reducing the accuracy of aluminosilicate saturation states.

Moderately pre-weathered sediments tend to Mg-K consumption, broadly consistent with observations from deeper (> 10 m below sediment surface) anoxic slope, fan and deep-sea sediments that are rich in feldspar and detrital clay (Aloisi et al., 2004; Meister et al., 2022; Torres et al., 2022; Wallmann et al., 2023). However, Mg-K consumption in these scenarios decreases by about an order of magnitude at the onset of sulfidic conditions (figs. 5, S3). The pattern emerges from the effect of evolving solution chemistry, particularly Fe^{2+} concentrations, that induce changes in the authigenic mineral assemblage from green clay to smectite-chrysotile +/- illite, and is intensified by decreasing $Al(OH)_3$ availability in time. Thus, these patterns of weathering and related cation and alkalinity fluxes appear to be pre-determined by terrestrial sediment sources, but they emerge time-dependent in response to OM oxidation along the TEA sequence.

Specifically, decreasing Fe^{2+} and pH during later DIR and early sulfate reduction and an associated shift from green clay to aluminous clay precipitation facilitate the transition to alkalinity-neutral or net forward weathering and cation-release, particularly of Mg. The timing and shape of the transition from Mg consumption to Mg release strongly depend on precipitation kinetics and clay identity. High rates of chrysotile and smectite formation may significantly retard or even inhibit this transition, resulting in approximately stable Mg profiles. For example, depending on the relative rates of bSi and detrital silicate dissolution, and choices of clay nucleation barriers, Mg would not necessarily increase at 0%Amz, but only in the transitional, more acidic scenarios. Moreover, Mg-rich clays tend to precipitate in response to the dissolution of Mg-rich silicates, narrowing the net alkalinity impact. Forward weathering under basaltic-sulfidic conditions further raises pH and promotes carbonate formation. Only ~10% of the Ca consumed by calcite can be supplied by coeval detrital silicate dissolution (figs. 6, S3) so that the effect of silicate weathering on pH is more relevant to enhancing carbonate formation than the supply of Ca in our model. Again, reaction patterns are very similar in both model setups, but there are some differences in the details of evolution of carbonate and clay assemblages (illite, mixed-layer smectite), and in the shape of the trends in solution chemistry.

4.3. Sensitivity and interaction in the diagenetic reaction network

The previous section evaluated the sensitivity of the diagenetic reaction network towards the input of terrestrial minerals. Here, we present a linear analysis of the sensitivity of H^+, DIC, Ca, Mg, K, Si, and Fe concentration changes to group-wise perturbations of reaction kinetics. As expected from the similarity of the reaction patterns modelled with the PHA and TIP setup, respectively, the model sensitivities are largely consistent (figs. 7, S5–S10). The unexplained variance (100 (1-R^2)) is low (< 5 % in most cases, Fig. S10) and implies limited non-linear effects over small perturbation ranges (+/- 10%) ranges. However, early-stage Ca, K, Mg and late-stage K and H^+ seem to be affected by significant non-linearity (high unexplained variance), less so in

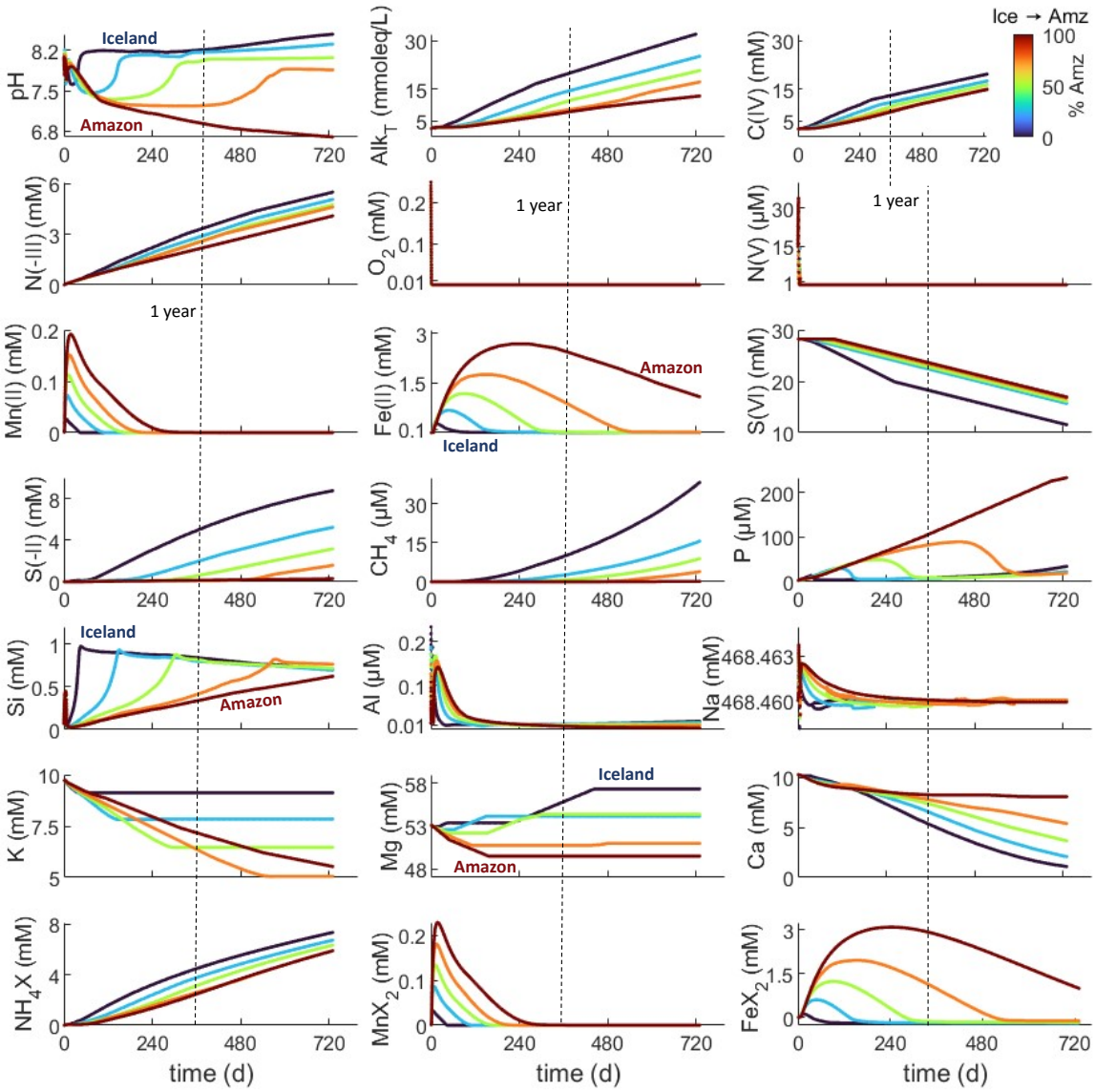

Figure 5. Evolution of porewater chemistry in progressive transitions from the Amz to Ice scenarios (TIP setup).

the PHA than in the TIP setup. These relationships reflect a specific situation and cannot necessarily be quantitatively extrapolated to other particle input mixtures and depositional environments. However, the general trends appear to be robust, compared to observations.

The sensitivity analysis revealed a strong response of dissolution and precipitation reactions to the non-linearity of OM degradation pathways with time (figs. 8, S10). We present in detail three time slices that are representative for oxic ([O_2] ⩾ 1 µM; day 1), suboxic ([O_2] < 1 µM, Mn-Fe dominated; day 70) and sulfidic conditions ([O_2] < 1 µM, total [S(-II)] > 1 µM; day 325; figs. 7–8, S5–S9). Besides a major influence of OM degradation, silicate weathering processes (dissolution of bSi (D bSi) and detrital silicates (D Sil) and precipitation of silicates (P Sil)) dominate major cation and Si concentration patterns, and details of pH evolution particularly under suboxic and sulfidic conditions (fig. 8). Fe and Ca concentration responses are complex and drivers vary substantially in time. DIC is primarily influenced by the rate of organic matter degradation. In the following, we will examine the details of these reaction dynamics.

Under oxygenated conditions (day 1), H^+, DIC and Ca increase (pH decreases) primarily in response to aerobic OM oxidation. Although calcite remains supersaturated, Ca concentrations increase with organic matter degradation rates due to exchange with NH_4^+ at surface sites, and with detrital silicate dissolution (pyroxene, plagioclase). Moreover, detrital silicate dissolution increases Mg and K concentrations and decreases H^+ by ~20 %, i.e., forward weathering partly buffering acidification through aerobic respiration (fig. 8). In the TIP setup, K decreases in response to increasing detrital silicate dissolution and significant non-linearity is involved, reflecting effects on illite saturation and cation exchange. Si increases are largely driven by bSi dissolution in both setups, while Fe concentrations increase in response to detrital silicate dissolution and OM degradation equally.

During the suboxic, Fe^{2+}-dominated stage (70 days), H^+ levels are primarily regulated by decreases through detrital

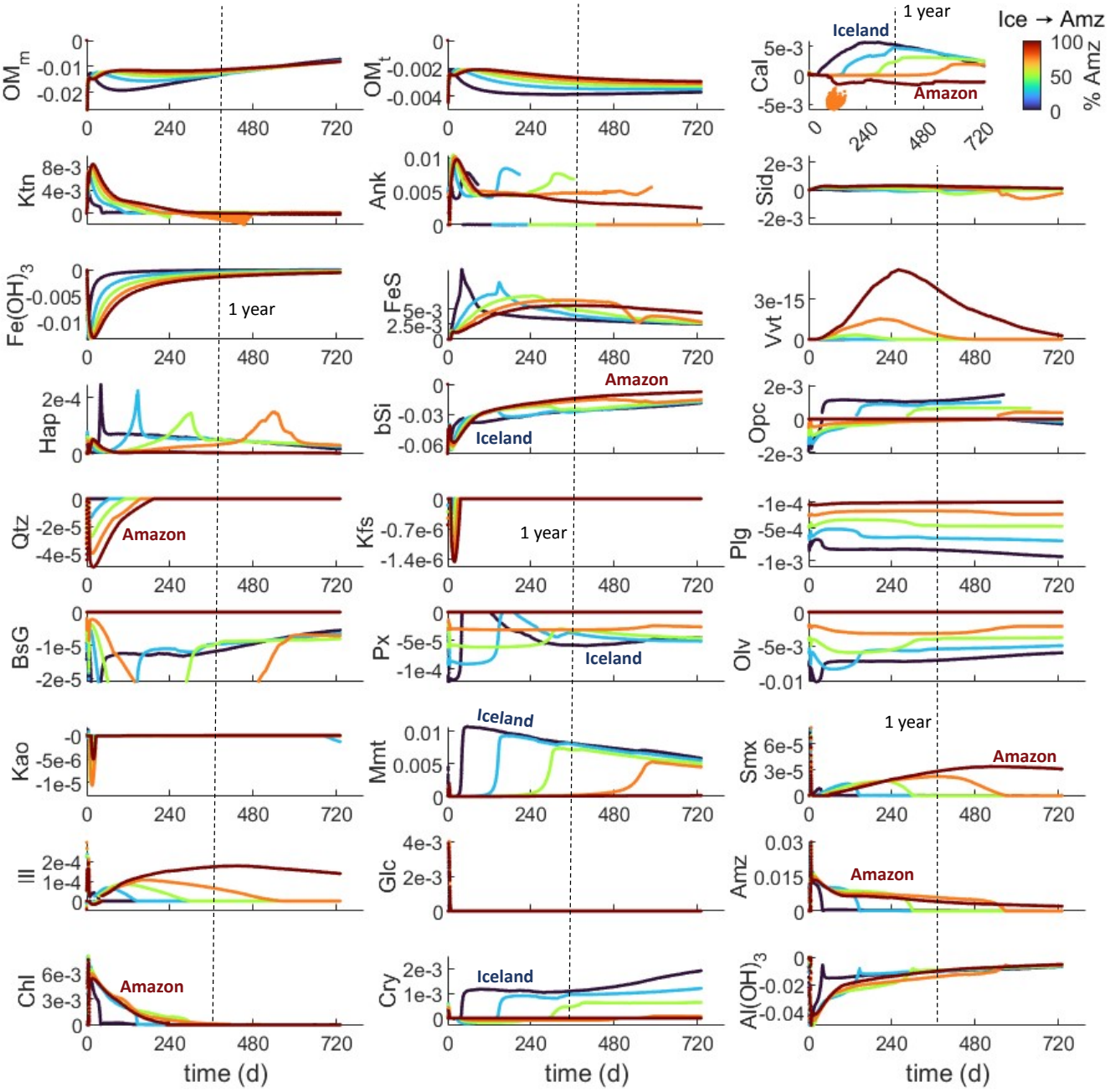

Figure 6. Evolution of reaction rates in progressive transitions from the Amz to Ice scenarios (TIP setup).

silicate dissolution and increases through clay precipitation (PHA, fig. S10) and/or bSi dissolution (TIP, fig. 8), resulting in slightly net forward weathering. Forward weathering under suboxic conditions is facilitated by the presence of basaltic reactants, especially olivine, but is strongly reduced by the acid effects of bSi dissolution coupled to silicate (green clay) precipitation. DIC and Ca are still dominated by the rate of OM degradation and forward detrital silicate weathering that together lower Ca concentration by enhancing calcite saturation. A significant effect of linear carbonate precipitation rate coefficients on Ca is evident under suboxic conditions in the TIP setup (fig. 8). Moreover, bSi dissolution appears to slightly reduce Ca sequestration, probably by increasing the reverse component of the net silicate weathering balance. Mg concentrations under suboxic conditions are dominated by the interplay of detrital and biogenic silica dissolution, the latter promoting K-rich over Mg-rich clay precipitation. In the TIP setup, the effect of bSi dissolution on clay concurrence is much weaker and detrital silicate dissolution exerts a stronger positive influence on Mg concentrations. In both setups, K consumption is clearly dominated by the beneficial effect of bSi dissolution on the precipitation of the Si-rich Amz clay. Dissolved Si levels during the suboxic stage are largely governed by the balance of bSi dissolution and authigenic silicate precipitation. Fe concentrations mainly decrease with detrital and biogenic silicate dissolution, implying a stronger sen-

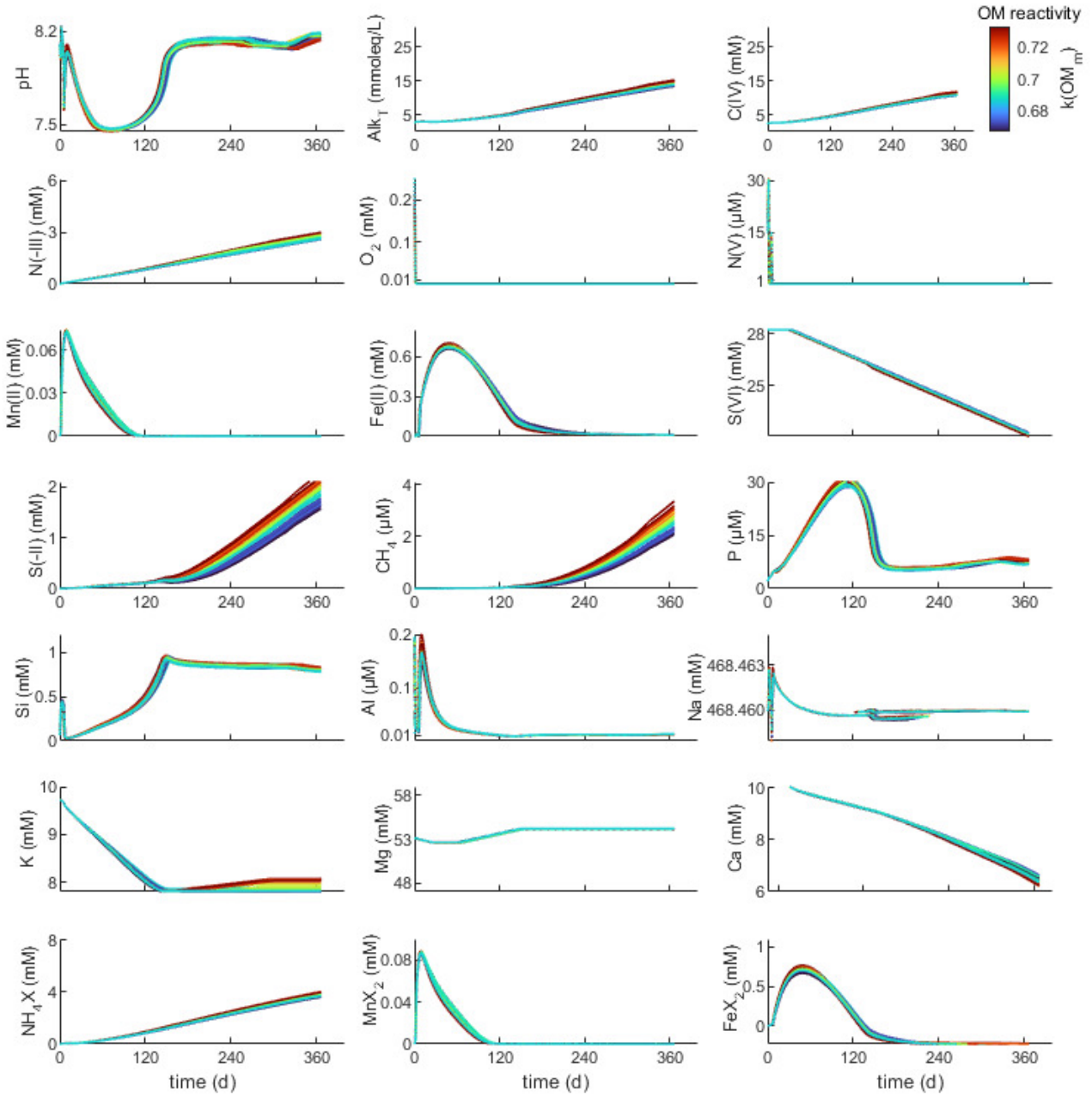

Figure 7. Response of solution chemistry to groupwise perturbations in the TIP setup (30% Amz, $\gamma_{Fe(OH)3}$ = 115). Colors scale with the linear rate constant of marine organic matter degradation (k_{OmM} in yr^{-1}).

sitivity of Fe sequestration to silicate than to carbonate processes.

Under sulfidic conditions (325 days), H^+ concentrations decrease primarily in response to detrital silicate dissolution, reflecting net forward weathering. OM degradation and bSi dissolution slightly increase H^+ as they stimulate FeS, smectite and chrysotile formation, respectively (fig. S10). In the TIP setup, this also applies to carbonate (calcite) precipitation rates (fig. 8). This is also reflected in Ca decreases that are primarily driven by the positive influence of OM degradation and detrital silicate dissolution on calcite saturation. DIC concentrations still increase primarily with increasing OM degradation rates, but detrital silicate dissolution now exerts a minor negative influence reflecting silicate-carbonate coupling in the PHA setup (fig. S10). OM degradation and bSi dissolution seem to limit increases of Mg under sulfidic conditions by increasing the clay sink through pH and Si increases, while detrital silicate dissolution and carbonate precipitation appear to elevate Mg through direct Mg release and competitive effects of calcite and siderite (fig. 8). In both setups, K concentrations increase in response to OM degradation, reflecting the concurrence of OM-driven FeS formation and silicate precipitation, and increase in response to bSi dissolution, promoting sequestration in silicates (figs. 8, S10). However, in the TIP setup, a strong influence of silicate precipitation is indi-

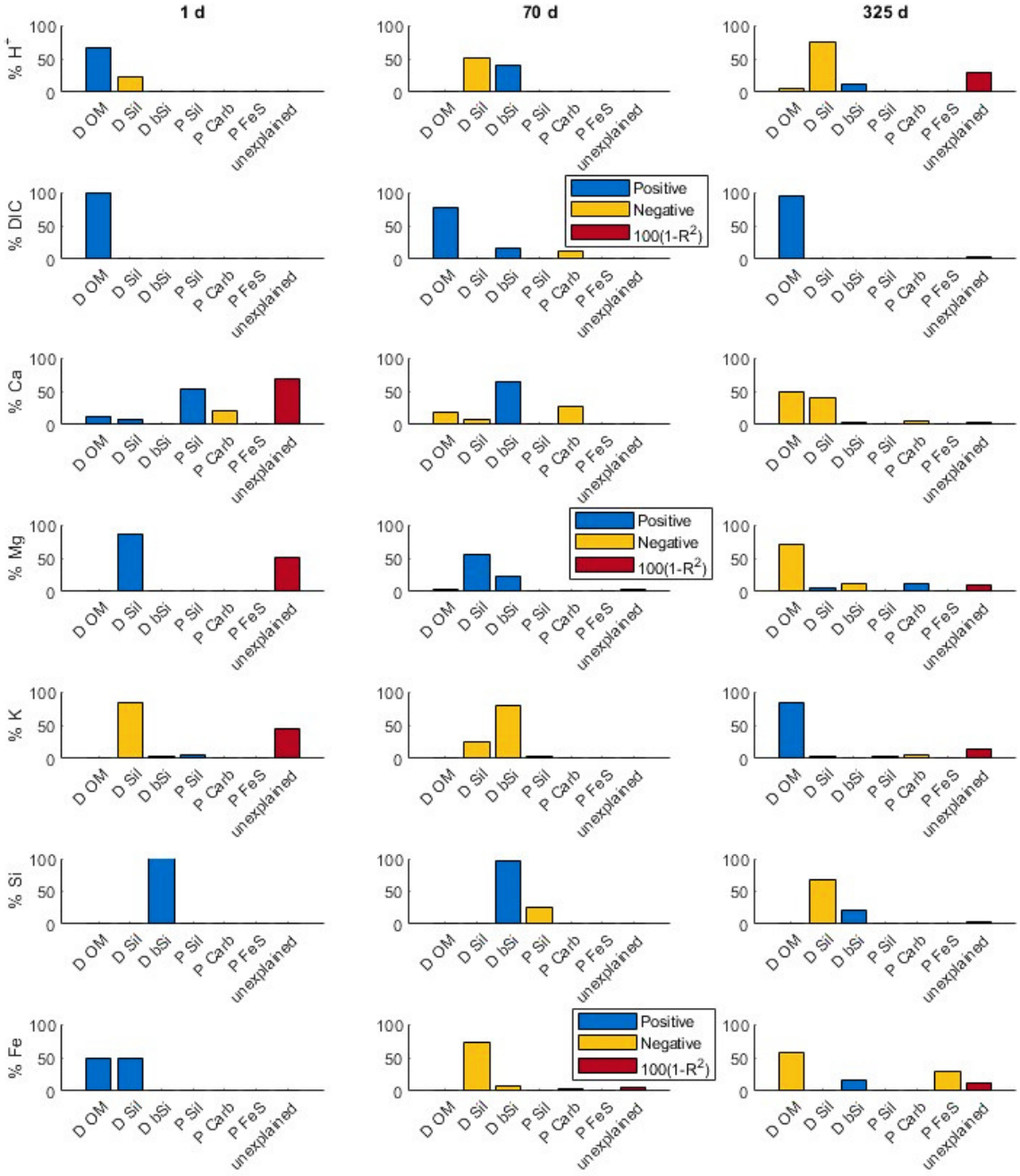

Figure 8. Results of the global kinetic sensitivity analysis (GSA based on the TIP approach). Three time-slices are shown representing aerobic-nitrogenous conditions (1 days), deeply ferruginous conditions (70 days) and deeply sulfidic-incipient methanogenic conditions (325 d). Each bar represents the influence (blue positive correlation, yellow negative correlation, red: unexplained fraction (1-R^2)) measured as the ratio of the squared standardized regression coefficient (Methods) of a process and the total explained fraction (R^2). Processes: D OM: degradation of OM, D bSi: dissolution of bSi, D Sil: Dissolution of non-biogenic silicates (incl Opal-CT), P Sil: precipitation of secondary silicates (incl Opal-CT), P Carb: precipitation of carbonates, P FeS: precipitation of FeS.

cated directly along with strong non-linear and/or interaction effects (~40% unexplained fraction, fig. S10), possibly reflecting the hyperbolic function regulating the dependence on saturation in the TIP rate law. However, such a high unexplained fraction renders the linear model insufficient for quantitative evaluation. Late-stage Si levels increase with bSi dissolution and, slightly, with OM degradation, and decrease with increasing detrital (alumino-)silicate dissolution. This is because detrital silicate dissolution releases Si, Al, and alkalinity, driving silicate precipitation, while acidification through organic matter degradation and reverse weathering of bSi inhibit clay formation (relative to Si release). Finally, late-stage Fe concentrations decrease in response to increasing OM degradation and coupled FeS precipitation, with a positive effect of bSi dissolution, reflecting concurrence with the less efficient clay sinks, in both setups.

5. DISCUSSION

5.1. Links between organic matter, authigenic minerals and silicate weathering

During diagenesis, the degradation of organic matter along the terminal electron acceptor sequence (O_2, NO_3^-, MnO_2, $Fe(OH)_3$, SO_4^{2-}, CO_2) exerts a large influence on the balance of silicate dissolution and precipitation, on the secondary phase assemblage (Aplin & Taylor, 2012; Baldermann et al., 2013; R. A. Berner, 1981; Burst, 1958) and on the resulting biogeochemical fluxes (fig. 8) (R. C. Aller & Wehrmann, 2025; Wallmann et al., 2023). The magnitude and direction of diagenetic weathering fluxes can change with sediment depth in redox-stratified sediments (Middelburg, 1990; Scholz et al., 2013; Wallmann et al., 2008), and certain types of authigenic minerals are characteristic of specific biogeochemical environments (Aplin & Taylor, 2012; R. A. Berner, 1981). For example, glauconite is thought to form under incipient suboxic (Mn-Fe reducing) or fluctuating oxic-anoxic conditions (R. A. Berner, 1981; Cloud, 1955), while FeS_x and MnS_x are indicative of sulfidic conditions and authigenic Ca-Mg-Fe carbonates for methanic environments (figs. 7, 9) (R. A. Berner, 1981; Suess, 1979). These patterns have implications for diagenetic reaction balances:

Net cation (Na, K, Ca, Mg, Fe^{2+}) fluxes (ΣCat) in our model simulations indicate distinct trends in silicate-related cation and alkalinity cycling with reactant composition and the evolution of biogeochemical conditions in time (fig. 9). These favor cation consumption and reverse weathering at high terrestrial weathering intensity and under suboxic conditions, while cation release and forward weathering are promoted by unweathered, basaltic reactant pools and either oxic or sulfidic-methanic conditions (fig. 9). The variation in time is driven by the variation of precipitates with transient biogeochemical conditions, superimposing the baseline cation-release related to crustal silicate dissolution. Here, we compare our modelled trends of inorganic reactions coupled with organic matter degradation to published concepts and observations from a range of marine settings to arrive at a generalized, explanatory framework of diagenetic weathering products and fluxes (fig. 10). We will discuss reaction dynamics during oxic ($[O_2] \geqslant 1$ µM), suboxic ($[O_2] < 1$ µM, Mn-Fe dominated) and sulfidic conditions ($[O_2] < 1$ µM , $[S(-II)]_{tot} > 1$ µM), and how this sequence affects authigenic mineral assemblages and weathering fluxes.

5.1.1. Oxic conditions

Under aerobic to nitrogenous conditions, smectite +/- illite precipitation results from the interplay of biogenic silica and detrital silicate dissolution, consistent with widespread occurrences (Burdige, 2006; Cole & Shaw, 1983; Müller, 1967; Steiner et al., 2022), with our modelled trends (figs. 4, 8) and with Si isotope dynamics in open ocean surface sediments (Closset et al., 2022). The structure (dioctahedral, mixed layer or trioctahedral) and composition (Si vs Al vs Fe) of these authigenic smectites may vary as a function of local porewater chemistry (pH, Si, salinity) and Fe-Al availability (Aplin & Taylor, 2012; Baldermann et al., 2017; Cole, 1985; Tosca & Masterson, 2014). The ratio of illite to smectite may vary with the relative availability of Si and Al, and, perhaps, with the ratio of detrital and biogenic silicate dissolution. Because of decreasing pH in response to aerobic respiration and lack of dissolved Si build-up, clay authigenesis in oxic sediments may proceed rather slowly, about an order of magnitude slower than green clays formed under suboxic conditions in our model. In volcanogenic surface sediments, zeolites (phillipsite) and palagonites (complexly patterned, amorphous alteration products of volcanic glasses) may accompany smectite instead of illite (Hay, 1966; Kastner, 1979; Stroncik & Schmincke, 2002) (fig. 10). This is common in the Pacific Ocean (Hay, 1966; Kastner, 1979), possibly constituting a globally significant, but so far unassessed sink of Na and K. While detrital Si-release is common (Closset et al., 2022; Tréguer & De La Rocha, 2013; Wallmann et al., 2023), the magnitude and direction of related alkalinity and major element cycling depends on the fine balance of local dissolution and precipitation rates so that both, slightly reverse and slightly forward weathering seem possible (fig. 10). This tight balance is in line with our model (fig. 5), with observations of Si-dependent reverse weathering (acidification) upon immersion of aluminous clays in standard seawater (Mackenzie & Garrels, 1965; Mackin, 1986), and with variable results upon immersion of mafic minerals in standard seawater (Fuhr et al., 2022; Montserrat et al., 2017). Without detailed constraints on reaction balances and fractionation factors, Si dynamics alone do not provide sufficient constraints to infer associated alkalinity and element cycling.

5.1.2. Manganous and ferruginous conditions

Dissimilatory manganese reduction (DMR) increases pH, DIC and dissolved Mn concentrations and induces the formation of Mn-Ca(-Fe-Mg)-carbonates like kutnahorite and ankerite (Middelburg et al., 1987; Mucci, 2004; Z. Zhu et al., 2002) (fig. 10). The relatively high pH and reoxidation of Fe^{2+} released by simultaneous dissimilatory iron reduc-

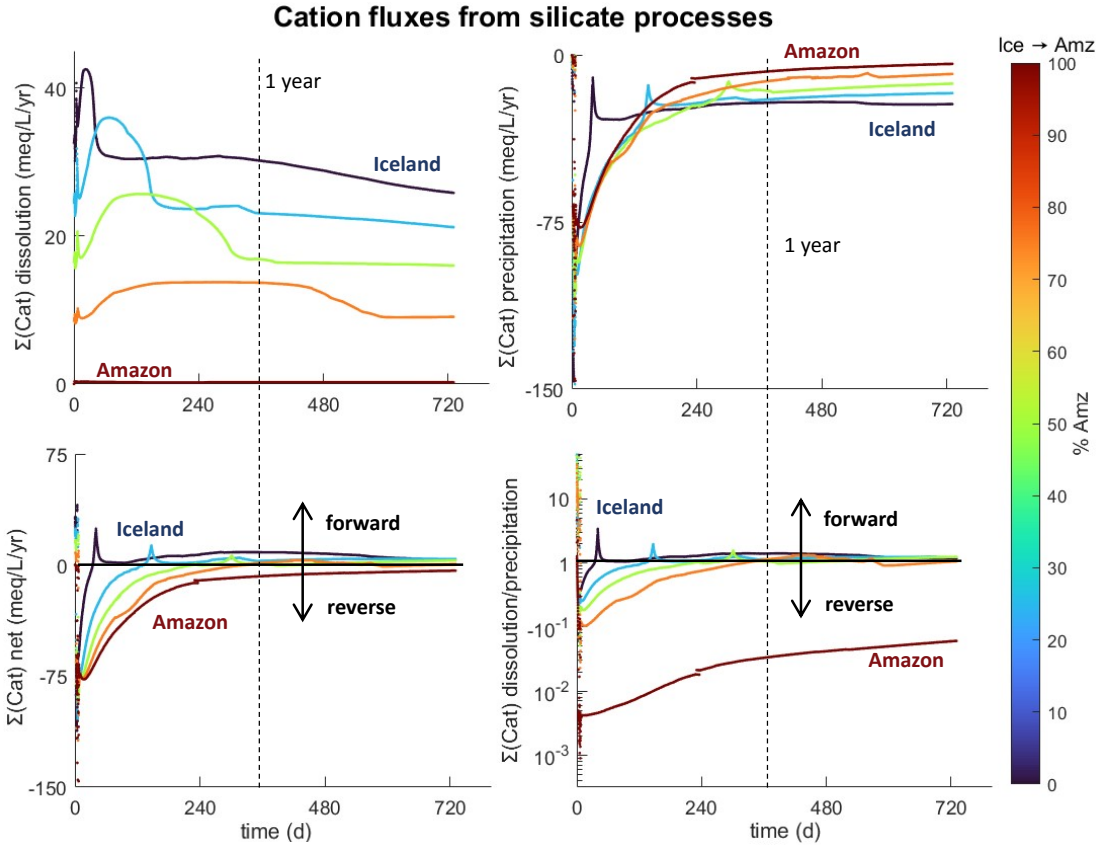

Figure 9. Total cation fluxes (Scat, including Na, K, Ca, Mg and Fe^{2+}) related to silicate dissolution and precipitation in the Amazon-to-Iceland transition (TIP setup). Positive fluxes indicate alkalinity generation and forward weathering, negative fluxes alkalinity consumption and reverse weathering. Bold black lines mark alkalinity-neutral reaction balances, i.e., the transition between forward and reverse weathering. Dotted lines indicate a timespan of one year that corresponds to the maximum timescale of episodic deposition in most deltaic mud belts.

tion (DIR) (R. C. Aller, 2004; R. C. Aller & Rude, 1988) also facilitate the concurrent, rapid growth of complex ferriferous green clays, such as odinite ($(Fe^{3+}_{0.784}Mg_{0.772}Al_{0.556}Fe^{2+}_{0.279}Ti_{0.016}Mn_{0.015})_{2.422}(Si_{1.788}Al_{0.212})O_5(OH)_4$) (Bailey, 1988; Odin, 1990), and Fe-rich interstratified mixed layer smectites and illite that may subsequently evolve into chlorite and glauconite, respectively (Baldermann et al., 2013, 2017; Cloud, 1955; Giresse, 2022; Odin, 1990). Despite significant overlap, the different ranges of Fe^{2+}/Fe^{3+} ratios in different green clays suggest that their occurrences relate to local redox potential and Fe supplies (fig. 10), which is supported by the solubility-driven trend of clay speciation with OM degradation, particularly DIR, in our model (smectite +/- illite smectite + chrysotile glauconite + smectite Amazon clay + chlorite Amazon clay +/- smectite +/- illite smectite +/- illite +/- chrysotile (Mg-clay) in figs. 4, 9). Basic thermodynamic and kinetic information for odinite and similar minerals are lacking, but the timing of chrysotile (Mg-serpentine) formation in our model approximately coincides with this expectation in both model setups. Under somewhat more reducing, Fe^{2+}-dominated conditions, chlorite and ferrous micas (celadonite, Amazon clay) may dominate the green clay assemblage. Depending on the quality and quantity of organic matter and Fe (oxy-)hydroxides, ankerite and/or siderite will complement the ferruginous assemblage, in concurrence with silicate and sulfide precipitation (figs. 4, 6, 8–9). Our results indicate that silicate precipitation increases Ca concentrations and inhibits carbonate formation through reverse weathering, consistent with inferences from mudstone petrography (Milliken & Land, 1991, 1993), and by positive feedback between clay formation and plagioclase dissolution (Du et al., 2022; Wallmann et al., 2023). These effects and OM degradation appear to more strongly influence Ca concentrations under metal (oxy-)hydroxide reducing conditions than do carbonate precipitation rates. The net effect of silicate weathering on DIC is negligible compared to OM degradation (fig. 8).

Green clays occur mostly in shallow sediments at water depth < 500 m and at low latitudes, except (Fe^{3+}-rich) glauconite which is widespread across latitudes and down to ~2000 m water depth (Aplin & Taylor, 2012; Odin & Morton, 1988; Porrenga, 1967). Moreover, green clays form extensively in microenvironments, such as fecal pellets and fillings of carbonaceous shells (Baldermann et al., 2013; Giresse et al., 1988; Odin & Morton, 1988), or as replacements of biogenic and detrital silicates (Baldermann et al., 2013; Geilert et al., 2023; Giresse et al., 1988; Michalopou-

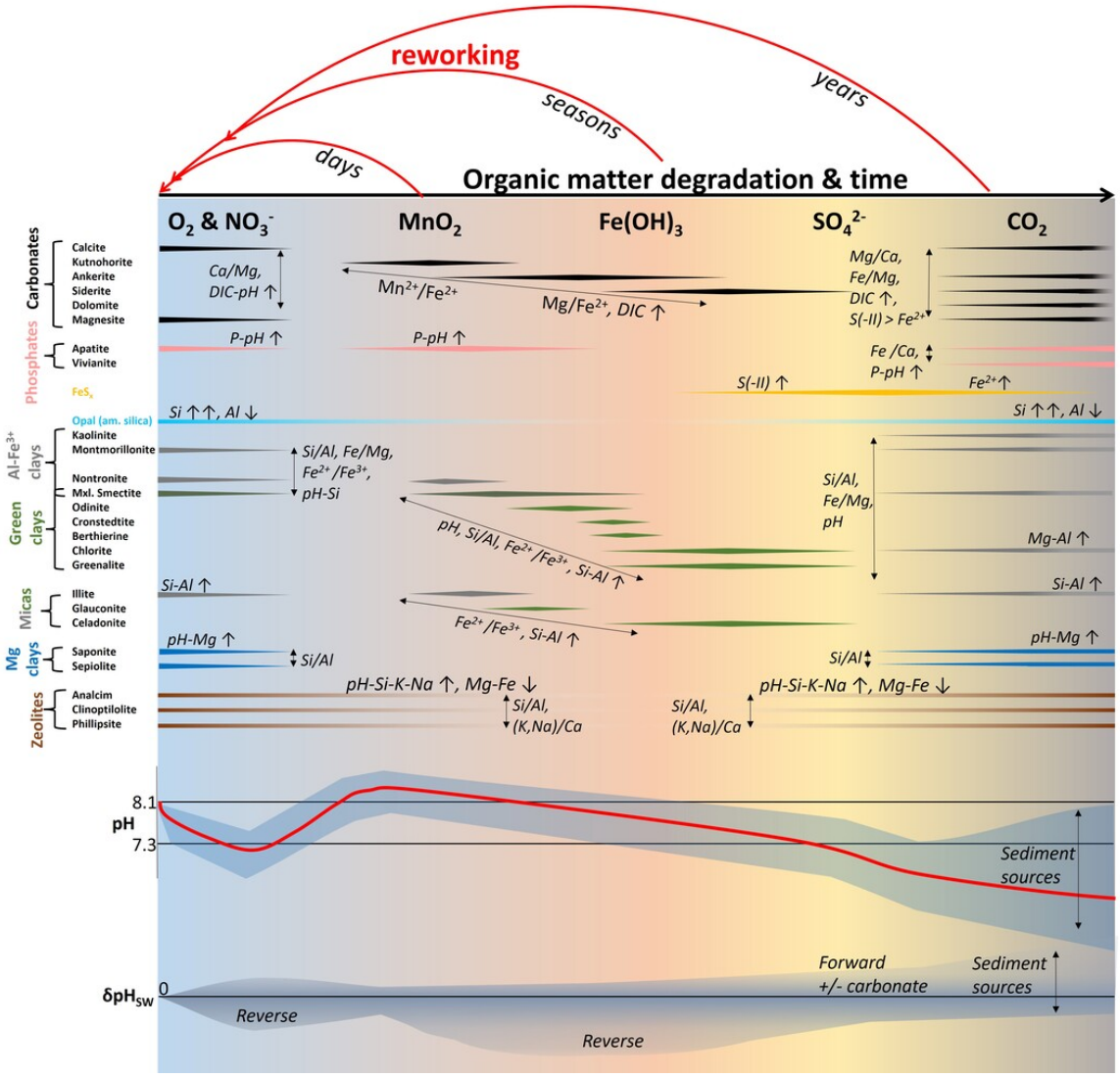

Figure 10. Schematic of likely authigenic phase assemblages at different stages of organic matter degradation and the chemical characteristics that may decide which phase forms. Specific mineral assemblages can be predicted from sediment inputs and environmental conditions. The tendencies of pH evolution and contribution of diagenetic silicate weathering to acidification (reverse, $\delta pH_{SW} < 0$) or alkalinization and/or carbon storage (forward or carbonate-forming, $\delta pH_{SW} > 0$) depends on local sediment sources and depositional environment, with a bistability in Fe-S cycling that is related to the input ratio of organic matter/$Fe(OH)_3$. Because sediments are heterogeneous and host microenvironments, different conditions and corresponding assemblages in this graph may coexist. Red arrows indicate episodic reworking events at daily, seasonal and (multi-)annual scales, typically affecting increasing sediment volumes. Reworking frequency and extent determine how far a given sediment can progress through the sequence, regulating its residence time in the different biogeochemical zones and reaction refluxing.

los et al., 2000; Odin & Morton, 1988). There are physical and biogeochemical limits to the maintenance of Fe-rich conditions in the modern ocean, particularly within the relatively narrow stability fields of ferriferous clays (fig. 10). Thus, Fe^{2+}/Fe^{3+} ratios constrain green clay formation to periodically reworked or ventilated surface sediments, marginal deep-sea environments, and diffusive boundary zones within the sediment (Baldermann et al., 2015, 2017; R. A. Berner, 1981; Cloud, 1955; Giresse, 2022; Michalopoulos & Aller, 2004; Odin, 1990). Many surface sediments are reworked and remobilized multiple times before long-term deposition, particularly on the shelf (Kuehl et al., 1986, 2019; Liu et al., 2018; J. P. M. Syvitski et al., 1988), and are, thus, subjected to such unsteady, suboxic conditions multiple times and for sustained periods, either within restricted locales or progressively along sediment dispersal paths.

In line with available quantitative data, the prevalence of nonsulfidic, suboxic conditions in deltaic mobile muds gives rise to the highest rates of K-Mg consumption and potentially reverse weathering so far observed in marine sur-

face sediments (Michalopoulos & Aller, 1995; Rahman et al., 2016). Extensive mobilization of Fe and Al and growth of green clays in deltaic sediments during the suboxic stage lower porewater Si concentrations (Mackin, 1986, 1989; Mackin & Aller, 1984b), eventually inhibiting opal precipitation (Riech & von Rad, 1979) (fig. 10) and, possibly, zeolite formation (fig. 10). In contrast, opal commonly coexists with Si-rich Mg clays, clinoptilolite and illite (Calvert, 1971; Keene & Kastner, 1974). Moreover, extensive green clay precipitation sustains silicate dissolution and the overall weathering process (Wallmann et al., 2023). The most common green clays are comparably cation-rich (Isson & Planavsky, 2018), so that weathering reactions producing them have an inherent tendency towards reverse weathering (fig. 10), particularly if compared to weathering reactions producing opal or montmorillonite. If detrital plagioclase were the main source of Si and Al to green clay formation, the weathering process would result in a near alkalinity-neutral reaction balance (Trapp-Müller et al., in press; Wallmann et al., 2023). However, while plagioclase is a likely Si and Al source even in the most pre-weathered coastal sediments (R. C. Aller et al., 1986; Odin & Morton, 1988; Wallmann et al., 2023), green clays in deltaic mobile muds have largely been observed as replacements of bSi (Michalopoulos et al., 2000; Presti & Michalopoulos, 2008) and on lateritic clay coatings (Rude & Aller, 1989) rather than plagioclase. Feldspar sources to the low-latitude, extensively pre-weathered deltaic muds, in which green clays prevail (Aplin & Taylor, 2012; Michalopoulos et al., 2000; Odin, 1990; Rahman et al., 2016), are likely pre-weathered and coated, further passivating them. Moreover, quantitative models of porewater Al-dynamics in organic-rich, muddy sediments (Mackin & Aller, 1984b), and our kinetic assessment (figs. 4, S2) suggest the involvement of cation-depleted and non-silicate Al sources (e.g., Al (oxy-)hydroxides or associated with metal (oxy-)hydroxides in various physical forms) in deltaic green clay authigenesis (figs. 8, S10). The corresponding changes in bulk sediment geochemistry may be nearly undetectable (in the range of a few wt% or mmol/g at maximum) but become visible in operational leaches (Michalopoulos & Aller, 2004), and episodic reworking of materials may drive comparable large biogeochemical fluxes that are easy to overlook (R. C. Aller, 2004; McKee et al., 2004; Moore et al., 1995).

5.1.3. Sulfidic and methanic conditions

Iron sulfide (FeS) precipitation upon microbial sulfate reduction rapidly consumes Fe^{2+} and acidifies the system, eventually destabilizing green clays and outcompeting carbonate and phosphate minerals (R. A. Berner, 1981) (fig. 10). While diagenetic serpentine dissolution (Geilert et al., 2020; Milliken et al., 1996) and carbonation of green clays seem feasible (Zhang & Tutolo, 2021), stoichiometric flexibility within the chlorite group of authigenic clays (Müller, 1967) or deep-seated Fe-sources (Egger, Rasigraf, et al., 2015; Luo et al., 2020) may stabilize Mg-Fe^{2+} clays under more deeply anoxic conditions. However, precipitation of aluminous, Fe-poor clays like smectite, illite or kaolinite appears most likely under Fe-depleted sulfidic and methanic conditions, consistent with the downcore evolution of authigenic clay mineralogy and porewater chemistry in a range of anoxic surficial and deeper subsurface sediments (Aloisi et al., 2004; Iacoviello et al., 2012; McKinley et al., 1999; Müller, 1967; Torres et al., 2022). In Fe-rich sediments, pH may further decrease (towards ~6.5) in response to sustained FeS formation and methanogenesis, increasingly promoting the formation of more acid-tolerant cation-poor clays (motmorillonite, illite, kaolinite) and/or opal rather than trioctahedral smectite and chlorites. Because of the particularly low pH, carbonate formation may require additional stimulation through DIC generation and silicate weathering (Torres et al., 2020). In contrast, pH and alkalinity increase because Fe-limitation of FeS formation results in dissolved sulfide accumulation and, eventually, in response to anaerobic oxidation of methane and/or silicate reactions, driving supersaturation of Ca(-Mg-Fe) carbonates (including dolomite) and Mn sulfides (R. A. Berner, 1981; Middelburg et al., 1990; Suess, 1979; Torres et al., 2020; Turchyn et al., 2021), and/or of Mg-rich clays (e.g., crysotile or trioctaheral smectite) (figs. 6, 9). Thus, the bistability of the coupled Fe-S cycles (R. A. Berner, 1970; van de Velde et al., 2020; Wijsman et al., 2002) affects mineral authigenesis patterns and diagenetic weathering fluxes.

These changes in authigenic mineral assemblages imply a change in net reaction balance and, consequently, biogeochemical cycling. Invariant concentration vs depth profiles of K and other cations indicate an approximate balance of dissolution and precipitation fluxes during (incipient) sulfate reduction in both, model and nature (fig. 5) (B. Zhao et al., 2017). In our model, a smectite-illite assemblage consumes cations at least an order of magnitude more slowly under sulfidic conditions than the preceding green clay assemblage under suboxic conditions. In the presence of cation-rich and reactive detrital silicates, e.g., mafic minerals, ashes or plagioclase, this may facilitate a shift to forward and carbonate-forming silicate weathering. In fact, carbonate precipitation in marine sediments may be intimately coupled to local Ca, Mg and alkalinity generation through forward weathering, particularly of fresh (ultra-)mafic and volcaniclastic materials (Bonatti et al., 1974; Hong et al., 2020; Torres et al., 2020). However, cation-accumulation and increasing pH in response to forward weathering may stabilize Mg-rich clays, such as chrysotile in our basaltic scenarios, eventually limiting net alkalinity and cation release (fig. 5). This stabilization is consistent with the common observations of Mg-rich serpentine and saponite as low temperature diagenetic weathering products of ultramafic detritus and volcanogenic sediments, respectively (Barale et al., 2022; Bonatti et al., 1984; Iacoviello et al., 2012). Moreover, zeolites and opal or palagonite may form instead of, or in concert with, authigenic clays and/or carbonates, depending on the nature of the silicates supplied and the evolution of *local* solution chemistry (fig. 10). For example, clinoptilolite or phillipsite, opal, smectite and carbonates may form where volcanic ashes, glasses and biogenic silica are the main reac-

tants (Bonatti, 1965; Luo et al., 2023; Petzing & Chester, 1979; Stroncik & Schmincke, 2002).

Thus, continental, volcanogenic and biogenic sediment sources will influence authigenic mineralogy, diagenetic weathering fluxes, and associated alkalinity cycling. The influence of input silicate mineralogy appears to be pronounced under oxygenated and anoxic conditions but becomes overshadowed by rapid green clay precipitation under suboxic conditions. Our results suggest that the duration of the different biogeochemical stages (or their relativ spatial extent) and a possible transition from reverse to forward diagenetic weathering is governed by the interplay of organic matter degradation and the relative intensities of the different silicate processes and, hence, may be predicted from silicate mineralogy and the relative amounts and reactivities of organic matter and metal (oxy-)hydroxides. However, the physical and biogeochemical boundary conditions of a specific depositional environment, and the presence of sedimentary microenvironments determine which situation in figure 10 is realized. There are some limitations to the application of this predictive concept. The amount of silicate weathering-related alkalinity consumption is intimately tied to the cation- and silica-content of the various Al-sources, including crustal silicate, secondary clays, as well as Al-Fe-Mn (oxy-)hydroxides and highly reactive nanoparticles. Moreover, significant variation in reactant abundances may superimpose multiple modeled trends over longer timescales, and there may be distinct relationships between reactants and products, i.e., favored pathways in figure 10, such as a preference for Mg-rich clays (e.g., chrysotile or saponite) in response to Mg-rich silicate dissolution (e.g., olivine). Better defining the relative contributions of these different aluminum pools to clay authigenesis, identifying reactant-product relationships, and assessing the scale-dependence of weathering fluxes will alleviate the current limitations of predicting diagenetic weathering fluxes.

5.2. Depositional environments, weathering fluxes and global biogeochemistry

The depositional environment of a given reactant mixture determines the physical and biogeochemical conditions and, thus, the trajectory through the biogeochemical sequence in figure 10. As noted earlier, terrestrial sediment sources, particularly metal (oxy-)hydroxide content, and the timescale of episodic reworking have a clear and dramatic effect on the evolution of the metabolic pathways of organic matter degradation, porewater composition, mineral authigenesis and weathering balances. Many subaqueous deltaic muds are seasonally reworked, essentially resetting the diagenetic sequence (red arrows in fig. 10, if the overlying water column remains oxygenated) and trapping the sediment in a repeating, transient, and often iron-dominated biogeochemical state (R. C. Aller, 2004). Moreover, particle advection, mixing and collisions during reworking may erode passivating coatings, enhance organic and inorganic particle reactivities, and entrain fresh, biogenic materials (bSi, OM, $CaCO_3$) (R. C. Aller & Blair, 2006; Bao et al., 2018; Fabre et al., 2019; McKee et al., 2004; Verhagen et al., 2020) (fig. 1). *In situ* production of bacterial biomass may contribute fresh and degradable organic matter in relatively stable areas (J. Y. Aller & Aller, 1986; Ruttenberg & Goñi, 1997). In addition, 'priming' due to redox oscillation and physical reworking further stimulates organic matter reactivity (R. C. Aller & Cochran, 2019; Bianchi, 2011; Blair & Aller, 2012; Q.-Z. Zhu et al., 2024), while physical associations with pedogenic metal (oxy-)hydroxides and clays in terigenous nearshore sediments tends to decrease organic matter reactivity (Mayer, 1994; Ransom et al., 1998; B. Zhao et al., 2023). In dynamic, deltaic environments, the characteristic frequency and intensity of reworking determine the dominant biogeochemical stage, diagenetic reaction patterns and rates (fig. 10). Frequency and intensity of physical mixing events are often inversely related: Smaller layers (< ~0.1 m) are typically reworked on scales of hours to weeks, e.g., through tides, smaller weather events or biological reworking (Boudreau, 1994; Kineke et al., 1996). Reworking of ~10s of meter thick sediment layers and shelf edge or upper slope sediments rather occurs on interannual and decadal timescales, and deeper slope and pelagic sediments may stabilize for thousands or millions of years (J. P. M. Syvitski et al., 1988). Seasonal reworking of 10s–100s of cm thick layers in response to floods and storms is common along continental shelves across latitudes and appears to be the norm along river-dominated ocean margins (R. C. Aller et al., 2008; Bao et al., 2019; Kuehl et al., 1986, 2019; Malmgren & Brydsten, 1992; McKee et al., 2004).

Seasonal reworking often results in the prevalence of suboxic or incipient sulfidic conditions in deltaic muds, depending on the relative abundance and reactivity of organic matter and metal (oxy-)hydroxides (R. C. Aller et al., 1996, 2008; Bao et al., 2018; B. Zhao et al., 2017). High Si-based biological productivity, excessive riverine metal (oxy-)hydroxides and mud supply, as well as the most extensive reworked surface sediment layers coincide at low latitude deltas (Hayes, 1967; Hulskamp et al., 2023; Poulton & Raiswell, 2002; Rahman et al., 2016; Song et al., 2022), producing efficient, suboxic batch reactors and global hotspots of K-Mg sequestration, green clay formation and net reverse weathering (Aplin & Taylor, 2012; Ku & Walter, 2003; Michalopoulos & Aller, 2004; Rahman et al., 2017). Most sediments leaving the continents transit through these unsteady coastal systems for ~10–1000 years before reaching more stable depocenters (Anthony et al., 2010; Kuehl et al., 2019), driving large biogeochemical fluxes (Bao et al., 2018; McKee et al., 2004; Michalopoulos & Aller, 2004; Rahman et al., 2016). Re-oxidation of reduced diagenetic products, especially FeS (R. C. Aller & Rude, 1988), the production of strong acid, and re-dissolution of authigenic minerals during reworking events are relevant in nature, although not covered by our model. This reoxidation-dissolution phenomenon alters the regional and global relative to the local biogeochemical impact (R. C. Aller & Wehrmann, 2025; Gustafsson et al., 2019; Hu & Cai, 2011). However, continuously increasing K and Si at a stable mica-like ratio in leaching fractions representing authigenic clays (Michalopoulos & Aller, 2004), and converging Mg/Fe ratios in altered clay coatings (Rude & Aller, 1989)

along the Amazon-Guianas dispersal system suggest progressive silicate transformation, element sequestration and reverse weathering.

In contrast, undisturbed, organic-rich sediments that steadily accumulate, eventually acquire the typical redox reaction stratification while approaching steady state (R. C. Aller & Wehrmann, 2025; R. A. Berner, 1980; Froelich et al., 1979). In these sediments, the residence times of individual particles in the different biogeochemical zones depend on sedimentation rate and sediment composition, particularly OM and metal (oxy-)hydroxide content and reactivity (R. A. Berner, 1980). Chemical exchange with the water column occurs primarily through upward diffusion and surficial biological reworking, so that dissolved reaction products are extensively recycled (R. C. Aller & Wehrmann, 2025; Boudreau & Canfield, 1993; Burdige, 1993). Extensive zones of forward weathering under methanic conditions may be overlain by comparably small, suboxic zones of reverse weathering that largely recycle the cations and alkalinity produced below (Wallmann et al., 2008). Moreover, extensive authigenesis and the development of reaction textures eventually affect particle reactivities and exchange with the overlying water column by passivation, surface area generation and/or permeability reduction (Altree-Williams et al., 2015, 2019; Deng et al., 2021; Lönartz et al., 2023). This variation of weathering dynamics with environmental boundary conditions and transport of particles and solutes between (sub-)environments imply that net silicate weathering fluxes are scale-dependent in respect to time and space. This scale-dependence and the effect of repeated episodic deposition or long-term stabilization on diagenetic reaction balances should be investigated in future studies.

In Earth's recent history, anthropogenic and natural environmental perturbations have resulted in significant variation of nutrient and sediment delivery, dispersal and deposition, altering coastal communities, diagenesis patterns and weathering fluxes at the global scale (Beusen et al., 2016; Bianchi et al., 2021, 2024; Regnier et al., 2022; J. Syvitski et al., 2022; J. P. M. Syvitski & Milliman, 2007; van de Velde et al., 2018). A direct response of diagenetic weathering dynamics in coastal marine sediment to El Niño-related short-term sediment pulses has recently been documented (Geilert et al., 2023). Clearly, such effects require more attention in the modern times of rapid environmental change with, for instance, increasing extreme weather frequencies and marine (geo-)engineering (De Borger et al., 2021; Eisaman et al., 2023; Gattuso et al., 2018; Intergovernmental Panel on Climate Change (IPCC), 2023). Moreover, reconstructions of past global biogeochemical cycles and weathering fluxes through geological time (Caves et al., 2016; Isson et al., 2020; Krause et al., 2023; Kump & Arthur, 1997; Pogge von Strandmann et al., 2021) will profit from considering variations in the relative abundances of different marine sedimentary environments, residence times of particles within them, and corresponding diagenetic weathering fluxes. Our models demonstrate that responses to these changing conditions are predictable.

5.3. Sedimentary microenvironments

While our discussion has focused on bulk sediment trends, the biogeochemical reaction framework (fig. 10) can also be applied to sedimentary 'microenvironments'. Sediments are heterogeneous at the micro-scale, where chemical gradients extend from individual reacting particles and aggregates, eventually merging in the 'bulk porewater' (Boudreau, 1997; Steefel et al., 2015). Sedimentary microenvironments develop where the influence of local reactions on solution chemistry exceeds the exchange with the bulk solution and/or where local enhancement or inhibition of transport phenomena decouples specific areas within the sediment from the bulk (e.g., authigenic coatings, local fluid channeling, porosity clogging or burrow construction) (R. C. Aller, 1980; Bachmat & Bear, 1986; Boudreau, 1997). Common sedimentary microenvironments that favor mineral authigenesis include aggregates, pellets and biominerals (Baldermann et al., 2013; R. A. Berner, 1980; R. Jahnke, 1985; Jørgensen, 1977; Odin & Morton, 1988). In such transport-limited microenvironments, the influence of local reactions on solution chemistry and on each other is enhanced. In the case of pseudomorphic replacements, e.g., of green clay after biogenic silica (Michalopoulos et al., 2000), internal feedbacks between dissolution, precipitation, solution chemistry and transport phenomena at the reaction front determine the evolution of reaction rates and products (Müller et al., 2022; Odin & Morton, 1988; A. Putnis, 2009).

However, sufficient supplies of Fe and Al, and porosity are needed to sustain high reaction rates and are pre-requisite for the completion of a (bSi-) replacement process (Loucaides et al., 2010; A. Putnis, 2015). Chemical gradient may develop at the µm to cm-scale at diffusive boundary layers in vertically stratified sediments or at the margins of micro-environment. In such boundary layers, otherwise transient redox conditions can be maintained, facilitating the sustained, rapid production of authigenic minerals with relatively small stability windows. For instance, green clays may form in organic-rich microenvironments or layers in nominally Fe^{2+}-poor settings, continuously producing sufficient Fe^{2+} and Fe^{3+} (Baldermann et al., 2013; De Lange & Rispens, 1986; R. Jahnke, 1985). The formation of Ca-Mg carbonate may be facilitated where upward diffusing methane is oxidized by sulfate, increasing alkalinity (Middelburg et al., 1990), or in wider areas influenced by spatially separate forward weathering reactions (Torres et al., 2022). Thus, local reaction-transport phenomena and the presence of microenvironments facilitate the co-existence of different assemblages of figure 10 in bulk sediments, extending and overlapping the potential areas of authigenic mineral occurrences, and altering averaged reaction kinetics.

5.4. Advances and challenges

5.4.1. Weathering kinetics and models

As previously noted, (e.g., Aradóttir, Sonnenthal, & Jónsson, 2012; Velbel, 1993), the description of reaction-limited

dissolution dynamics and relative dissolution rates by TST can provide a reasonable first-order approximation of dissolution dynamics, if the surface parameter (RSA) can be scaled to field observations. Improved, dynamic surface reactivity and accessibility factors may be obtained from microscopic observations or explicit modeling of sediment texture (Altree-Williams et al., 2015, 2019; Beckingham et al., 2017). Moreover, the simplified nucleation-growth rate law (PHA) and our novel composite rate law (TIP) seem promising models to predict the nature of an authigenic mineral assemblage and, by using field observations, approximate precipitation rates and diagenetic reaction balances. Despite quantitative difference in rate evolution, both model setups (TIP & PHA), produce similar and robust, mineral solubility-driven precipitation patterns and provide insights into the biogeochemical dynamics of diagenetic silicate weathering, including interactions between secondary phases *via* solution chemistry. More phase-specific parameters were required for the PHA approach than for TIP, so that the fit to observations from the Amazon delta appears more 'forced'. However, these specifics could reflect real tendencies, such as preferred nucleation at specific grain surfaces (Fodor et al., 2020; Haile et al., 2015; Wooldridge et al., 2019). Moreover, nucleation-growth kinetics are generally more difficult to scale, particularly over a wide range of ambient conditions, because of its exponential dependence on saturation and many poorly known parameters. The TIP approach with its strong Si dependence at high supersaturation appears to be a simple, functional way to describe the transition between thermodynamic limitations and control by element supply through dissolution and/or transport, which appears mechanistically reasonable (Ehlert et al., 2016; Michalopoulos & Aller, 2004). For carbonate precipitation, the exponential nature of the nucleation rate law in the PHA approach allows for a stricter separation of the different carbonates along the TEA sequence than the linear bulk rate laws (or TIP-like formulations) as the variation in saturations states between carbonates (model Ω_{max} < ~10^4) is generally narrower than those between silicates (model Ω_{max} often > 10^6). This enhances the predictability of authigenic carbonate identity (e.g., kutnahorite vs ankerite vs siderite), which is in line with findings in rock carbonation studies (Hellevang et al., 2013; Pham et al., 2011). Precipitation kinetics are further complicated by the various dependencies of nucleation (Haile et al., 2015; Kashchiev & van Rosmalen, 2003; Tosca & Masterson, 2014; Wolthers et al., 2012), solid solutions, and the involvement of molecular clusters, colloids, nanoparticles, and precursor phases (Gebauer et al., 2014; Steefel & Van Cappellen, 1990; Tosca et al., 2016).

5.4.2. Diagenesis, silicate weathering and global biogeochemistry

Our relatively simple batch model reproduces observed diagenetic conditions and product suites over timescales characteristic of natural sedimentary dynamics in common deltaic and estuarine systems. It allowed us to investigate in detail the influences of reactant mixtures and evolving biogeochemical conditions on silicate weathering and diagenetic reaction balances. Moreover, it enables a quantitative comparison of field observations to conceptual frameworks and thermodynamic-kinetic constraints. Together with a broad range of observations from marine sediments (Aloisi et al., 2004; Aplin & Taylor, 2012; R. A. Berner, 1981; Bonatti, 1963; Bonatti et al., 1984; Kastner, 1979; Michalopoulos & Aller, 2004; Müller, 1967; Suess, 1979; Torres et al., 2020, 2022; Wallmann et al., 2008), these insights provide a consistent explanatory framework for the occurrences of authigenic marine minerals, reaction timescales, their relationships to silicate weathering and diagenetic reaction balances based on sediment sources (reactant mixtures), and depositional environments (physical and biogeochemical boundary conditions) (figs. 9–10). Such a framework can be used to predict sedimentary reaction patterns and sediment-water exchange fluxes or to reconstruct depositional conditions and fluxes from the rock record. Moreover, our model has elucidated the dynamic coupling between the sedimentary cycles of C, P, Fe, S, Si, Mg, K, and Ca, and revealed a strong bidirectional influence of diagenetic silicate weathering on porewater concentrations of various elements, acid-base balances and mineral authigenesis (figs. 9–10).

These systematic and predictable patterns allow for a comparison of the role and relative importance of different depositional environments with respect to the global biogeochemical cycles, including alkalinity generation and/or carbon storage through 'enhanced weathering' in targeted environments. In particular, seasonally reworked deltaic muds are efficient suboxic batch reactors and prone to element sequestration and dominant reverse weathering through the precipitation-driven conversion of pre-weathered river sediments and biogenic silica to K-Mg-rich green clays. Despite this tendency to reverse weathering, silicate weathering in deltaic muds releases appreciable amounts of lithogenic Si, Na and Ca. This forward component could be strengthened through cation-rich mineral addition (e.g., olvine, ash), although increasing silica and aluminum release will also enhance precipitation, limiting the net enhanced weathering potential of these environments. Authigenic Mn-Fe-rich carbonates and iron sulfide compete with green clays and recycle part of the cations and alkalinity released from detrital silicates. As these conditions are typical of areas with the greatest sediment fluxes on Earth and lead to efficient exchange with the water column, it is clear that deltaic mobile and fluid muds play a major role in the main global biogeochemical cycles. Steadily accumulating, sustained anoxic and iron-poor sediments promote alkalinity generation, silicate carbonation and phosphate authigenesis, particularly in the presence of mafic minerals and ashes. These relatively quiescent systems eventually release lithogenic silica, exchange cations with seawater, and enhance carbon and nutrient burial over wider areas and sediment volumes across the continental slopes. Thus, they may be similarly important to the global biogeochemical cycles. However, because of redox stratification, alkalinity and many solutes are internally recycled so that the influence on overlying water-column chemistry of such deep-seated forward weathering zones may be limited.

Models extending over multiple depositional cycles and environments will be required to investigate the scale dependences of net weathering and alkalinity fluxes.

6. CONCLUSIONS

We developed a batch reaction model that combines equilibrium aqueous chemistry and kinetic concepts from sediment biogeochemistry and mineral sciences to explore the solution-mediated interplay of organic and inorganic matter alteration in episodically reworked deltaic and estuarine sediments. Representative end-member reactant mixtures were chosen to reflect terrestrial inputs from highly weathered (Amazon) and minimally weathered (Iceland) terrains. Two kinetic approaches to precipitation were tested, (I) a mechanistic nucleation-growth model and (II) an improved phenomenological pH-Si-dependent batch rate law. Despite the scarcity of information on precipitation kinetics and parametrizations, microenvironments and transport-feedbacks, the models can reasonably reproduce observed diagenetic conditions and product suites over timescales characteristic of natural sedimentary dynamics in deltaic systems. This general agreement allowed us to investigate in detail the influences of reactant mixtures and evolving biogeochemical conditions on silicate weathering and diagenetic reaction balances.

Both model approaches consistently lead to robust, mineral solubility-based patterns of coupled silicate, carbonate, sulfide and phosphate reactions with progression of organic matter oxidation through the sequence of terminal electron acceptors (O_2, NO_3^-, MnO_2, $Fe(OH)_3$, SO_4^{2-}, CO_2). The patterns emerge from the dynamic feedback between inorganic dissolution and precipitation and their response to organic matter degradation. In combination with a wide range of field observations and previous conceptual frameworks of authigenic mineral occurrences, we used the model to develop a generalized explanatory framework for silicate weathering fluxes and diagenetic reaction balances in marine sediments. The concept is based on the evolution of porewater chemistry through organic matter degradation, silicate weathering and mineral authigenesis, and implies a dynamic coupling between the sedimentary cycles of H^+, C, P, Fe, S, Si, Mg, K, and Ca. In this framework, reverse (acid) silicate weathering is most likely and intense under suboxic, Fe-rich conditions that promote the green clay formation and are sustained through seasonal reworking in major sedimentary environments, such as deltaic mobile muds. Moreover, rapid rates of green clay authigenesis, as observed in Amazon delta sediments, likely require supplies from cation-depleted, highly reactive, likely amorphous and nanoparticulate Al(-Si-Fe-Mn) sources in addition to feldspar. This implies a general tendency to green clay formation and reverse weathering near tropical river deltas and in many bio-siliceous sediments, supporting published theories that link occurrences of authigenic minerals to climate-dependent, terrestrial supplies of metastable reactants and biomineralization. High sediment fluxes and protracted reworking and refluxing drive large biogeochemical fluxes from and into these deltaic sediments (Aplin & Taylor, 2012; Michalopoulos & Aller, 2004; Odin, 1990; Porrenga, 1967).

In contrast, forward (alkaline) and carbonate-producing diagenetic weathering is facilitated by relatively fresh and reactive material with high ratios of cations (Na, K, Mg, Ca, Mn, Fe) to structural elements that are needed for silicate precipitation (Si, Al, Fe), e.g., basaltic rocks and tephra. The tendency to forward weathering increases under sulfidic, Fe-depleted conditions, as relatively cation-poor aluminous clays and non-silicates stabilize at the expanse of green clays. Anoxic forward silicate weathering promotes carbonate, phosphate, and sulfide precipitation and burial, but may have limited influence on the overlying water due to sedimentary redox stratification and internal recycling.

These results support the 'weathering continuum' concept (Trapp-Müller et al., in press) and demonstrate a potential for Earth system feedbacks involving endogenic and exogenic forces, and physical, chemical and biological processes. Moreover, our conceptual framework of silicate weathering dynamics and diagenetic reaction balances in marine sediments can aid the quantification of global biogeochemical fluxes between sediment and seawater, the interpretation of the geological record, and targeted enhanced weathering approaches to carbon dioxide reduction and environmental governance.

ACKNOWLEDGMENTS

We thank Josephine Aller for logistical assistance, and Olivier Sulpis and Wytze Lenstra for useful comments on the contextualization and presentation of our model results. Further, we appreciate the valuable comments and suggestions from our reviewers and associate editor, which have substantially improved the manuscript.

FUNDING

This work was carried out under the umbrella of the Netherlands Earth System Science Center (NESSC) and supported by a NESSC travel grant. The project received funding from the European Union Horizon 2020 research and innovation program under Marie Skłodowska-Curie grant agreement No 847504. RCA was supported by US NSF grant OCE-2321875.

STATEMENT OF ORIGINALITY

The content of this paper, *"Silicate weathering and diagenetic reaction balances in deltaic muds"*, is original and has not been submitted, accepted, or published elsewhere. The content forms part of the first author's PhD thesis at Utrecht University.

CONFLICT OF INTEREST

The authors declare no conflicts of interest.

Editor: C. Page Chamberlain, Associate Editor: Donald Canfield

Submitted: June 18, 2024 EDT. Accepted: April 08, 2025 EDT.
Published: May 19, 2025 EDT.

REFERENCES

Aagaard, P., & Helgeson, H. C. (1982). Thermodynamic and kinetic constraints on reaction rates among minerals and aqueous solutions; I, Theoretical considerations. *American Journal of Science*, *282*(3), 237–285. https://doi.org/10.2475/ajs.282.3.237

Aller, J. Y., & Aller, R. C. (1986). General characteristics of benthic faunas on the Amazon inner continental shelf with comparison to the shelf off the Changjiang River, East China Sea. *Continental Shelf Research*, *6*(1–2), 291–310. https://doi.org/10.1016/0278-4343(86)90065-8

Aller, R. C. (1980). Quantifying solute distributions in the bioturbated zone of marine sediments by defining an average microenvironment. *Geochimica et Cosmochimica Acta*, *44*(12), 1955–1965. https://doi.org/10.1016/0016-7037(80)90195-7

Aller, R. C. (1994). Bioturbation and remineralization of sedimentary organic matter: effects of redox oscillation. *Chemical Geology*, *114*(3–4), 331–345. https://doi.org/10.1016/0009-2541(94)90062-0

Aller, R. C. (1998). Mobile deltaic and continental shelf muds as suboxic, fluidized bed reactors. *Marine Chemistry*, *61*(3–4), 143–155. https://doi.org/10.1016/S0304-4203(98)00024-3

Aller, R. C. (2004). Conceptual models of early diagenetic processes: the muddy seafloor as an unsteady, batch reactor. *Journal of Marine Research*, *62*(6), 815–835. https://doi.org/10.1357/0022240042880837

Aller, R. C., & Blair, N. E. (2006). Carbon remineralization in the Amazon-Guianas tropical mobile mudbelt: a sedimentary incinerator. *Continental Shelf Research*, *26*(17–18), 2241–2259. https://doi.org/10.1016/j.csr.2006.07.016

Aller, R. C., Blair, N. E., & Brunskill, G. J. (2008). Early diagenetic cycling, incineration, and burial of sedimentary organic carbon in the central Gulf of Papua (Papua New Guinea). *Journal of Geophysical Research: Earth Surface*, *113*(F1). https://doi.org/10.1029/2006JF000689

Aller, R. C., Blair, N. E., Xia, Q., & Rude, P. D. (1996). Remineralization rates, recycling, and storage of carbon in Amazon shelf sediments. *Continental Shelf Research*, *16*(5–6), 753–786. https://doi.org/10.1016/0278-4343(95)00046-1

Aller, R. C., & Cochran, J. K. (2019). The critical role of bioturbation for particle dynamics, priming potential, and organic C remineralization in marine sediments: local and basin scales. *Frontiers in Earth Science*, *7*, 157. https://doi.org/10.3389/feart.2019.00157

Aller, R. C., Mackin, J. E., & Cox, R. T., Jr. (1986). Diagenesis of Fe and S in Amazon inner shelf muds: apparent dominance of Fe reduction and implications for the genesis of ironstones. *Continental Shelf Research*, *6*(1–2), 263–289. https://doi.org/10.1016/0278-4343(86)90064-6

Aller, R. C., & Rude, P. D. (1988). Complete oxidation of solid phase sulfides by manganese and bacteria in anoxic marine sediments. *Geochimica et Cosmochimica Acta*, *52*(3), 751–765. https://doi.org/10.1016/0016-7037(88)90335-3

Aller, R. C., & Wehrmann, L. M. (2025). Sedimentary diagenesis, depositional environments, and benthic fluxes. *Treatise on Geochemistry*, 573–629. https://doi.org/10.1016/b978-0-323-99762-1.00095-4

Aloisi, G., Wallmann, K., Drews, M., & Bohrmann, G. (2004). Evidence for the submarine weathering of silicate minerals in Black Sea sediments: possible implications for the marine Li and B cycles. *Geochemistry, Geophysics, Geosystems*, *5*(4), QO4007. https://doi.org/10.1029/2003GC000639

Altree-Williams, A., Brugger, J., Pring, A., & Bedrikovetsky, P. (2019). Coupled reactive flow and dissolution with changing reactive surface and porosity. *Chemical Engineering Science*, *206*, 289–304. https://doi.org/10.1016/j.ces.2019.05.016

Altree-Williams, A., Pring, A., Ngothai, Y., & Brugger, J. (2015). Textural and compositional complexities resulting from coupled dissolution-reprecipitation reactions in geomaterials. *Earth-Science Reviews*, *150*, 628–651. https://doi.org/10.1016/j.earscirev.2015.08.013

Anthony, E. J., Gardel, A., Gratiot, N., Proisy, C., Allison, M. A., Dolique, F., & Fromard, F. (2010). The Amazon-influenced muddy coast of South America: a review of mud-bank-shoreline interactions. *Earth-Science Reviews*, *103*(3–4), 99–121. https://doi.org/10.1016/j.earscirev.2010.09.008

Aplin, A. C., & Taylor, K. G. (2012). Mineralogy of marine sediment systems: a geochemical framework. *Environmental Mineralogy II*, 123–176. https://doi.org/10.1180/EMU-notes.13.4

Aradóttir, E. S. P., Sonnenthal, E. L., Björnsson, G., & Jónsson, H. (2012). Multidimensional reactive transport modeling of CO2 mineral sequestration in basalts at the Hellisheidi geothermal field, Iceland. *International Journal of Greenhouse Gas Control*, *9*, 24–40. https://doi.org/10.1016/j.ijggc.2012.02.006

Aradóttir, E. S. P., Sonnenthal, E. L., & Jónsson, H. (2012). Development and evaluation of a thermodynamic dataset for phases of interest in CO_2 mineral sequestration in basaltic rocks. *Chemical Geology*, *304–305*, 26–38. https://doi.org/10.1016/j.chemgeo.2012.01.031

Bachmat, Y., & Bear, J. (1986). Macroscopic modelling of transport phenomena in porous media. 1: The continuum approach. *Transport in Porous Media*, *1*(3), 213–240. https://doi.org/10.1007/bf00238181

Bailey, S. W. (1988). Odinite, a new dioctahedral-trioctahedral Fe3+-rich 1:1 clay mineral. *Clay Minerals*, *23*(3), 237–247. https://doi.org/10.1180/claymin.1988.023.3.01

Baldermann, A., Dietzel, M., Mavromatis, V., Mittermayr, F., Warr, L. N., & Wemmer, K. (2017). The role of Fe on the formation and diagenesis of interstratified glauconite-smectite and illite-smectite: a case study of Upper Cretaceous shallow-water carbonates. *Chemical Geology*, *453*, 21–34. https://doi.org/10.1016/j.chemgeo.2017.02.008

Baldermann, A., Warr, L. N., Grathoff, G. H., & Dietzel, M. (2013). The rate and mechanism of deep-sea glauconite formation at the Ivory Coast-Ghana Marginal Ridge. *Clays and Clay Minerals*, *61*(3), 258–276. https://doi.org/10.1346/CCMN.2013.0610307

Baldermann, A., Warr, L. N., Letofsky-Papst, I., & Mavromatis, V. (2015). Substantial iron sequestration during green-clay authigenesis in modern deep-sea sediments. *Nature Geoscience*, *8*(11), 885–889. https://doi.org/10.1038/ngeo2542

Bao, R., van der Voort, T. S., Zhao, M., Guo, X., Montluçon, D. B., McIntyre, C., & Eglinton, T. I. (2018). Influence of Hydrodynamic Processes on the Fate of Sedimentary Organic Matter on Continental Margins. *Global Biogeochemical Cycles*, *32*(9), 1420–1432. https://doi.org/10.1029/2018GB005921

Bao, R., Zhao, M., McNichol, A., Galy, V., McIntyre, C., Haghipour, N., & Eglinton, T. I. (2019). Temporal constraints on lateral organic matter transport along a coastal mud belt. *Organic Geochemistry*, *128*, 86–93. https://doi.org/10.1016/j.orggeochem.2019.01.007

Barale, L., Petriglieri, J. R., Botta, S., & Piana, F. (2022). Low-temperature, diagenetic serpentinization of peridotite clasts in lower Miocene marine conglomerates, Torino Hill, NW Italy. *Marine and Petroleum Geology*, *143*, 105830. https://doi.org/10.1016/j.marpetgeo.2022.105830

Beckingham, L. E., Steefel, C. I., Swift, A. M., Voltolini, M., Yang, L., Anovitz, L. M., Sheets, J. M., Cole, D. R., Kneafsey, T. J., Mitnick, E. H., Zhang, S., Landrot, G., Ajo-Franklin, J. B., DePaolo, D. J., Mito, S., & Xue, Z. (2017). Evaluation of accessible mineral surface areas for improved prediction of mineral reaction rates in porous media. *Geochimica et Cosmochimica Acta*, *205*, 31–49. https://doi.org/10.1016/j.gca.2017.02.006

Berner, E. K., & Berner, R. A. (2012). *Global environment: water, air, and geochemical cycles* (2nd ed.). Princeton University Press. https://doi.org/10.1515/9781400842766

Berner, R. A. (1970). Sedimentary pyrite formation. *American Journal of Science*, *268*(1), 1–23. https://doi.org/10.2475/ajs.268.1.1

Berner, R. A. (1980). *Early diagenesis: a theoretical approach*. Princeton University Press. https://doi.org/10.1515/9780691209401

Berner, R. A. (1981). A new geochemical classification of sedimentary environments. *SEPM Journal of Sedimentary Research*, *51*(2), 359–365. https://doi.org/10.1306/212F7C7F-2B24-11D7-8648000102C1865D

Berner, R. A. (1991). A model for atmospheric CO_2 over Phanerozoic time. *American Journal of Science*, *291*(4), 339–376. https://doi.org/10.2475/ajs.291.4.339

Berner, R. A., Lasaga, A. C., & Garrels, R. M. (1983). The carbonate-silicate geochemical cycle and its effect on atmospheric carbon dioxide over the past 100 million years. *American Journal of Science*, *283*(7), 641–683. https://doi.org/10.2475/ajs.283.7.641

Berner, R. A., Scott, M. R., & Thomlinson, C. (1970). Carbonate alkalinity in the pore waters of anoxic marine sediments. *Limnology and Oceanography*, *15*(4), 544–549. https://doi.org/10.4319/lo.1970.15.4.0544

Beusen, A. H. W., Bouwman, A. F., Van Beek, L. P. H., Mogollón, J. M., & Middelburg, J. J. (2016). Global riverine N and P transport to ocean increased during the 20th century despite increased retention along the aquatic continuum. *Biogeosciences*, *13*(8), 2441–2451. https://doi.org/10.5194/bg-13-2441-2016

Bianchi, T. S. (2011). The role of terrestrially derived organic carbon in the coastal ocean: A changing paradigm and the priming effect. *Proceedings of the National Academy of Sciences*, *108*(49), 19473–19481. https://doi.org/10.1073/pnas.1017982108

Bianchi, T. S., Aller, R. C., Atwood, T. B., Brown, C. J., Buatois, L. A., Levin, L. A., Levinton, J. S., Middelburg, J. J., Morrison, E. S., Regnier, P., Shields, M. R., Snelgrove, P. V. R., Sotka, E. E., & Stanley, R. R. E. (2021). What global biogeochemical consequences will marine animal-sediment interactions have during climate change? *Elementa: Science of the Anthropocene*, *9*(1), 00180. https://doi.org/10.1525/elementa.2020.00180

Bianchi, T. S., Mayer, L. M., Amaral, J. H. F., Arndt, S., Galy, V., Kemp, D. B., Kuehl, S. A., Murray, N. J., & Regnier, P. (2024). Anthropogenic impacts on mud and organic carbon cycling. *Nature Geoscience*, *17*, 287–297. https://doi.org/10.1038/s41561-024-01405-5

Blair, N. E., & Aller, R. C. (2012). The fate of terrestrial organic carbon in the marine environment. *Annual Review of Marine Science*, *4*(1), 401–423. https://doi.org/10.1146/annurev-marine-120709-142717

Bonatti, E. (1963). Zeolites in Pacific pelagic sediments. *Transactions of the New York Academy of Sciences*, *25*(8), 938. https://doi.org/10.1111/j.2164-0947.1963.tb01930.x

Bonatti, E. (1965). Palagonite, hyaloclastites and alteration of volcanic glass in the ocean. *Bulletin Volcanologique*, *28*(8), 257–269. https://doi.org/10.1007/BF02596930

Bonatti, E., Emiliani, C., Ferrara, G., Honnorez, J., & Rydell, H. (1974). Ultramafic-carbonate breccias from the Equatorial Mid Atlantic Ridge. *Marine Geology*, *16*(2), 83–102. https://doi.org/10.1016/0025-3227(74)90057-7

Bonatti, E., Lawrence, J. R., & Morandi, N. (1984). Serpentinization of oceanic peridotites: temperature dependence of mineralogy and boron content. *Earth and Planetary Science Letters*, *70*(1), 88–94. https://doi.org/10.1016/0012-821X(84)90211-5

Boudreau, B. P. (1994). Is burial velocity a master parameter for bioturbation? *Geochimica et Cosmochimica Acta*, *58*(4), 1243–1249. https://doi.org/10.1016/0016-7037(94)90378-6

Boudreau, B. P. (1996). A method-of-lines code for carbon and nutrient diagenesis in aquatic sediments. *Computers & Geosciences*, *22*(5), 479–496. https://doi.org/10.1016/0098-3004(95)00115-8

Boudreau, B. P. (1997). *Diagenetic models and their implementation: modelling transport and reactions in aquatic sediments*. Springer.

Boudreau, B. P., & Canfield, D. E. (1988). A provisional diagenetic model for pH in anoxic porewaters: application to the FOAM Site. *Journal of Marine Research*, *46*(2), 429–455. https://doi.org/10.1357/002224088785113603

Boudreau, B. P., & Canfield, D. E. (1993). A comparison of closed- and open-system models for porewater pH and calcite-saturation state. *Geochimica et Cosmochimica Acta*, *57*(2), 317–334. https://doi.org/10.1016/0016-7037(93)90434-X

Brantley, S. L., Shaughnessy, A., Lebedeva, M. I., & Balashov, V. N. (2023). How temperature-dependent silicate weathering acts as Earth's geological thermostat. *Science*, *379*(6630), 382–389. https://doi.org/10.1126/science.add2922

Brown, E., Colling, A., Park, D., Phillips, J., Rothery, D., & Wright, J. (1995). *Seawater: its Composition, Properties and Behaviour*. Butterworth Heinemann and The Open University. https://doi.org/10.1016/c2013-0-10208-5

Burdige, D. J. (1993). The biogeochemistry of manganese and iron reduction in marine sediments. *Earth-Science Reviews*, *35*(3), 249–284. https://doi.org/10.1016/0012-8252(93)90040-E

Burdige, D. J. (2006). *Geochemistry of Marine Sediments*. Princeton University Press. https://doi.org/10.2307/j.ctv131bw7s.22

Burst, J. F. (1958). "Glauconite" pellets: their mineral nature and applications to stratigraphic interpretations. *AAPG Bulletin*, *42*(2), 310–3277. https://doi.org/10.1306/0BDA5A7D-16BD-11D7-8645000102C1865D

Burton, W. K., Cabrera, N., & Frank, F. C. (1949). Role of Dislocations in Crystal growth. *Nature*, *163*(4141), 398–399. https://doi.org/10.1038/163398a0

Caillère, S., & Hénin, S. (1949). Experimental formation of chlorites from montmorillonite. *Mineralogical Magazine and Journal of the Mineralogical Society*, *28*(205), 612–620. https://doi.org/10.1180/minmag.1949.028.205.10

Caldeira, K. (1995). Long-term control of atmospheric carbon dioxide; low-temperature seafloor alteration or terrestrial silicate-rock weathering. *American Journal of Science*, *295*(9), 1077–1114. https://doi.org/10.2475/ajs.295.9.1077

Calvert, S. E. (1971). Composition and origin of North Atlantic Deep Sea cherts. *Contributions to Mineralogy and Petrology*, *33*(4), 273–288. https://doi.org/10.1007/bf00382569

Canfield, D. E., Thamdrup, B., & Hansen, J. W. (1993). The anaerobic degradation of organic matter in Danish coastal sediments: Iron reduction, manganese reduction, and sulfate reduction. *Geochimica et Cosmochimica Acta*, *57*(16), 3867–3883. https://doi.org/10.1016/0016-7037(93)90340-3

Caves, J. K., Jost, A. B., Lau, K. V., & Maher, K. (2016). Cenozoic carbon cycle imbalances and a variable weathering feedback. *Earth and Planetary Science Letters*, *450*, 152–163. https://doi.org/10.1016/j.epsl.2016.06.035

Cetiner, J. E. P., Berelson, W. M., Rollins, N. E., Barnhart, H. A., Liu, X., Dong, S., Byrne, R. H., & Adkins, J. F. (2023). Novel device to collect deep-sea porewater in situ: a focus on benthic carbonate chemistry. *Limnology and Oceanography: Methods*, *21*(2), 82–97. https://doi.org/10.1002/lom3.10530

Chanda, P., Kohli, A., Teng, F.-Z., & Fantle, M. S. (2023). Clay authigenesis in carbonate-rich sediments and its impact on carbonate diagenesis. *Geochimica et Cosmochimica Acta*, *346*, 76–101. https://doi.org/10.1016/j.gca.2023.02.002

Closset, I., Brzezinski, M. A., Cardinal, D., Dapoigny, A., Jones, J. L., & Robinson, R. S. (2022). A silicon isotopic perspective on the contribution of diagenesis to the sedimentary silicon budget in the Southern Ocean. *Geochimica et Cosmochimica Acta*, *327*, 298–313. https://doi.org/10.1016/j.gca.2022.04.010

Cloud, P. E., Jr. (1955). Physical limits to glauconite formation. *AAPG Bulletin*, *39*(4), 484–492. https://doi.org/10.1306/5CEAE166-16BB-11D7-8645000102C1865D

Cole, T. G. (1985). Composition, oxygen isotope geochemistry and origin of smectite in the metalliferous sediments of the Bauer Deep, southeast Pacific. *Geochimica et Cosmochimica Acta*, *49*(1), 221–235. https://doi.org/10.1016/0016-7037(85)90206-6

Cole, T. G., & Shaw, H. F. (1983). The nature and origin of authigenic smectites in some recent marine sediments. *Clay Minerals*, *18*(3), 239–252. https://doi.org/10.1180/claymin.1983.018.3.02

De Borger, E., Tiano, J., Braeckman, U., Rijnsdorp, A. D., & Soetaert, K. (2021). Impact of bottom trawling on sediment biogeochemistry: A modelling approach. *Biogeosciences*, *18*(8), 2539–2557. https://doi.org/10.5194/bg-18-2539-2021

De Lange, G. J., Cranston, R. E., Hydes, D. H., & Boust, D. (1992). Extraction of pore water from marine sediments: a review of possible artifacts wit pertinent examples from the North Atlantic. *Marine Geology*, *109*(1–2), 53–76. https://doi.org/10.1016/0025-3227(92)90220-C

De Lange, G. J., & Rispens, F. B. (1986). Indication of a diagenetically induced precipitate of an Fe-Si mineral in sediment from the Nares abyssal plain, Western North Atlantic. *Marine Geology*, *73*(1–2), 85–97. https://doi.org/10.1016/0025-3227(86)90112-X

Delerce, S., Heřmanská, M., Bénézeth, P., Schott, J., & Oelkers, E. H. (2023). Experimental determination of the reactivity of basalts as a function of their degree of alteration. *Geochimica et Cosmochimica Acta*, *360*, 106–121. https://doi.org/10.1016/j.gca.2023.09.007

Deng, H., Tournassat, C., Molins, S., Claret, F., & Steefel, C. I. (2021). A pore-scale investigation of mineral precipitation driven diffusivity change at the column-scale. *Water Resources Research*, *57*, e2020WR028483. https://doi.org/10.1029/2020WR028483

Du, J., Haley, B. A., Mix, A. C., Abbott, A. N., McManus, J., & Vance, D. (2022). Reactive-transport modeling of neodymium and its radiogenic isotope in deep-sea sediments: The roles of authigenesis, marine silicate weathering and reverse weathering. *Earth and Planetary Science Letters*, *596*, 117792. https://doi.org/10.1016/j.epsl.2022.117792

Ébelmen, J.-J. (1845). Sur les produits de la décomposition des espèces minérales de la famille des silicates. *Annales Des Mines*, *7*(3), 66.

Egger, M., Jilbert, T., Behrends, T., Rivard, C., & Slomp, C. P. (2015). Vivianite is a major sink for phosphorus in methanogenic coastal surface sediments. *Geochimica et Cosmochimica Acta*, *169*, 217–235. https://doi.org/10.1016/j.gca.2015.09.012

Egger, M., Rasigraf, O., Sapart, C. J., Jilbert, T., Jetten, M. S. M., Röckmann, T., van Der Veen, C., Bânda, N., Kartal, B., Ettwig, K. F., & Slomp, C. P. (2015). Iron-mediated anaerobic oxidation of methane in brackish coastal sediments. *Environmental Science & Technology*, *49*(1), 277–283. https://doi.org/10.1021/es503663z

Ehlert, C., Doering, K., Wallmann, K., Scholz, F., Sommer, S., Grasse, P., Geilert, S., & Frank, M. (2016). Stable silicon isotope signatures of marine pore waters – biogenic opal dissolution versus authigenic clay mineral formation. *Geochimica et Cosmochimica Acta*, *191*, 102–117. https://doi.org/10.1016/j.gca.2016.07.022

Eisaman, M. D., Geilert, S., Renforth, P., Bastianini, L., Campbell, J., Dale, A. W., Foteinis, S., Grasse, P., Hawrot, O., Löscher, C. R., Rau, G. H., & Rønning, J. (2023). Assessing technical aspects of ocean alkalinity enhancement approaches. *State of Planet Discussions*, 1–52. https://doi.org/10.5194/sp-2-oae2023-3-2023

Fabre, S., Jeandel, C., Zambardi, T., Roustan, M., & Almar, R. (2019). An overlooked silica source of the modern oceans: are sandy beaches the key? *Frontiers in Earth Science*, *7*, 231. https://doi.org/10.3389/feart.2019.00231

Fodor, M. A., Ható, Z., Kristóf, T., & Pósfai, M. (2020). The role of clay surfaces in the heterogeneous nucleation of calcite: molecular dynamics simulations of cluster formation and attachment. *Chemical Geology*, *538*, 119497. https://doi.org/10.1016/j.chemgeo.2020.119497

Frings, P. J., De La Rocha, C., Struyf, E., van Pelt, D., Schoelynck, J., Hudson, M. M., Gondwe, M. J., Wolski, P., Mosimane, K., Gray, W., Schaller, J., & Conley, D. J. (2014). Tracing silicon cycling in the Okavango Delta, a sub-tropical flood-pulse wetland using silicon isotopes. *Geochimica et Cosmochimica Acta*, *142*, 132–148. https://doi.org/10.1016/j.gca.2014.07.007

Froelich, P. N., Klinkhammer, G. P., Bender, M. L., Luedtke, N. A., Heath, G. R., Cullen, D., Dauphin, P., Hammond, D., Hartman, B., & Maynard, V. (1979). Early oxidation of organic matter in pelagic sediments of the eastern equatorial Atlantic: suboxic diagenesis. *Geochimica et Cosmochimica Acta*, *43*(7), 1075–1090. https://doi.org/10.1016/0016-7037(79)90095-4

Fuhr, M., Geilert, S., Schmidt, M., Liebetrau, V., Vogt, C., Ledwig, B., & Wallmann, K. (2022). Kinetics of olivine weathering in seawater: an experimental study. *Frontiers in Climate*, *4*. https://doi.org/10.3389/fclim.2022.831587

Gattuso, J. P., Magnan, A. K., Bopp, L., Cheung, W. W. L., Duarte, C. M., Hinkel, J., Mcleod, E., Micheli, F., Oschlies, A., Williamson, P., Billé, R., Chalastani, V. I., Gates, R. D., Irisson, J. O., Middelburg, J. J., Pörtner, H. O., & Rau, G. H. (2018). Ocean solutions to address climate change and its effects on marine ecosystems. *Frontiers in Marine Science*, *5*, 337. https://doi.org/10.3389/fmars.2018.00337

Gebauer, D., Kellermeier, M., Gale, J. D., Bergström, L., & Cölfen, H. (2014). Pre-nucleation clusters as solute precursors in crystallisation. *Chemical Society Reviews*, *43*(7), 2348–2371. https://doi.org/10.1039/c3cs60451a

Geilert, S., Frick, D. A., Garbe-Schönberg, D., Scholz, F., Sommer, S., Grasse, P., Vogt, C., & Dale, A. W. (2023). Coastal El Niño triggers rapid marine silicate alteration on the seafloor. *Nature Communications*, *14*(1). https://doi.org/10.1038/s41467-023-37186-5

Geilert, S., Grasse, P., Wallmann, K., Liebetrau, V., & Menzies, C. D. (2020). Serpentine alteration as source of high dissolved silicon and elevated δ30Si values to the marine Si cycle. *Nature Communications*, *11*(1). https://doi.org/10.1038/s41467-020-18804-y

Gibbs, R. J. (1967). The Geochemistry of the Amazon River System: Part I. The Factors that Control the Salinity and the Composition and Concentration of the Suspended Solids. *Geological Society of America Bulletin*, *78*(10), 1203–1232. https://doi.org/10.1130/0016-7606(1967)78[1203:TGOTAR]2.0.CO;2

Gibbs, R. J. (1973). Mechanisms of Trace Metal Transport in Rivers. *Science*, *180*(4081), 71–73. https://doi.org/10.1126/science.180.4081.71

Giffaut, E., Grivé, M., Blanc, P., Vieillard, P., Colàs, E., Gailhanou, H., Gaboreau, S., Marty, N., Madé, B., & Duro, L. (2014). Andra thermodynamic database for performance assessment: ThermoChimie. *Applied Geochemistry*, *49*, 225–236. https://doi.org/10.1016/j.apgeochem.2014.05.007

Giresse, P. (2022). Quaternary glauconitization on Gulf of Guinea, glauconite factory: overview of and new data on tropical Atlantic continental shelves and deep slopes. *Minerals*, *12*(7), 908. https://doi.org/10.3390/min12070908

Giresse, P., Bayon, G., Tallobre, C., & Loncke, L. (2021). Neodymium isotopes in glauconite for palaeoceanographic reconstructions at continental margins: a preliminary investigation from Demerara rise. *Frontiers in Earth Science*, *9*. https://doi.org/10.3389/feart.2021.652501

Giresse, P., Wiewiora, A., & Lacka, B. (1988). Mineral phases and processes within green peloids from two recent deposits near the Congo River mouth. *Clay Minerals*, *23*(4), 447–458. https://doi.org/10.1180/claymin.1988.023.4.11

Gruber, C., Harlavan, Y., Pousty, D., Winkler, D., & Ganor, J. (2019). Enhanced chemical weathering of albite under seawater conditions and its potential effect on the Sr ocean budget. *Geochimica et Cosmochimica Acta*, *261*, 20–34. https://doi.org/10.1016/j.gca.2019.06.049

Gustafsson, E., Hagens, M., Sun, X., Reed, D. C., Humborg, C., Slomp, C. P., & Gustafsson, B. G. (2019). Sedimentary alkalinity generation and long-term alkalinity development in the Baltic Sea. *Biogeosciences*, *16*(2), 437–456. https://doi.org/10.5194/bg-16-437-2019

Haile, B. G., Hellevang, H., Aagaard, P., & Jahren, J. (2015). Experimental nucleation and growth of smectite and chlorite coatings on clean feldspar and quartz grain surfaces. *Marine and Petroleum Geology*, *68*, 664–674. https://doi.org/10.1016/j.marpetgeo.2015.02.006

Hartmann, J., Moosdorf, N., Lauerwald, R., Hinderer, M., & West, A. J. (2014). Global chemical weathering and associated p-release — the role of lithology, temperature and soil properties. *Chemical Geology*, *363*, 145–163. https://doi.org/10.1016/j.chemgeo.2013.10.025

Hartmann, J., West, A. J., Renforth, P., Köhler, P., De La Rocha, C. L., Wolf-gladrow, D. A., Dürr, H. H., & Scheffran, J. (2013). Enhanced chemical weathering as a geoengineering strategy to reduce atmospheric carbon dioxide, supply nutrients, and mitigate ocean acidification. *Reviews of Geophysics*, *51*(2), 113–149. https://doi.org/10.1002/rog.20004

Hay, R. L. (1966). Zeolites and Zeolitic Reactions in Sedimentary Rocks. *Geological Society of America Special Papers*, 85. https://doi.org/10.1130/SPE85

Hayes, M. O. (1967). Relationships between coastal climate and bottom sediment type on the inner continental shelf. *Marine Geology*, *5*(2), 111–132. https://doi.org/10.1016/0025-3227(67)90074-6

Hellevang, H., Pham, V. T. H., & Aagaard, P. (2013). Kinetic modelling of CO2–water–rock interactions. *International Journal of Greenhouse Gas Control*, *15*, 3–15. https://doi.org/10.1016/j.ijggc.2013.01.027

Hellmann, R., Wirth, R., Daval, D., Barnes, J.-P., Penisson, J.-M., Tisserand, D., Epicier, T., Florin, B., & Hervig, R. L. (2012). Unifying natural and laboratory chemical weathering with interfacial dissolution-reprecipitation: A study based on the nanometer-scale chemistry of fluid-silicate interfaces. *Chemical Geology*, *294–295*, 203–216. https://doi.org/10.1016/j.chemgeo.2011.12.002

Heřmanská, M., Voigt, M. J., Marieni, C., Declercq, J., & Oelkers, E. H. (2022). A comprehensive and internally consistent mineral dissolution rate database: Part I: primary silicate minerals and glasses. *Chemical Geology*, *597*, 120807. https://doi.org/10.1016/j.chemgeo.2022.120807

Heřmanská, M., Voigt, M. J., Marieni, C., Declercq, J., & Oelkers, E. H. (2023). A comprehensive and consistent mineral dissolution rate database: Part II: secondary silicate minerals. *Chemical Geology*, *636*, 121632. https://doi.org/10.1016/j.chemgeo.2023.121632

Higgins, J. A., & Schrag, D. P. (2015). The Mg isotopic composition of Cenozoic seawater - evidence for a link between Mg-clays, seawater Mg/Ca, and climate. *Earth and Planetary Science Letters*, *416*, 73–81. https://doi.org/10.1016/j.epsl.2015.01.003

Hilton, R. G., & West, A. J. (2020). Mountains, erosion and the carbon cycle. *Nature Reviews Earth & Environment*, *1*(6), 284–299. https://doi.org/10.1038/s43017-020-0058-6

Hong, W. L., Torres, M. E., & Kutterolf, S. (2020). Towards a global quantification of volcanogenic aluminosilicate alteration rates through the mass balance of strontium in marine sediments. *Chemical Geology*, *550*, 119743. https://doi.org/10.1016/j.chemgeo.2020.119743

Hu, X., & Cai, W.-J. (2011). An assessment of ocean margin anaerobic processes on oceanic alkalinity budget. *Global Biogeochemical Cycles*, *25*(3). https://doi.org/10.1029/2010GB003859

Hulskamp, R., Luijendijk, A., van Maren, B., Moreno-Rodenas, A., Calkoen, F., Kras, E., Lhermitte, S., & Aarninkhof, S. (2023). Global distribution and dynamics of muddy coasts. *Nature Communications*, *14*(1). https://doi.org/10.1038/s41467-023-43819-6

Iacoviello, F., Giorgetti, G., Nieto, F., & Memmi, I. T. (2012). Evolution with depth from detrital to authigenic smectites in sediments from AND-2A drill core (McMurdo Sound, Antarctica). *Clay Minerals*, *47*(4), 481–498. https://doi.org/10.1180/claymin.2012.047.4.07

Intergovernmental Panel on Climate Change (IPCC). (2023). *Climate Change 2021: The Physical Science Basis*. Cambridge University Press. https://doi.org/10.1017/9781009157896

Isson, T. T., & Planavsky, N. J. (2018). Reverse weathering as a long-term stabilizer of marine pH and planetary climate. *Nature*, *560*(7719), 471–475. https://doi.org/10.1038/s41586-018-0408-4

Isson, T. T., Planavsky, N. J., Coogan, L. A., Stewart, E. M., Ague, J. J., Bolton, E. W., Zhang, S., McKenzie, N. R., & Kump, L. R. (2020). Evolution of the global carbon cycle and climate regulation on earth. *Global Biogeochemical Cycles*, *34*(2), 1–28. https://doi.org/10.1029/2018GB006061

Jahnke, R. (1985). A model of microenvironments in deep-sea sediments: formation and effects on porewater profiles. *Limnology and Oceanography*, *30*(5), 966–971. https://doi.org/10.4319/lo.1985.30.5.0956

Jahnke, R. A., Emerson, S. R., Roe, K. K., & Burnett, W. C. (1983). The present day formation of apatite in Mexican continental margin sediments. *Geochimica et Cosmochimica Acta*, *47*(2), 259–266. https://doi.org/10.1016/0016-7037(83)90138-2

Jeandel, C., & Oelkers, E. H. (2015). The influence of terrigenous particulate material dissolution on ocean chemistry and global element cycles. *Chemical Geology*, *395*, 50–66. https://doi.org/10.1016/j.chemgeo.2014.12.001

Jones, M. T., Pearce, C. R., Jeandel, C., Gislason, S. R., Eiriksdottir, E. S., Mavromatis, V., & Oelkers, E. H. (2012). Riverine particulate material dissolution as a significant flux of strontium to the oceans. *Earth and Planetary Science Letters*, *355–356*, 51–59. https://doi.org/10.1016/j.epsl.2012.08.040

Jørgensen, B. B. (1977). Distribution of colorless sulfur bacteria (Beggiatoa spp.) in a coastal marine sediment. *Marine Biology*, *41*(1), 19–28. https://doi.org/10.1007/BF00390577

Kashchiev, D. (2011). Note: On the critical supersaturation for nucleation. *Journal of Chemical Physics*, *134*(19), 10–12. https://doi.org/10.1063/1.3593401

Kashchiev, D., & van Rosmalen, G. M. (2003). Nucleation in solutions revisited. *Crystal Research and Technology*, *38*(7–8), 555–574. https://doi.org/10.1002/crat.200310070

Kastner, M. (1979). Chapter 4. Zeolites. In *Marine Minerals* (pp. 111–122). De Gruyter. https://doi.org/10.1515/9781501508646-008

Kastner, M. (1999). Oceanic minerals: Their origin, nature of their environment, and significance. *Proceedings of the National Academy of Sciences of the United States of America*, *96*(7), 3380–3387. https://doi.org/10.1073/pnas.96.7.3380

Keene, J. B., & Kastner, M. (1974). Clays and formation of deep-sea chert. *Nature*, *249*(5459), 754–755. https://doi.org/10.1038/249754a0

Khalil, K., Rabouille, C., Gallinari, M., Soetaert, K., DeMaster, D. J., & Ragueneau, O. (2007). Constraining biogenic silica dissolution in marine sediments: a comparison between diagenetic models and experimental dissolution rates. *Marine Chemistry*, *106*(1–2), 223–238. https://doi.org/10.1016/j.marchem.2006.12.004

Kineke, G. C., Sternberg, R. W., Trowbridge, J. H., & Geyer, W. R. (1996). Fluid-mud processes on the Amazon continental shelf. *Continental Shelf Research*, *16*(5–6), 667–696. https://doi.org/10.1016/0278-4343(95)00050-X

Krause, A. J., Sluijs, A., van der Ploeg, R., Lenton, T. M., & Pogge von Strandmann, P. A. E. (2023). Enhanced clay formation key in sustaining the Middle Eocene Climatic Optimum. *Nature Geoscience*, *16*(8), 730–738. https://doi.org/10.1038/s41561-023-01234-y

Krissansen-Totton, J., & Catling, D. C. (2020). A coupled carbon-silicon cycle model over Earth history: reverse weathering as a possible explanation of a warm mid-Proterozoic climate. *Earth and Planetary Science Letters*, *537*, 116181. https://doi.org/10.1016/j.epsl.2020.116181

Ku, T. C. W., & Walter, L. M. (2003). Syndepositional formation of Fe-rich clays in tropical shelf sediments, San Blas Archipelago, Panama. *Chemical Geology*, *197*(1–4), 197–213. https://doi.org/10.1016/S0009-2541(02)00363-7

Kuehl, S. A., DeMaster, D. J., & Nittrouer, C. A. (1986). Nature of sediment accumulation on the Amazon continental shelf. *Continental Shelf Research*, *6*(1–2), 209–225. https://doi.org/10.1016/0278-4343(86)90061-0

Kuehl, S. A., Williams, J., Liu, J. P., Harris, C., Aung, D. W., Tarpley, D., Goodwyn, M., & Aye, Y. Y. (2019). Sediment dispersal and accumulation off the Ayeyarwady delta – Tectonic and oceanographic controls. *Marine Geology*, *417*, 106000. https://doi.org/10.1016/j.margeo.2019.106000

Kump, L. R., & Arthur, M. A. (1997). Global Chemical Erosion during the Cenozoic: Weatherability Balances the Budgets. In W. F. Ruddiman (Ed.), *Tectonic Uplift and Climate Change* (pp. 399–426). https://doi.org/10.1007/978-1-4615-5935-1_18

Kump, L. R., Brantley, S. L., & Arthur, M. A. (2000). Chemical weathering, atmospheric CO_2, and climate. *Annual Review of Earth and Planetary Sciences*, *28*(1), 611–667. https://doi.org/10.1146/annurev.earth.28.1.611

Lasaga, A. C., & Luttge, A. (2001). Variation of Crystal Dissolution Rate Based on a Dissolution Stepwave Model. *Science*, *291*(5512), 2400–2404. https://doi.org/10.1126/science.1058173

Li, W., Liu, X.-M., Wang, K., McManus, J., Haley, B. A., Takahashi, Y., Shakouri, M., & Hu, Y. (2022). Potassium isotope signatures in modern marine sediments: Insights into early diagenesis. *Earth and Planetary Science Letters*, *599*. https://doi.org/10.1016/j.epsl.2022.117849

Liu, J. T., Hsu, R. T., Yang, R. J., Wang, Y. P., Wu, H., Du, X., Li, A., Chien, S. C., Lee, J., Yang, S., Zhu, J., Su, C.-C., Chang, Y., & Huh, C.-A. (2018). A comprehensive sediment dynamics study of a major mud belt system on the inner shelf along an energetic coast. *Scientific Reports*, *8*, 4229. https://doi.org/10.1038/s41598-018-22696-w

Lönartz, M. I., Yang, Y., Deissmann, G., Bosbach, D., & Poonoosamy, J. (2023). Capturing the dynamic processes of porosity clogging. *Water Resources Research*, *59*(11). https://doi.org/10.1029/2023WR034722

Longman, J., Palmer, M. R., & Gernon, T. M. (2020). Viability of greenhouse gas removal via artificial addition of volcanic ash to the ocean. *Anthropocene*, *32*, 100264. https://doi.org/10.1016/j.ancene.2020.100264

Loucaides, S., Michalopoulos, P., Presti, M., Koning, E., Behrends, T., & Van Cappellen, P. (2010). Seawater-mediated interactions between diatomaceous silica and terrigenous sediments: results from long-term incubation experiments. *Chemical Geology*, *270*(1–4), 68–79. https://doi.org/10.1016/j.chemgeo.2009.11.006

Luo, M., Hong, W. L., Torres, M. E., Kutterolf, S., Pank, K., Hopkins, J. L., Solomon, E. A., Wang, K. L., & Lee, H. Y. (2023). Volcanogenic aluminosilicate alteration drives formation of authigenic phases at the northern Hikurangi margin: implications for subseafloor geochemical cycles. *Chemical Geology*, *619*, 121317. https://doi.org/10.1016/j.chemgeo.2023.121317

Luo, M., Li, W., Geilert, S., Dale, A. W., Song, Z., & Chen, D. (2022). Active silica diagenesis in the deepest hadal trench sediments. *Geophysical Research Letters*, *49*(14), e2022GL099365. https://doi.org/10.1029/2022GL099365

Luo, M., Torres, M. E., Hong, W.-L., Pape, T., Fronzek, J., Kutterolf, S., Mountjoy, J. J., Orpin, A., Henkel, S., Huhn, K., Chen, D., & Kasten, S. (2020). Impact of iron release by volcanic ash alteration on carbon cycling in sediments of the northern Hikurangi margin. *Earth and Planetary Science Letters*, *541*, 116288. https://doi.org/10.1016/j.epsl.2020.116288

Luttge, A., Arvidson, R. S., Fischer, C., & Kurganskaya, I. (2019). Kinetic concepts for quantitative prediction of fluid-solid interactions. *Chemical Geology*, *504*, 216–235. https://doi.org/10.1016/j.chemgeo.2018.11.016

Mackenzie, F. T., & Garrels, R. M. (1965). Silicates: reactivity with sea water. *Science*, *150*(3692), 57–58. https://doi.org/10.1126/science.150.3692.57

Mackenzie, F. T., & Garrels, R. M. (1966). Chemical mass balance between rivers and oceans. *American Journal of Science*, *264*(7), 507–525. https://doi.org/10.2475/ajs.264.7.507

Mackin, J. E. (1986). Control of dissolved Al distributions in marine sediments by clay reconstitution reactions: Experimental evidence leading to a unified theory. *Geochimica et Cosmochimica Acta*, *50*(2), 207–214. https://doi.org/10.1016/0016-7037(86)90170-5

Mackin, J. E. (1989). Relationships between Si, Al, and Fe deposited on filter-covered glass substrates in marine sediments and in suspensions of sediments and standard clays. *Marine Chemistry*, *26*(1), 101–117. https://doi.org/10.1016/0304-4203(89)90055-8

Mackin, J. E., & Aller, R. C. (1984a). Ammonium adsorption in marine sediments 1. *Limnology and Oceanography*, *29*(2), 250–257. https://doi.org/10.4319/lo.1984.29.2.0250

Mackin, J. E., & Aller, R. C. (1984b). Diagenesis of dissolved aluminum in organic-rich estuarine sediments. *Geochimica et Cosmochimica Acta*, *48*(2), 299–313. https://doi.org/10.1016/0016-7037(84)90252-7

Mackin, J. E., & Aller, R. C. (1984c). Dissolved Al in sediments and waters of the East China Sea: implications for authigenic mineral formation. *Geochimica et Cosmochimica Acta*, *48*(2), 281–297. https://doi.org/10.1016/0016-7037(84)90251-5

Mackin, J. E., & Aller, R. C. (1986). The effects of clay mineral reactions on dissolved Al distributions in sediments and waters of the Amazon continental shelf. *Continental Shelf Research*, *6*(1–2), 245–262. https://doi.org/10.1016/0278-4343(86)90063-4

Mackin, J. E., Aller, R. C., & Ullman, W. J. (1988). The effects of iron reduction and nonsteady-state diagenesis on iodine, ammonium, and boron distributions in sediments from the Amazon continental shelf. *Continental Shelf Research*, *8*(4), 363–386. https://doi.org/10.1016/0278-4343(88)90009-X

Maher, K., Steefel, C. I., DePaolo, D. J., & Viani, B. E. (2006). The mineral dissolution rate conundrum: insights from reactive transport modeling of U isotopes and pore fluid chemistry in marine sediments. *Geochimica et Cosmochimica Acta*, *70*(2), 337–363. https://doi.org/10.1016/j.gca.2005.09.001

Malmgren, L., & Brydsten, L. (1992). Sedimentation of river-transported particles in the Öre estuary, northern Sweden. *Hydrobiologica*, *235*, 59–69. https://doi.org/10.1007/BF00026200

Martens, C. S., & Berner, R. A. (1977). Interstitial water chemistry of anoxic long island sound sediments. 1. Dissolved gases. *Limnology and Oceanography*, *22*(1), 10–25. https://doi.org/10.4319/lo.1977.22.1.0010

Marty, N. C. M., Claret, F., Lassin, A., Tremosa, J., Blanc, P., Madé, B., Giffaut, E., Cochepin, B., & Tournassat, C. (2015). A database of dissolution and precipitation rates for clay-rocks minerals. *Applied Geochemistry*, *55*, 108–118. https://doi.org/10.1016/j.apgeochem.2014.10.012

Matter, J. M., Stute, M., Snæbjörnsdottir, S. Ó., Oelkers, E. H., Gislason, S. R., Aradottir, E. S., Sigfusson, B., Gunnarsson, I., Sigurdardottir, H., Gunnlaugsson, E., Axelsson, G., Alfredsson, H. A., Wolff-Boenisch, D., Mesfin, K., Fernandez de la Reguera Taya, D., Hall, J., Dideriksen, K., & Broecker, W. S. (2016). Rapid carbon mineralization for permanent disposal of anthropogenic carbon dioxide emissions. *Science*, *352*(6291), 1312–1314. https://doi.org/10.1126/science.aad8132

Mayer, L. M. (1994). Surface area control of organic carbon accumulation in continental shelf sediments. *Geochimica et Cosmochimica Acta*, *58*(4), 1271–1284. https://doi.org/10.1016/0016-7037(94)90381-6

McKee, B. A., Aller, R. C., Allison, M. A., Bianchi, T. S., & Kineke, G. C. (2004). Transport and transformation of dissolved and particulate materials on continental margins influenced by major rivers: Benthic boundary layer and seabed processes. *Continental Shelf Research*, *24*(7–8), 899–926. https://doi.org/10.1016/j.csr.2004.02.009

McKinley, J. M., Worden, R. H., & Ruffell, A. H. (1999). Smectite in sandstones: a review of the controls on occurrence and behaviour during diagenesis. In R. H. Worden & S. Morad (Eds.), *Clay Mineral Cements in Sandstones* (pp. 109–128). Wiley. https://doi.org/10.1002/9781444304336.ch5

Meister, P., Herda, G., Petrishcheva, E., Gier, S., Dickens, G. R., Bauer, C., & Liu, B. (2022). Microbial alkalinity production and silicate alteration in methane charged marine sediments: implications for porewater chemistry and diagenetic carbonate formation. *Frontiers in Earth Science*, *9*. https://doi.org/10.3389/feart.2021.756591

Meysman, F. J. R., & Montserrat, F. (2017). Negative CO2 emissions via enhanced silicate weathering in coastal environments. *Biology Letters*, *13*(4). https://doi.org/10.1098/rsbl.2016.0905

Michalopoulos, P., & Aller, R. C. (1995). Rapid clay mineral formation in Amazon delta sediments: reverse weathering and oceanic elemental cycles. *Science*, *270*(5236), 614–617. https://doi.org/10.1126/science.270.5236.614

Michalopoulos, P., & Aller, R. C. (2004). Early diagenesis of biogenic silica in the Amazon delta: Alteration, authigenic clay formation, and storage. *Geochimica et Cosmochimica Acta*, *68*(5), 1061–1085. https://doi.org/10.1016/j.gca.2003.07.018

Michalopoulos, P., Aller, R. C., & Reeder, R. J. (2000). Conversion of diatoms to clays during early diagenesis in tropical, continental shelf muds. *Geology*, *28*(12), 1095–1098. https://doi.org/10.1130/0091-7613(2000)28%3C1095:CODTCD%3E2.0.CO;2

Middelburg, J. J. (1990). Early diagenesis and authigenic mineral formation in anoxic sediments of Kau Bay, Indonesia [Ph.D. Thesis, Utrecht University]. In *Geologica Ultraiectina* (pp. 1–177). http://dspace.library.uu.nl/handle/1874/238641

Middelburg, J. J., de Lange, G. J., & Kreulen, R. (1990). Dolomite formation in anoxic sediments of Kau Bay, Indonesia. *Geology*, *1*, 399–402. https://doi.org/10.1130/0091-7613(1990)018%3C0399:DFIASO%3E2.3.CO;2

Middelburg, J. J., De Lange, G. J., & van Der Wejjden, C. H. (1987). Manganese solubility control in marine pore waters. *Geochimica et Cosmochimica Acta*, *51*(3), 759–763. https://doi.org/10.1016/0016-7037(87)90086-X

Middelburg, J. J., Soetaert, K., & Hagens, M. (2020). Ocean alkalinity, buffering and biogeochemical processes. *Reviews of Geophysics*, *58*(3). https://doi.org/10.1029/2019RG000681

Milliken, K. L. (2003). Late diagenesis and mass transfer in sandstone-shale sequences. In H. D. Holland & K. K. Turekian (Eds.), *Treatise in Geochemistry* (2nd ed., Vol. 7, pp. 159–190). https://doi.org/10.1016/B0-08-043751-6/07091-2

Milliken, K. L., & Land, L. S. (1991). Reverse weathering, the carbonate-feldspar system, and porosity evolution during burial of sandstones. *American Association of Petroleum Geologists Bulletin*, *75*(3).

Milliken, K. L., & Land, L. S. (1993). The origin and fate of silt sized carboante in subsurface miocene oligocene mudstones. *Sedimentology*, *40*(1), 107–124. https://doi.org/10.1111/j.1365-3091.1993.tb01094.x

Milliken, K. L., Lynch, F. L., & Seifert, K. E. (1996). Marine weathering of serpentinite and serpentinite breccias, Sites 897 and 899, Iberia abyssal plain. *Proceedings of the Ocean Drilling Program, Scientific Results*, *149*, 529–540. https://doi.org/10.2973/odp.proc.sr.149.222.1996

Montserrat, F., Renforth, P., Hartmann, J., Leermakers, M., Knops, P., & Meysman, F. J. R. (2017). Olivine dissolution in seawater: implications for CO2 sequestration through enhanced weathering in coastal environments. *Environmental Science & Technology*, *51*(7), 3960–3972. https://doi.org/10.1021/acs.est.6b05942

Moore, W. S., Astwood, H., & Lindstrom, C. (1995). Radium isotopes in coastal waters on the Amazon shelf. *Geochimica et Cosmochimica Acta*, *59*(20), 4285–4298. https://doi.org/10.1016/0016-7037(95)00242-R

Mucci, A. (2004). The behavior of mixed Ca-Mn carbonates in water and seawater: controls of manganese concentrations in marine porewaters. *Aquatic Geochemistry*, *10*, 139–169. https://doi.org/10.1023/B:AQUA.0000038958.56221.b4

Müller, G. (1967). Diagenesis in argillaceous sediments. *Developments in Sedimentology*, *8*, 127–177. https://doi.org/10.1016/S0070-4571(08)70843-4

Müller, G., Fritzsche, M. B. K., Dohmen, L., & Geisler, T. (2022). Feedbacks and non-linearity of silicate glass alteration in hyperalkaline solution studied by in operando fluid-cell Raman spectroscopy. *Geochimica et Cosmochimica Acta*, *329*, 1–21. https://doi.org/10.1016/j.gca.2022.05.013

Müller, G., Middelburg, J. J., & Sluijs, A. (2021). Introducing GloRiSe - A global database on river sediment composition. *Earth System Science Data*, *13*(7), 3565–3575. https://doi.org/10.5194/essd-13-3565-2021

Niedermeier, D. R. D., Putnis, A., Geisler, T., Golla-Schindler, U., & Putnis, C. V. (2009). The mechanism of cation and oxygen isotope exchange in alkali feldspars under hydrothermal conditions. *Contributions to Mineralogy and Petrology*, *157*(1), 65–76. https://doi.org/10.1007/s00410-008-0320-2

Odin, G. S. (1990). Clay mineral formation at the continent-ocean boundary: the verdine facies. *Clay Minerals*, *25*(4), 477–483. https://doi.org/10.1180/claymin.1990.025.4.06

Odin, G. S., & Morton, A. C. (1988). Authigenic green particles from marine environments. *Developments in Sedimentology*, *43*, 213–264. https://doi.org/10.1016/S0070-4571(08)70009-8

O'Neil, J. R., & Taylor, H. P. (1967). The oxygen isotope and cation exchange chemistry of feldspars. *American Mineralogist*, *52*(9–10), 1414–1437.

Palandri, J. L., & Kharaka, Y. K. (2004). *A compilation of rate parameters of water-mineral interaction kinetics for application to geochemical modeling* (Open File Report Nos. 2004–1068). U.S. Geological Survey. https://doi.org/10.3133/ofr20041068

Parkhurst, D. L., & Appelo, C. A. J. (2013). *Description of Input and Examples for PHREEQC Version 3: A Computer Program for Speciation, Batch-Reaction, One-Dimensional Transport, and Inverse Geochemical Calculations* [Techniques and Methods 6-A43]. U.S. Geological Survey. https://doi.org/10.3133/tm6A43

Petzing, J., & Chester, B. (1979). Authigenic marine zeolites and their relationship to global volcanism. *Marine Geology*, *29*(1–4), 253–271. https://doi.org/10.1016/0025-3227(79)90112-9

Pham, V. T. H., Lu, P., Aagaard, P., Zhu, C., & Hellevang, H. (2011). On the potential of CO2-water-rock interactions for CO2 storage using a modified kinetic model. *International Journal of Greenhouse Gas Control*, *5*(4), 1002–1015. https://doi.org/10.1016/j.ijggc.2010.12.002

Pogge von Strandmann, P. A. E., Jones, M. T., West, A. J., Murphy, M. J., Stokke, E. W., Tarbuck, G., Wilson, D. J., Pearce, C. R., & Schmidt, D. N. (2021). Lithium isotope evidence for enhanced weathering and erosion during the Paleocene-Eocene Thermal Maximum. *Science Advances*, *7*(42), eabh4224. https://doi.org/10.1126/sciadv.abh4224

Porrenga, D. H. (1967). Glauconite and chamosite as depth indicators in the marine environment. *Marin Geology*, *5*(5–6), 495–501. https://doi.org/10.1016/0025-3227(67)90056-4

Postma, D. (1993). The reactivity of iron oxides in sediments: a kinetic approach. *Geochimica et Cosmochimica Acta*, *57*(21–22), 5027–5034. https://doi.org/10.1016/S0016-7037(05)80015-8

Poulton, S. W., & Raiswell, R. (2002). The low-temperature geochemical cycle of iron: from continental fluxes to marine sediment deposition. *American Journal of Science*, *302*(9), 774–805. https://doi.org/10.2475/ajs.302.9.774

Presti, M., & Michalopoulos, P. (2008). Estimating the contribution of the authigenic mineral component to the long-term reactive silica accumulation on the western shelf of the Mississippi River Delta. *Continental Shelf Research*, *28*(2), 823–838. https://doi.org/10.1016/j.csr.2007.12.015

Putnis, A. (2009). Mineral replacement reactions. *Reviews in Mineralogy and Geochemistry*, *70*(1), 87–124. https://doi.org/10.2138/rmg.2009.70.3

Putnis, A. (2015). Transient porosity resulting from fluid-mineral interaction and its consequences. *Reviews in Mineralogy and Geochemistry*, *80*(1), 1–23. https://doi.org/10.2138/rmg.2015.80.01

Putnis, C. V., & Ruiz-Agudo, E. (2021). Nanoparticles formed during mineral-fluid interactions. *Chemical Geology*, *586*, 120614. https://doi.org/10.1016/j.chemgeo.2021.120614

Rahman, S., Aller, R. C., & Cochran, J. K. (2016). Cosmogenic 32Si as a tracer of biogenic silica burial and diagenesis: major deltaic sinks in the silica cycle. *Geophysical Research Letters*, *43*(13), 7124–7132. https://doi.org/10.1002/2016GL069929

Rahman, S., Aller, R. C., & Cochran, J. K. (2017). The missing silica sink: revisiting the marine sedimentary Si cycle using cosmogenic 32Si. *Global Biogeochemical Cycles*, *31*(10), 1559–1578. https://doi.org/10.1002/2017GB005746

Rahman, S., & Trower, E. J. (2023). Probing surface Earth reactive silica cycling using stable Si isotopes: mass balance, fluxes, and deep time implications. *Science Advances*, *9*(49), eadi2440. https://doi.org/10.1126/sciadv.adi2440

Raiswell, R., & Canfield, D. E. (2012). The iron biogeochemical cycle past and present. *Geochemical Perspectives*, *1*(1), 1–220. https://doi.org/10.7185/geochempersp.1.1

Ransom, B., Kim, D., Kastner, M., & Wainwright, S. (1998). Organic matter preservation on continental slopes: importance of mineralogy and surface area. *Geochimica et Cosmochimica Acta*, *62*(8), 1329–1345. https://doi.org/10.1016/S0016-7037(98)00050-7

Regnier, P., Resplandy, L., Najjar, R. G., & Ciais, P. (2022). The land-to-ocean loops of the global carbon cycle. *Nature*, *603*(7901), 401–410. https://doi.org/10.1038/s41586-021-04339-9

Riech, V., & von Rad, U. (1979). Silica diagenesis in the Atlantic Ocean: diagenetic potential and transformations. In M. Talwani, W. Hay, & W. B. F. Ryan (Eds.), *Deep Drilling Results in the Atlantic Ocean: Continental Margins and Paleoenvironment* (Vol. 3, pp. 315–340). https://doi.org/10.1029/ME003p0315

Rimstidt, J. D., Zhang, Y., & Zhu, C. (2016). Rate equations for sodium catalyzed amorphous silica dissolution. *Geochimica et Cosmochimica Acta*, *195*, 120–125. https://doi.org/10.1016/j.gca.2016.09.020

Rousseau, T. C. C., Roddaz, M., Moquet, J.-S., Handt Delgado, H., Calves, G., & Bayon, G. (2019). Controls on the geochemistry of suspended sediments from large tropical South American rivers (Amazon, Orinoco and Maroni). *Chemical Geology*, *522*, 38–54. https://doi.org/10.1016/j.chemgeo.2019.05.027

Rude, P. D., & Aller, R. C. (1989). Early diagenetic alteration of lateritic particle coatings in Amazon continental shelf sediments. *Journal of SedimentaryResearch*, *59*(5), 704–716. https://doi.org/10.1306/212F9052-2B24-11D7-8648000102C1865D

Rude, P. D., & Aller, R. C. (1994). Fluorine uptake by Amazon continental shelf sediment and its impact in the global fluorine cycle. *Continental Shelf Research*, *14*(7/8), 883–907. https://doi.org/10.1016/0278-4343(94)90078-7

Ruiz-Agudo, E., King, H. E., Patiño-López, L. D., Putnis, C. V., Geisler, T., Rodriguez-Navarro, C., & Putnis, A. (2016). Control of silicate weathering by interface-coupled dissolution-precipitation processes at the mineral-solution interface. *Geology*, *44*(7), 567–570. https://doi.org/10.1130/G37856.1

Ruiz-Agudo, E., Putnis, C. V., Rodriguez-Navarro, C., & Putnis, A. (2012). Mechanism of leached layer formation during chemical weathering of silicate minerals. *Geology*, *40*(10), 947–950. https://doi.org/10.1130/G33339.1

Ruttenberg, K. C. (1992). Development of a sequential extraction method for different forms of phosphorus in marine sediments. *Limnology and Oceanography*, *37*(7), 1460–1482. https://doi.org/10.4319/lo.1992.37.7.1460

Ruttenberg, K. C., & Goñi, M. A. (1997). Phosphorus distribution, C:N:P ratios, and δ13Coc in arctic, temperate, and tropical coastal sediments: tools for characterizing bulk sedimentary organic matter. *Marine Geology*, *139*(1–4), 123–145. https://doi.org/10.1016/S0025-3227(96)00107-7

Saltelli, A., Ratto, M., Andres, T., Campolongo, F., Cariboni, J., Gatelli, D., Saisana, M., & Tarantola, S. (2008). *Global Sensitivity Analysis. The Primer*. Wiley. https://doi.org/10.1002/9780470725184

Santiago Ramos, D. P., Morgan, L. E., Lloyd, N. S., & Higgins, J. A. (2018). Reverse weathering in marine sediments and the geochemical cycle of potassium in seawater: insights from the K isotopic composition (41K/39K) of deep-sea pore-fluids. *Geochimica et Cosmochimica Acta*, *236*, 99–120. https://doi.org/10.1016/j.gca.2018.02.035

Sayles, F. L., & Mangelsdorf, P. C., Jr. (1977). The equilibration of clay minerals with sea water: exchangereactions. *Geochimica et Cosmochimica Acta*, *41*(7), 951–960. https://doi.org/10.1016/0016-7037(77)90154-5

Schnoor, J. L. (1990). Kinetics of chemical weathering: a comparison of laboratory and field weathering rates. In W. Stumm (Ed.), *Aquatic chemical kinetics: reaction rates of processes in natural waters* (pp. 475–504). John Wiley and Sons.

Scholz, F., Hensen, C., Schmidt, M., & Geersen, J. (2013). Submarine weathering of silicate minerals and the extent of pore water freshening at active continental margins. *Geochimica et Cosmochimica Acta*, *100*, 200–216. https://doi.org/10.1016/j.gca.2012.09.043

Schrag, D. P., Higgins, J. A., Macdonald, F. A., & Johnston, D. T. (2013). Authigenic carbonate and the history of the global carbon cycle. *Science*, *339*(6119), 540–543. https://doi.org/10.1126/science.1229578

Schwertmann, U., & Taylor, R. M. (1989). Iron oxides. In B. Dixon & S. B. Weed (Eds.), *Minerals in Soil Environments* (Vol. 1, pp. 379–427). https://doi.org/10.2136/sssabookser1.2ed.c8

Siever, R., Beck, K. C., & Berner, R. A. (1965). Composition of interstitial waters of modern sediments. *The Journal of Geology*, *73*(1), 39–73. https://doi.org/10.1086/627045

Sillén, L. G. (1967). The ocean as a chemical system. *Science*, *156*, 1189–1196. https://doi.org/10.1126/science.156.3779.1189

Soetaert, K., Herman, P. M. J., & Middelburg, J. J. (1996). A model of early diagenetic processes from the shelf to abyssal depths. *Geochimica et Cosmochimica Acta*, *60*(6), 1019–1040. https://doi.org/10.1016/0016-7037(96)00013-0

Soetaert, K., Hofmann, A. F., Middelburg, J. J., Meysman, F. J. R., & Greenwood, J. (2007). The effect of biogeochemical processes on pH. *Marine Chemistry*, *105*(1–2), 30–51. https://doi.org/10.1016/j.marchem.2006.12.012

Song, S., Santos, I. R., Yu, H., Wang, F., Burnett, W. C., Bianchi, T. S., Dong, J., Lian, E., Zhao, B., Mayer, L., Yao, Q., Yu, Z., & Xu, B. (2022). A global assessment of the mixed layer in coastal sediments and implications for carbon storage. *Nature Communications*, *13*(1). https://doi.org/10.1038/s41467-022-32650-0

Spiegel, T., Vosteen, P., Wallmann, K., Paul, S. A. L., Gledhill, M., & Scholz, F. (2021). Updated estimates of sedimentary potassium sequestration and phosphorus release on the Amazon shelf. *Chemical Geology*, *560*, 120017. https://doi.org/10.1016/j.chemgeo.2020.120017

Stallard, R. F. (1985). River chemistry, geology, geomorphology, and soils in the amazon and orinoco basins. In J. I. Drever (Ed.), *The Chemistry of Weathering* (Vol. 149, pp. 293–314). Springer. https://doi.org/10.1007/978-94-009-5333-8_17

Steefel, C. I., Beckingham, L. E., & Landrot, G. (2015). Micro-continuum approaches for modeling pore-scale geochemical processes. *Reviews in Mineralogy and Geochemistry*, *80*(1), 217–246. https://doi.org/10.2138/rmg.2015.80.07

Steefel, C. I., & Van Cappellen, P. (1990). A new kinetic approach to modeling water-rock interaction: the role of nucleation, precursors, and Ostwald ripening. *Geochimica et Cosmochimica Acta*, *54*(10), 2651–2611. https://doi.org/10.1016/0016-7037(90)90003-4

Steiner, Z., Rae, J. W. B., Berelson, W. M., Adkins, J. F., Hou, Y., Dong, S., Lampronti, G. I., Liu, X., Achterberg, E. P., Subhas, A. V., & Turchyn, A. V. (2022). Authigenic formation of clay minerals in the Abyssal North Pacific. *Global Biogeochemical Cycles*, *36*(11). https://doi.org/10.1029/2021gb007270

Stroncik, N. A., & Schmincke, H.-U. (2001). Evolution of palagonite: crystallization, chemical changes, and element budget. *Geochemistry, Geophysics, Geosystems*, *2*(7), 2000GC000102. https://doi.org/10.1029/2000GC000102

Stroncik, N. A., & Schmincke, H.-U. (2002). Palagonite - a review. *International Journal of Earth Sciences*, *91*(4), 680–697. https://doi.org/10.1007/s00531-001-0238-7

Stumm, W., & Morgan, J. J. (2013). *Aquatic Chemistry: Chemical Equilibria and Rates in Natural Waters*. John Wiley & Sons.

Suess, E. (1979). Mineral phases formed in anoxic sediments by microbial decomposition of organic matter. *Geochimica et Cosmochimica Acta*, *43*(3), 339–352. https://doi.org/10.1016/0016-7037(79)90199-6

Sulpis, O., Humphreys, M. P., Wilhelmus, M. M., Carroll, D., Berelson, W. M., Menemenlis, D., Middelburg, J. J., & Adkins, J. F. (2022). RADIv1: a non-steady-state early diagenetic model for ocean sediments in Julia and MATLAB/GNU Octave. *Geoscientific Model Development*, *15*(5), 2105–2131. https://doi.org/10.5194/gmd-15-2105-2022

Swindale, L. D., & Fan, P.-F. (1967). Transformation of gibbsite to chlorite in ocean bottom sediments. *Science*, *157*(3790), 799–800. https://doi.org/10.1126/science.157.3790.799

Syvitski, J., Ángel, J. R., Saito, Y., Overeem, I., Vörösmarty, C., Wang, H., & Olago, D. (2022). Earth's sediment cycle during the Anthropocene. *Nature Reviews Earth & Environment*, *3*, 179–196. https://doi.org/10.1038/s43017-021-00253-w

Syvitski, J. P. M., & Milliman, J. D. (2007). Geology, geography, and humans battle for dominance over the delivery of fluvial sediment to the coastal ocean. *The Journal of Geology*, *115*(1), 1–19. https://doi.org/10.1086/509246

Syvitski, J. P. M., Smith, J. N., Calabrese, E. A., & Boudreau, B. P. (1988). Basin sedimentation and the growth of prograding deltas. *Journal of Geophysical Research: Oceans*, *93*(C6), 6895–6908. https://doi.org/10.1029/jc093ic06p06895

The MathWorks, Inc. (2023). *MATLAB* (Version R2023b) [Computer software]. The MathWorks, Inc. https://www.mathworks.com/

Thorpe, M. T., Hurowitz, J. A., & Dehouck, E. (2019). Sediment geochemistry and mineralogy from a glacial terrain river system in southwest Iceland. *Geochimica et Cosmochimica Acta*, *263*, 140–166. https://doi.org/10.1016/j.gca.2019.08.003

Torres, M. E., Hong, W.-L., Solomon, E. A., Milliken, K., Kim, J. H., Sample, J. C., Teichert, B. M. A., & Wallmann, K. (2020). Silicate weathering in anoxic marine sediment as a requirement for authigenic carbonate burial. *Earth-Science Reviews*, *200*, 102960. https://doi.org/10.1016/j.earscirev.2019.102960

Torres, M. E., Milliken, K. L., Hüpers, A., Kim, J. H., & Lee, S. G. (2022). Authigenic clays versus carbonate formation as products of marine silicate weathering in the input sequence to the Sumatra Subduction Zone. *Geochemistry, Geophysics, Geosystems*, *23*(4), e2022GC010338. https://doi.org/10.1029/2022GC010338

Tosca, N. J., Guggenheim, S., & Pufahl, P. K. (2016). An authigenic origin for Precambrian greenalite: implications for iron formation and the chemistry of ancient seawater. *Geological Society of America Bulletin*, *128*(3–4), 511–530. https://doi.org/10.1130/b31339.1

Tosca, N. J., & Masterson, A. L. (2014). Chemical controls on incipient Mg-silicate crystallization at 25°C: implications for early and late diagenesis. *Clay Minerals*, *49*(2), 165–194. https://doi.org/10.1180/claymin.2014.049.2.03

Trapp-Müller, G., Caves Rugenstein, J., Conley, D., Geilert, S., Hagens, M., Van Hinsbergen, D. J. J., Hong, W.-L., Jeandel, C., Longman, J., Mason, P., Middelburg, J. J., Milliken, K. L., Navarre-Sitchler, A., Planavsky, N., Reichart, G.-J., Slomp, C. P., Sluijs, A., & Zhang, X. Y. (in press). Earth's weathering continuum. *Nature Geoscience*.

Tréguer, P. J., & De La Rocha, C. L. (2013). The world ocean silica cycle. *Annual Review of Marine Science*, *5*(1), 477–501. https://doi.org/10.1146/annurev-marine-121211-172346

Truesdale, V. W., & Greenwood, J. E. (2015). Improved templating of the net-rate of mineral batch-dissolutions. *Geochimica et Cosmochimica Acta*, *164*, 428–440. https://doi.org/10.1016/j.gca.2015.04.055

Tsukimura, K., Miyoshi, Y., Takagi, T., Suzuki, M., & Wada, S. -i. (2021). Amorphous nanoparticles in clays, soils and marine sediments analyzed with a small angle X-ray scattering (SAXS) method. *Scientific Reports*, *11*(1), 6997. https://doi.org/10.1038/s41598-021-86573-9

Turchyn, A. V., Bradbury, H. J., Walker, K., & Sun, X. (2021). Controls on the precipitation of carbonate minerals within marine sediments. *Frontiers in Earth Science*. https://doi.org/10.3389/feart.2021.618311

Urey, H. C. (1952). On the Early Chemical History of the Earth and the Origin of Life. *Proceedings of the National Academy of Sciences*, *38*(4), 351–363. https://doi.org/10.1073/pnas.38.4.351

van Bennekom, A. J., Fred Jansen, J. H., van der Gaast, S. J., van Iperen, J. M., & Pieters, J. (1989). Aluminium-rich opal: an intermediate in the preservation of biogenic silica in the Zaire (Congo) deep-sea fan. *Deep Sea Research Part A. Oceanographic Research Papers*, *36*(2), 173–190. https://doi.org/10.1016/0198-0149(89)90132-5

Van Cappellen, P., Dixit, S., & van Beusekom, J. (2002). Biogenic silica dissolution in the oceans: Reconciling experimental and field-based dissolution rates. *Global Biogeochemical Cycles*, *16*(4). https://doi.org/10.1029/2001gb001431

Van Cappellen, P., & Wang, Y. (1996). Cycling of iron and manganese in surface sediments; a general theory for the coupled transport and reaction of carbon, oxygen, nitrogen, sulfur, iron, and manganese. *American Journal of Science*, *296*(3), 197–243. https://doi.org/10.2475/ajs.296.3.197

van de Velde, S. J., Reinhard, C. T., Ridgwell, A., & Meysman, F. J. R. (2020). Bistability in the redox chemistry of sediments and oceans. *Proceedings of the National Academy of Sciences of the United States of America*, *117*(52), 33043–33050. https://doi.org/10.1073/PNAS.2008235117

van de Velde, S. J., Van Lancker, V., Hidalgo-Martinez, S., Berelson, W. M., & Meysman, F. J. R. (2018). Anthropogenic disturbance keeps the coastal seafloor biogeochemistry in a transient state. *Scientific Reports*, *8*(1). https://doi.org/10.1038/s41598-018-23925-y

van Hoek, W. J., Wang, J., Vilmin, L., Beusen, A. H. W., Mogollón, J. M., Müller, G., Pika, P. A., Liu, X., Langeveld, J. J., Bouwman, A. F., & Middelburg, J. J. (2021). Exploring spatially explicit changes in carbon budgets of global river basins during the 20th century. *Environmental Science & Technology*, *55*(24), 16757–16769. https://doi.org/10.1021/acs.est.1c04605

Velbel, M. A. (1993). Constancy of silicate-mineral weathering-rate ratios between natural and experimental weathering: implications for hydrologic control of differences in absolute rates. *Chemical Geology*, *105*(1–3), 89–99. https://doi.org/10.1016/0009-2541(93)90120-8

Verhagen, I. T. E., Crisóstomo-Figueroa, A., Utley, J. E. P., & Worden, R. H. (2020). Abrasion of detrital grain-coating clays during sediment transport: implications for diagenetic clay coats. *Sedimentary Geology*, *403*, 105653. https://doi.org/10.1016/j.sedgeo.2020.105653

von Blanckenburg, F. (2005). The control mechanisms of erosion and weathering at basin scale from cosmogenic nuclides in river sediment. *Earth and Planetary Science Letters*, *237*(3–4), 462–479. https://doi.org/10.1016/j.epsl.2005.06.030

Wallmann, K., Aloisi, G., Haeckel, M., Tishchenko, P., Pavlova, G., Greinert, J., Kutterolf, S., & Eisenhauer, A. (2008). Silicate weathering in anoxic marine sediments. *Geochimica et Cosmochimica Acta*, *72*(12), 2895–2918. https://doi.org/10.1016/j.gca.2008.03.026

Wallmann, K., Geilert, S., & Scholz, F. (2023). Chemical alteration of riverine particles in seawater and marine sediments: effects on seawater composition and atmospheric CO_2. *American Journal of Science*, *323*, 7. https://doi.org/10.2475/001c.87455

Wang, K., Shi, X., Qiao, S., Kornkanitnan, N., & Khokiattiwong, S. (2015). Distribution and composition of authigenic minerals in surface sediments of the western Gulf of Thailand. *Acta Oceanologica Sinica*, *34*(12), 125–136. https://doi.org/10.1007/s13131-015-0772-y

Wang, Y., & Van Cappellen, P. (1996). A multicomponent reactive transport model of early diagenesis: Application to redox cycling in coastal marine sediments. *Geochimica et Cosmochimica Acta*, *60*(16), 2993–3014. https://doi.org/10.1016/0016-7037(96)00140-8

Ward, J. P. J., Hendry, K. R., Arndt, S., Faust, J. C., Freitas, F. S., Henley, S. F., Krause, J. W., März, C., Ng, H. C., Pickering, R. A., & Tessin, A. C. (2022). Stable silicon isotopes uncover a mineralogical control on the benthic silicon cycle in the Arctic Barents Sea. *Geochimica et Cosmochimica Acta*, *329*, 206–230. https://doi.org/10.1016/j.gca.2022.05.005

West, A. J., Galy, A., & Bickle, M. (2005). Tectonic and climatic controls on silicate weathering. *Earth and Planetary Science Letters*, *235*(1–2), 211–228. https://doi.org/10.1016/j.epsl.2005.03.020

White, A. F., & Brantley, S. L. (2003). The effect of time on the weathering of silicate minerals: why do weathering rates differ in the laboratory and field? *Chemical Geology*, *202*(3–4), 479–506. https://doi.org/10.1016/j.chemgeo.2003.03.001

Wijsman, J. W. M., Herman, P. M. J., Middelburg, J. J., & Soetaert, K. (2002). A model for early diagenetic processes in sediments of the continental shelf of the Black Sea. *Estuarine, Coastal and Shelf Science*, *54*(3), 403–421. https://doi.org/10.1006/ecss.2000.0655

Wilkinson, M. (2015). Does the nucleation of clay minerals control the rate of diagenesis in sandstones? *Clay Minerals*, *50*(3), 275–281. https://doi.org/10.1180/claymin.2015.050.3.01

Wolthers, M., Nehrke, G., Gustafsson, J. P., & Van Cappellen, P. (2012). Calcite growth kinetics: modeling the effect of solution stoichiometry. *Geochimica et Cosmochimica Acta*, *77*, 121–134. https://doi.org/10.1016/j.gca.2011.11.003

Wooldridge, L. J., Worden, R. H., Griffiths, J., & Utley, J. E. P. (2019). Clay-coat diversity in marginal marine sediments. *Sedimentology*, *66*(3), 1118–1138. https://doi.org/10.1111/sed.12538

Worden, R. H., & Burley, S. D. (2003). Sandstone Diagenesis: the evolution of sand to stone. In D. Burley & R. H. Worden (Eds.), *Sandstone Diagenesis: Recent and Ancient* (pp. 1–44). Wiley. https://doi.org/10.1002/9781444304459.ch

Yang, L., & Steefel, C. I. (2008). Kaolinite dissolution and precipitation kinetics at 22 °C and pH 4. *Geochimica et Cosmochimica Acta*, *72*(1), 99–116. https://doi.org/10.1016/j.gca.2007.10.011

Zhang, Q., & Tutolo, B. M. (2021). Geochemical evaluation of glauconite carbonation during sedimentary diagenesis. *Geochimica et Cosmochimica Acta*, *306*, 226–244. https://doi.org/10.1016/j.gca.2021.05.036

Zhao, B., Yao, P., Bianchi, T. S., Wang, X., Shields, M. R., Schröder, C., & Yu, Z. (2023). Preferential preservation of pre-aged terrestrial organic carbon by reactive iron in estuarine particles and coastal sediments of a large river-dominated estuary. *Geochimica et Cosmochimica Acta*, *345*, 34–49. https://doi.org/10.1016/j.gca.2023.01.023

Zhao, B., Yao, P., Bianchi, T. S., Xu, Y., Liu, H., Mi, T., Zhang, X.-H., Liu, J., & Yu, Z. (2017). Early diagenesis and authigenic mineral formation in mobile muds of the Changjiang Estuary and adjacent shelf. *Journal of Marine Systems*, *172*, 64–74. https://doi.org/10.1016/j.jmarsys.2017.03.001

Zhao, M., Zhang, S., Tarhan, L. G., Reinhard, C. T., & Planavsky, N. (2020). The role of calcium in regulating marine phosphorus burial and atmospheric oxygenation. *Nature Communications*, *11*(1). https://doi.org/10.1038/s41467-020-15673-3

Zhu, Q.-Z., Yin, X., Taubner, H., Wendt, J., Friedrich, M. W., Elvert, M., Hinrichs, K.-U., & Middelburg, J. J. (2024). Secondary production and priming reshape the organic matter composition in marine sediments. *Science Advances*, *10*(20), eadm8096. https://doi.org/10.1126/sciadv.adm8096

Zhu, Z., Aller, R. C., & Mak, J. (2002). Stable carbon isotope cycling in mobile coastal muds of Amapá, Brazil. *Continental Shelf Research*, *22*(15), 2065–2079. https://doi.org/10.1016/S0278-4343(02)00071-7

SUPPLEMENTARY MATERIALS

Supplement to: Silicate weathering and diagenetic reaction balances in deltaic muds

Download: https://ajsonline.org/article/134118-silicate-weathering-and-diagenetic-reaction-balances-in-deltaic-muds/attachment/281069.docx

Supplementary Data S1

Download: https://ajsonline.org/article/134118-silicate-weathering-and-diagenetic-reaction-balances-in-deltaic-muds/attachment/281070.xlsx